# Electronic and Structural Factors in Modification and Functionalization of Clean and Passivated Semiconductor Surfaces with Aromatic Systems

Feng Tao,[†,‡] Steven L. Bernasek,[*,†] and Guo-Qin Xu[§]

*Department of Chemistry, Princeton University, Princeton, New Jersey 08544, Department of Chemistry, University of California, Berkeley, and Materials Science and Chemistry Divisions, Lawrence Berkeley National Laboratory, Berkeley, California, 94720, and Department of Chemistry, National University of Singapore, Singapore 119260*

## Contents

* To whom correspondence should be addressed.
† Princeton University.
‡ University of California, Berkeley and Lawrence Berkeley National Laboratory.
§ National University of Singapore.

## 1. Introduction

The chemistry of organic molecules on solid surfaces has been a central issue of surface and interfacial chemistry. The technologically important surfaces mainly include catalytic transition metal surfaces such as Pt(111),[1] semiconductor surfaces such as Si(100),[2] and insulator surfaces such as MgO.[3] The interactions between organic molecules and solid surfaces are quite diverse.[4] For example, the weak van der Waals interactions between organic molecules and solid surfaces such as graphite make the adsorbed organic molecules have the capability of self-assembling into various 2-D or even 3-D functional structures;[5,6] the metastable interactions of organic molecules such as cyclohexene and benzene on noble metals make heterogeneous catalysis such as hydrogenation and dehydrogenation possible;[7,8] the strong covalent binding of organic molecules on semiconductor surfaces makes those surfaces ideal for the immobilization of functional organic materials for the development of new hybrid materials and semiconductor-based molecular devices.[2,9−15] Thus, from weak van der Waals interactions to strong covalent binding the diverse interfacial chemistry between organic molecules and solid surfaces contributes to a wide spectrum of technological needs and the development of new hybrid materials, sensors, and electronic devices.

Feng Tao received his Master's degree from Sichuan University and did research at the Beijing Institute of Physics of the Chinese Academy of Science. He then worked as a research scientist studying organic modification and functionalization of semiconductor surfaces with Professor Xu Guo-Qin at the National University of Singapore. He obtained his Ph.D. from Princeton University in 2006, where he worked in the research group of Professor Steven L. Bernasek. During his Ph.D. studies at Princeton, he worked on two projects: functionalization of semiconductor surfaces and self-assembly of organic monolayers. Since August 2006, Feng Tao has worked on nanocatalysis in Professor Gabor A. Somorjai's group at Berkeley, as a chemistry postdoctoral fellow in the Department of Chemistry and the Materials Science and Chemistry Divisions of the Lawrence Berkeley National Laboratory. At Berkeley, he has worked on the synthesis and catalytic behavior of metallic nanoparticle catalysts. To carry out in situ studies of nanocatalysts under high-pressure conditions, he success-fully designed and built the first chamber-in-chamber high-pressure scanning tunneling microscope, which has been extensively used in catalysis studies under high pressure conditions. Using synchrotron-based ambient pressure X-ray photoelectron spectroscopy, he and his colleagues revealed the reaction-driven restructuring of core−shell structure bimetallic nanocatalysts under different reaction conditions. Feng Tao received the International Union of Pure and Applied Chemistry (IUPAC) Prize for Young Chemists based on his thesis work, and the Harold W. Dodds Honorific Fellowship, the Schering-Plough Presentation Award, and the Hugh Stott Taylor Merit Prize during his studies at Princeton. He was awarded the Materials Research Society Graduate Research Silver Award and the American Vacuum Science and Technology Society National Graduate Research Award.

Steven L. Bernasek graduated from Kansas State University with a B.S. in chemistry in 1971. He received his Ph.D. in physical chemistry from the University of California, Berkeley, in 1975, where he was an NSF Graduate Fellow working in the laboratory of Professor Gabor A. Somorjai. His thesis work examined hydrogen−deuterium exchange at stepped platinum surfaces using molecular beam scattering methods. Dr. Bernasek joined the faculty of Princeton University in 1975, where he is currently Professor of Chemistry. At Princeton he is an Associated Faculty Member of the Princeton Research Institute for the Science and Technology of Materials and the Princeton Environmental Institute, and he is a member of the Executive Committee for the Program in Plasma Science and Technology. The application of gas phase molecular reaction dynamics tools to the study of heterogeneous reactions has been the major focus of Dr. Bernasek's research. He has advised over thirty-five Ph.D. students and twenty postdoctoral associates in his laboratory at Princeton. Dr. Bernasek was elected a Fellow of the AAAS in 1994 and a Fellow of the AVS in 2001. In 1981, he was awarded the Exxon Faculty Fellowship in Solid State Chemistry, by the Division of Inorganic Chemistry of the American Chemical Society. He received the ACS Arthur W. Adamson Award for Distinguished Service in the Advancement of Surface Chemistry in 2006.

Professor Guo-Qin Xu graduated with his B.Sc. in chemistry from Fudan University, China, in 1982. He completed his Ph.D. studies with Professor Steven Bernasek at Princeton University in 1987. He then worked as a research associate with Dr. Jan Hrbek at the Brookhaven National Laboratory and Professor John Polanyi at the University of Toronto. In 1991, he joined the Department of Chemistry, the National University of Singapore. His research mainly focuses on semiconductor surface chemistry and nanomaterials. He has mentored over 20 graduate students at NUS. Professor Xu received the Singapore Youth Award (Science & Technology) in 1997. Currently, he is Professor and Head of Chemistry at the National University of Singapore.

A tremendous number of studies of organic functional-ization and modification of semiconductor surfaces[16−21] have been driven by significant technological requirements in several areas including the development of semiconductor-based sensing techniques, micro- and nanoscaled electro-mechanical devices, and a new generation of molecular electronic devices. Integration of organic materials into inorganic materials exhibits a great advantage for creating new functional materials and devices, as inorganic semicon-ductor surfaces are certainly absent of various functions of organic materials and these functions and properties can be tuned finely due to the availability of a myriad of organic molecules.

Aromatics are one of the most important categories of organic molecules and serve as an important building block of many organic materials.[22,23] Extensive studies of the surface chemistry of aromatic molecules on Si(100), Si(111)-7×7, and Ge(100) have been carried out recently. For each of these semiconductor surfaces, interactions with aromatic molecules, particularly heteroatom aromatic molecules, have complicated and diverse reaction mechanisms determined by several interacting electronic and structural factors. They mainly include the distribution of electron density on the molecule determined by the geometric arrangement of the carbon and heteroatoms (if any) on the aromatic ring, the electronegativity of the heteroatoms, and the electronic

contribution of the heteroatoms to the formation of aromatic π conjugation, as well as the overall molecular polarity. The competition and selectivity of different reaction channels is dependent on the intrinsic structural and electronic factors of the molecule. For each molecule on different semiconduc-tor surfaces, the various reaction mechanisms present a significant surface selectivity. The geometric and electronic
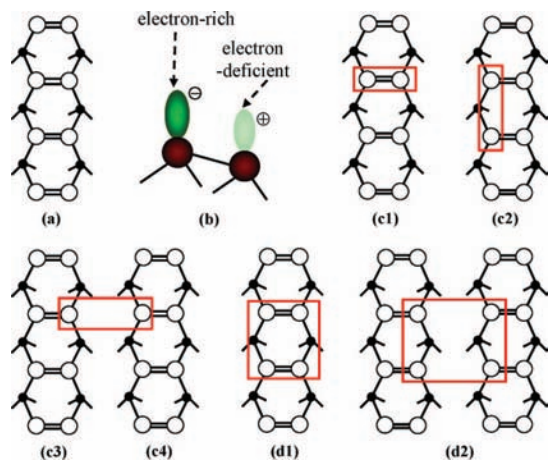
**Figure 1.** Surface structure and reactive sites of Si(100), Ge(100), and C(100). (a) Dimer and dimer row. (b) Electron transfer and distribution of buckled-down and buckled-up silicon atoms of a Si=Si (or Ge=Ge) dimer. (c1), (c2), (c3), and (c4) are disigma binding sites. (d1) and (d2) are tetrasigma binding sites.

structures of surface reactive sites are two other important factors shaping the reaction channel of an aromatic molecule on different semiconductor surfaces.

This article reviews the extensive studies on this topic from the view of electronic and structural factors of both the aromatic systems and the semiconductor surfaces, focusing on establishing the intrinsic connection between reaction mechanisms of aromatic molecules and their derivatives on semiconductor surfaces, and the complicated electronic and structural factors of aromatic molecules and surface reactive sites which result in the competition and selectivity among multiple reaction channels in this process. This review is organized by the class of aromatic systems from the simplest benzene to very much larger complicated carbon buckyballs and nanotubes. For each category of aromatic molecules, reaction mechanisms on different semiconductor surfaces will be reviewed to reveal the structural and electronic factors of the semiconductor surfaces that shape the selection of the reaction channels. In addition, the formation of monolayers of aromatic molecules and derivatives of aromatic molecules from solution on hydrogenated and halogenated semiconductor surfaces is reviewed.

## 2. Semiconductor Surface Structures and Study Techniques

Si(100), Si(111)-7×7, Ge(100), and diamond (100) are four main single crystal surfaces studied in molecular modification and functionalization of semiconductor surfaces. In the three 2 × 1 reconstructed surfaces (Si(100), Ge(100), C(100)),[18,19] two adjacent surface atoms pair into a dimer. Figure 1a schematically presents the structure of the (100) face of the three semiconductor single crystals. The bonding within a surface dimer can be described as a $\sigma$ bond coupled with a weak $\pi$ bond, analogous to the well-known C=C bond in organic chemistry. For Si(100) and Ge(100), the two atoms of a Si=Si (or Ge=Ge) dimer are tilted up and down, respectively, forming electron-rich buckled-up and electron-deficient buckled-down atoms as shown in Figure 1b. The extent of dimer tilting increases in the order C(100), Si(100), and Ge(100). In fact, there is no dimer buckling on C(100). Parts c1, c2, c3, c4, d1, and d2 of Figure 1 schematically present the multiple binding sites of the (100) face, particularly for Si(100). Recent investigations showed that organic

molecules can be bonded to the (100) surface through pericyclic addition, dissociative reactions, dative bonding, and other mechanisms.[18−20,24,25] For diamond (100), reaction mechanisms of unsaturated hydrocarbons such as ethylene, 1,3-butadiene, and cyclopentene have been extensively investigated.[26−28] Compared to Si(100) and Ge(100), diamond exhibits a weaker reactivity toward these molecules mentioned above. There is no report in the literature on reaction of aromatic molecules on diamond, likely due to the weak reactivity.

Si(111)-7×7 is a reconstructed surface of silicon. It is formed through a complicated layer-by-layer reconstruction on a base layer with 49 silicon atoms of the (111) surface, which reduces the number of 3-coordinated Si atoms from 49 to 19 in each unit cell. This surface structure is described with a dimer-adatom-stacking (DAS) faulted model.[29,30] A top view of a 7×7 unit cell is schematically presented in Figure 2a. Figure 2b1 and b2 are the unoccupied state and occupied state STM images of a clean Si(111)-7×7 surface, respectively. Nineteen dangling bonds of each unit cell are located at 12 adatoms, 6 rest atoms, and 1 corner hole. The charge transfer occurs preferentially from adatoms to rest atoms during reconstruction, thereby resulting in seven completely occupied dangling bonds at rest atoms and the corner hole as well as twelve partially occupied or empty dangling bonds at the twelve adatoms. Both experimental and theoretical studies have shown that the adjacent adatom-rest atom pair (Figure 2c) can serve as a diradical to react with organic molecules.[31,32]

All these semiconductor surfaces can be prepared by a combined annealing at high temperature and sputtering with $Ar^+$ ions to remove surface contamination such as oxides and carbides, and then annealing to high temperature followed by a slow cooling down for surface reconstruction. The annealing temperature for Ge(100) is much lower than those for Si(111) and Si(100). The main experimental techniques used to study the reaction mechanisms in modification and functionalization of semiconductor surfaces with aromatic molecules are electronic spectroscopies such as X-ray and ultraviolet photoelectron spectroscopies (XPS and UPS) for obtaining chemical shift of core-level and valence band structure, vibrational spectroscopies such as high-resolution electron energy loss spectroscopy (HREELS), and multiple internal reflection infrared spectroscopy (MIR-FTIR) for identifying vibrational modes of the organic layer, and surface microscopy techniques such as scanning tunneling microscopy (STM) for visualizing surface structure and molecular binding at the atomic level. Thermal desorption spectroscopy (TDS) is used to study molecular desorption behavior on these surfaces. In addition, various theoretical approaches are used to simulate the reaction mechanisms of these molecules on the semiconductor surfaces. In studies of organic layers formed on hydrogenated and halogenated semiconductor surfaces using wet chemistry, a few extra techniques such as scanning electron microscopy (SEM), atomic force microscopy (AFM), and scanning Auger electron spectroscopy (SAES) have been used.

## 3. Covalent Binding Mechanisms of Benzene

### 3.1. Multiple Binding Configurations of Benzene on Si(100)

Benzene is the prototype molecule for aromatic systems. Using both vibrational EELS and TDS, Taguchi et al.
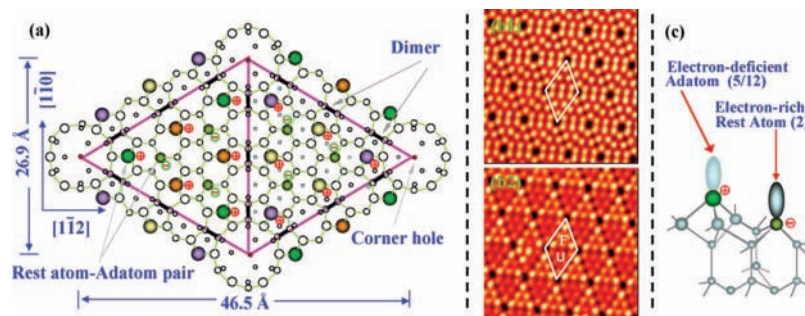
**Figure 2.** Surface structure and reactive sites of Si(111)-7×7. (a) Top view of a reconstructed 7×7 unit cell. (b1) STM images of unoccupied states of a clean Si(111)-7×7 surface. (b2) STM images of occupied states of a clean Si(111)-7×7 surface. (c) Electronic transfer and distribution of the reactive site, a pair of adatoms, and its adjacent rest atom.
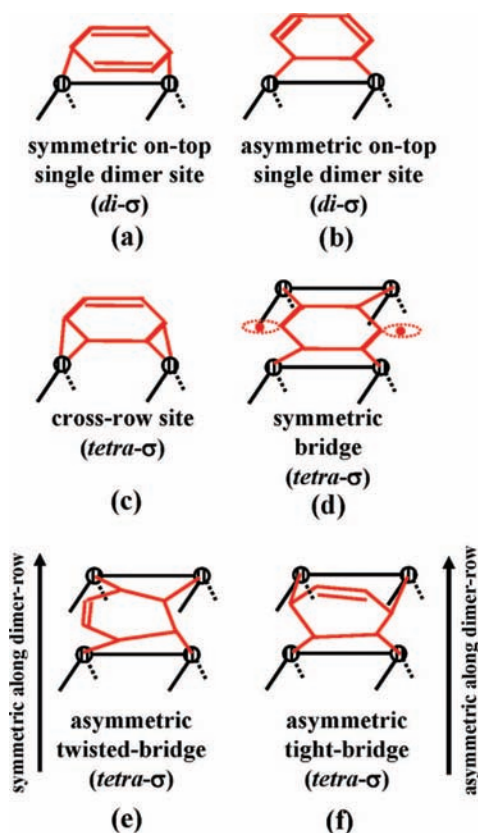


**Figure 3.** Six possible binding configurations of benzene molecules chemisorbed on Si(100).

explored the chemical binding of benzene on Si(100) at 300 K early on.[33] Two chemisorption states with desorption peaks at ∼432−460 and ∼500 K were identified.[33,34] They are attributed to benzene adsorbed on defect-free and near-defect regions, respectively. Several binding configurations were proposed for the molecularly chemisorbed benzene on Si(100).[33−39] Two disigma binding modes were initially proposed for benzene adsorbed on the defect-free region.[33] They are schematically shown in Figure 3a and b. One is formed via two Si−C covalent linkages at $C^1$ and $C^4$ atoms, producing a 1,4-cyclohexadiene-like product (Figure 3a), and the other involves the bonding at $C^5$ and $C^6$, giving rise to a 1,3-cyclohexadiene-like product (Figure 3b). Besides the two disigma binding modes, four tetrasigma binding modes involving two pairs of Si═Si dimers in each case giving three bridgelike configurations, as shown in Figure 3d, e, and f were proposed.[35−39] Figure 3c is a tetra-sigma binding mode involving two dangling bonds from two adjacent dimer rows. A symmetric bridge binding configuration was proposed as

shown in Figure 3d.[36,37] Parts e and f of Figure 3 are asymmetric twisted-bridge and tight-bridge binding modes on two adjacent dimers in a dimer row.[37]

STM and FTIR experimental techniques[37,40] revealed the coexistence of symmetric on-top single dimer binding (Figure 3a), asymmetric twisted-bridge binding (Figure 3e), and asymmetric tight-bridge binding (Figure 3f) on Si(100). Notably, the on-top disigma bound molecules can be converted into asymmetric bridge bound molecules by thermal promotion, suggesting that asymmetric tetrasigma bridge binding is thermodynamically more favorable than the on-top disigma binding.[37,38] It is interesting to note that the biased STM tip can be used to aid the conversion from the thermodynamically stable tetrasigma binding configuration to the on-top disigma binding one.[37,38,40] In addition, the chemisorption behavior of benzene on Si(100) exhibits an obvious coverage-dependence.[41] The ratio of disigma bonded product to tetrasigma bonded product is increased at a high coverage compared to that at a low coverage, though the formation of tetrasigma bonded product is thermodynamically favored at low coverage. This coverage-dependent binding behavior indicates the influence of the interaction between two adjacent adsorbate molecules on selecting binding sites.

## 3.2. Disigma Binding of Benzene on Si(111)-7×7

On Si(111)-7×7, early investigation using vibrational EELS with low resolution indicated that benzene chemisorbs on this surface at room temperature through a π-interaction.[42] Recent studies clearly show that benzene chemically binds to Si(111)-7×7 with two Si−C sigma bonds formed through a [4 + 2]-like pericyclic addition mechanism.[43−47] DFT calculations show that the [4 + 2]-like addition is both thermodynamically and kinetically preferred.[31,32,48,49] The binding site, an adatom and its adjacent rest atom, where the $C^1$ and $C^4$ atoms terminate on an adjacent adatom−rest atom pair, was confirmed in recent STM studies.[44,45,47,50] Compared to the multiple binding configurations of benzene on Si(100), the disigma bonded 1,4-cyclohexadiene-like product is the only one seen on Si(111)-7×7. This difference results from the accessible multiple reactive sites on Si(100) as shown in Figure 1a2, a3, a4, and a5. The difference among these binding sites on Si(100) which have different geometric and even electronic structures (Figure 1c1, c2, c3, c4, d1, and d2) is mainly their spatial arrangement. Alternatively, in general Si(111)-7×7 has only one reactive site, consisting of an adatom and its adjacent rest atom as shown in Figure 2c, which forms a binding configuration.
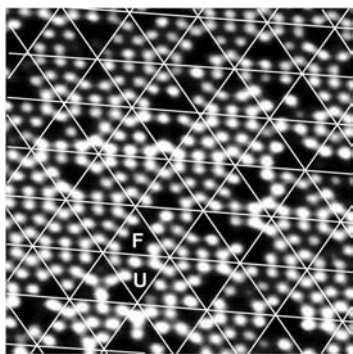
**Figure 4.** STM image of Si(111)-7×7 with the chemisorbed benzene molecules. F and U represent the faulted and unfaulted unit cells, respectively.

Figure 4 is an STM image of benzene on Si(111)-7×7. Clearly, each half unit cell contains at most three reacted adatoms appearing as dark features, which do not align in a straight line. This observation provides evidence for a nondissociated, disigma binding of benzene on an adatom–rest atom pair on Si(111)-7×7.[44,45,47,50] Each unit cell of the Si(111)-7×7 has six corner-adatoms and six center-adatoms. On average, each center-adatom–rest atom pair has more opportunity to react with benzene in contrast to a corner-adatom–rest atom pair. This is because each center-adatom faces two adjacent rest atoms in contrast to only one for the corner-adatom due to the geometric arrangement of adatoms on Si(111)-7×7. A similar difference in binding density was also observed for the binding of thiophene on Si(111)-7×7 by STM.[51]

## 3.3. Weak Binding of Benzene on Ge(100)

Compared to the disigma binding of benzene on Si(100), benzene weakly binds to Ge(100). TDS revealed two desorption peaks for benzene on Ge(100) at 234 and 252 K,[34,52] corresponding to molecular adsorption at terrace and step sites, respectively. However, the adsorbed benzene on Si(100) desorbs at ∼432−460 K and ∼500 K,[33,34] corresponding to the chemisorbed benzene at terrace and step sites, respectively. DFT calculations[52] rationalized the experimentally observed difference in the adsorption of benzene on Ge(100) and Si(100). The calculated adsorption energies for benzene on Ge(100) and Si(100) are 1.4 and 20.0 kcal/mol, respectively. This significant difference in adsorption energy could partially result from the larger Ge−C bond length compared to the Si−C bond length in the adsorbed benzene. In fact, a similar difference in molecular adsorption energy on the two semiconductor surfaces has been seen for other organic molecules.[53]

## 4. Five-Membered Aromatic Molecules Containing One Heteroatom

Thiophene, furan, and pyrrole are three representative five-membered ring aromatic molecules with one heteroatom, as shown in Figure 5. Their chemical binding on Si(111)-7×7, Si(100), and Ge(100) has been extensively studied. Compared to the simplest aromatic molecule, benzene, each of the three molecules exhibits different reaction mechanisms in the modification and functionalization of semiconductor surfaces due to the participation of their heteroatoms.
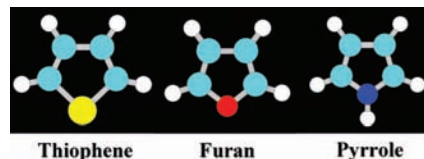


**Figure 5.** Molecular structures of thiophene, furan, and pyrrole. Yellow, red, and blue balls represent sulfur, oxygen, and nitrogen atoms, respectively.

## 4.1. Thiophene, Furan, and Pyrrole on Si(111)-7×7

Compared to the homogeneous distribution of electronic density on benzene, the electron density on the molecular ring of thiophene is unevenly distributed due to its heteroatom, sulfur. The electron density of the HOMO is mostly concentrated at the α-position, suggesting a highly nucleophilic nature of the $C^1$ and $C^4$ atoms. Thus, they are expected to interact with electrophilic dangling bonds on adatoms of Si(111)-7×7. Both experimental techniques and theoretical approaches reveal that thiophene can be chemically bound to one adatom–rest atom pair via two Si−C sigma bonds at the $C^1$ and $C^4$ atoms through a [4 + 2]-like addition.[32,51,54] STM studies[51,55] show the higher reactivity of the center-adatom in contrast to the corner-adatom due to its geometric arrangement in a unit cell and a smaller steric strain induced by thiophene bonded at the center adatom site. In addition, the faulted half-unit cell exhibits higher reactivity than the unfaulted half, due to a relatively higher electrophilicity of the adatom sites on the faulted subunit.

DFT calculations show that the binding of thiophene is initiated by the formation of a monosigma bonded intermediate ($LM_1$) through a transition state with a barrier of 5.4 kcal/mol.[32] The [4 + 2]-like addition process of thiophene on Si(111)-7×7 is exothermic by 36.0 kcal/mol, comparable to the adsorption energy of thiophene on Si(100) (−34.3 kcal/mol).[56] The energy of $LM_1$ of thiophene on Si(111)-7×7 is 4.6 kcal/mol lower than that of the initial reactants. Compared to the analogous intermediate of benzene on Si(111)-7×7, the lower energy intermediate of thiophene is possibly due to its lower resonance energy.

Compared to thiophene, furan (with an oxygen heteroatom) exhibits a significantly different reaction mechanism on interaction with Si(111)7×7. Both HREELS and TDS experiments revealed two chemisorbed states ($\beta1$ and $\beta2$) at both low temperature (110 K) and room temperature.[31,57] $\beta1$ is assigned to a [4 + 2]-like adduct linked to an adatom–rest atom pair through two Si−C sigma bonds (Figure 6a). $\beta2$ is a disigma linked dimerized furan formed through a diradical mechanism (Figure 6b). Both adstates are formed from the same intermediate, a monosigma complex. Due to the different adsorption energies of the two products, the product distribution exhibits a strong temperature dependence.

Theoretical simulations show that there is a common reaction pathway for 1,3-butadiene, benzene, and thiophene on Si(111)-7×7.[32] Isolated reactants initially form a monosigma bonded *radical*-like intermediate via a transition state. Passing another transition state, the monosigma intermediate converts into the final [4 + 2]-like adduct. The stability of the intermediate depends on the height of the barrier between the intermediate and the final [4 + 2]-like adduct. This barrier increases from *cis*-1,3-butadiene to benzene to thiophene because the increased separation between $C^4$ and the rest
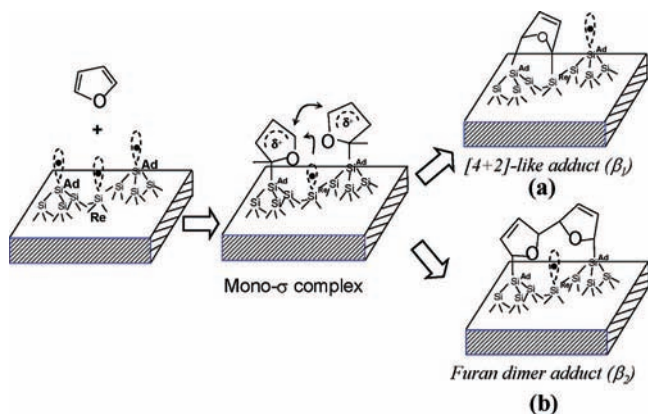
**Figure 6.** Scheme showing the mechanism for the formation of the [4 + 2]-like adduct ($\beta1$) (a) and dimerized product ($\beta2$) (b) of furan on Si(111)-7×7.



**Figure 7.** STM image of Si(111)-7×7 with the chemisorbed pyrrole showing the formation of the molecular chainlike structure on this surface.

atom due to the decreased $C^1-C^4$ distance in their monosigma intermediates results in a higher energy transition state. Following this dependence, furan may have a more stable intermediate due to its smaller $C^1-C^4$ distance (2.20 Å) in contrast to those of benzene and thiophene.

Based on the theoretical simulation of conjugated dienes including 1,3-butadiene, benzene, and thiophene,[32] all of them initially adsorb onto electrophilic adatoms by the electrostatic interaction with a nucleophilic $C^\alpha$ atom to form a monosigma-bonded intermediate. The unstable monosigma-bonded intermediate has two possible reaction channels: binding to an adjacent rest atom (Figure 6a) or coupling with an adjacent monosigma-bonded complex (Figure 6b). The monosigma-bonded complex of furan is expected to be more stable than those of benzene or thiophene, due to its smaller $C^1$ and $C^4$ separation, lower aromaticity, or lower resonance energy. This suggests the possible concurrent operation of these two reaction channels for furan on Si(111)-7×7. At a low temperature of 110 K, the monosigma-bonded furan intermediate is thermally stabilized and a high population of this intermediate can be built up on the surface. Two adjacent radical-like monosigma-bonded species can readily couple to each other to form a new C−C bond, giving rise to the $\beta2$ state (Figure 6b), the dimerized furan on Si(111)-7×7. Figure 6 is the scheme of the two reaction channels for furan on Si(111)-7×7. In fact, the formation of the more stable dimer complex ($\beta2$ state) for furan on Si(111)-7×7 was further supported by a PM3 semiempirical calculation.[57] The calculation results show that the resulting dimerized furan complex ($\beta2$) is about 23 kcal/mol more stable than the [4 + 2]-like adduct ($\beta1$).

Distinctly different from thiophene and furan, pyrrole is chemically bonded on Si(111)-7×7 through a dissociation of the N−H bond.[58] It forms silicon-based pyrroyl and Si−H species. Compared to the dissociation at the N−H bond, the [4 + 2]-like addition is expected to be thermodynamically and kinetically unfavorable for pyrrole. There is no theoretical simulation for the pathways of N−H dissociation of pyrrole on Si(111)-7×7. On the basis of theoretical calculations of the dissociation pathways of this molecule on Si(100) (section 4.2),[53] N−H dissociation on Si(111)-7×7 could occur through two possible pathways, including a direct pathway through an initial binding at the nitrogen atom and an alternative pathway through an initial binding at the $C^\alpha$ atom and a subsequent isomerization. For Si(100), the alternative pathway is both thermodynamically and kinetically favorable. Notably, this chemical binding through N−H
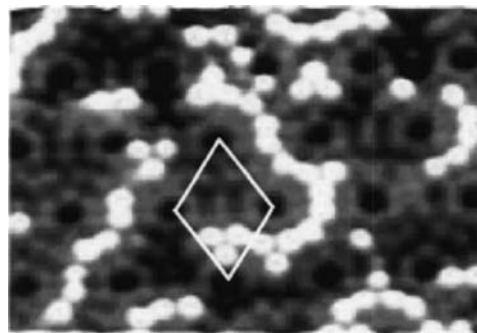
dissociation does not break the aromaticity of pyrrole, in contrast to loss of aromaticity of products in the addition reactions of benzene, thiophene, and furan. The preserved aromatic $\pi$ conjugation allows a weak $\pi-\pi$ electronic coupling between two adjacent pyrroyl groups bonded on the surface. This weak electronic coupling makes the next molecule preferentially bind to an unreacted site adjacent to the bonded pyrroyl ring, evidenced in the observation of molecular wirelike binding behavior at low exposure (Figure 7).[58]

## 4.2. Thiophene, Furan, and Pyrrole on Si(100)

Both thiophene and furan molecularly chemisorb on Si(100) through formation of Si−C sigma bonds. Both experimental studies and theoretical calculations show that the chemisorbed thiophene molecules have similar multiple binding configurations to that of benzene on Si(100).[56,59−64] Compared to the [4 + 2]-like addition on Si(111)-7×7,[5155] thiophene forms multiple products, including 2,3-dihydrothiophene-like species and 2,5-dihydrothiophene-like species through disigma binding, as well as twist bridge-like and tight bridge-like species with tetrasigma binding.[59−64]

For furan on Si(100),[56,61,64] no dimerized complex was observed, in contrast to the coexistence of a [4 + 2]-like adduct and dimerized complex on Si(111)-7×7.[57] Furan is chemisorbed on Si(100) through a [4 + 2]-like addition pathway.[56,61,64] This is probably due to the absence of a reactive site on Si(100), similar to two neighboring adatom−adjacent rest atom sites with a reasonable separation on Si(111)-7×7, which allows the electronic coupling of two adjacent monosigma complexes.

The chemical binding of thiophene and furan on Si(100) was investigated by hybrid density functional (B3LYP) calculation in combination with a cluster model approach.[56] The calculations show that the [4 + 2]-like addition is barrierless and favorable over the [2 + 2]-like addition, since the barriers of a [2 + 2]-like addition for thiophene and furan are 2.6 and 1.2 kcal/mol, respectively.

On Si(100),[3,53,58,65−68] pyrrole exhibits a major N−H dissociation pathway as on Si(111)-7×7[58] and a minor C−H dissociation pathway.[66] A direct dissociation pathway (Figure 8a) and an alternative dissociation channel (Figure 8b) through N−H cleavage were theoretically simulated.[53,69,70] DFT calculations suggest that this reaction takes place via a barrierless addition of the pyrrole molecule at the $C^\alpha$ position to a Si=Si dimer, followed by N−H dissociation and isomerization to form a pyrroyl group bonded to Si(100) through a Si−N covalent linkage.[53,69,70] Basically, this reaction can be divided into three steps[53] as shown in Figure
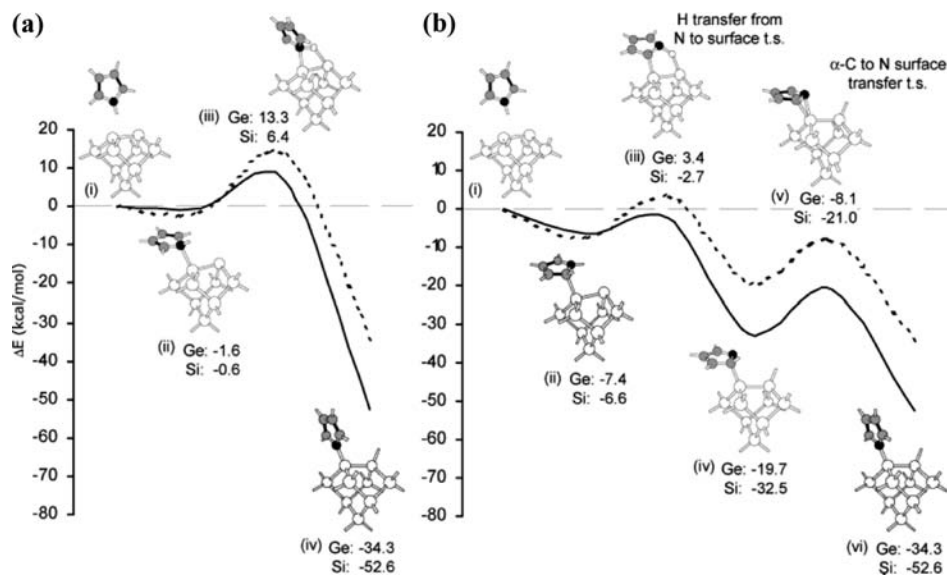
**Figure 8.** Critical points on the potential energy surfaces of the N−H dissociation reaction of pyrrole on Si(100) and Ge(100) through a direct pathway by an initial binding at the nitrogen atom (a) and an alternative pathway by an initial binding at $C^\alpha$ (b). (From ref 53.)

8b. The first step is the molecular adsorption of gaseous pyrrole onto the silicon surface through one of its $C^\alpha$ atoms to form a stable adsorbate (−6.6 kcal/mol referred to the reactants) without a barrier. In fact, this step is similar to the electrophilic attack of thiophene and furan at a $C^\alpha$ atom to form a monosigma intermediate for [4 + 2]-like addition on Si(111)-7×7. The second step is the dissociation of the intermediate formed in the first step to give $C_4H_4N^\bullet_{ads} + H_{ads}$ through a five-membered ring transition state (iii in Figure 8b) with a barrier of 3.9 kcal/mol. The last step is an isomerization of the dissociated intermediate to form final product $C_4H_4N-Si$ (−52.6 kcal/mol) through a transition state with a barrier of 11.5 kcal/mol. Notably, this reaction has no overall barrier for the dissociation of pyrrole to form $C_4H_4N-Si$ and H−Si species. Thus, the alternative dissociation channel (Figure 8b) is more kinetically favorable than a direct dissociative adsorption of pyrrole (Figure 8a) by the interaction of the lone pair electrons of the nitrogen atom with the unoccupied orbital of the Si≡Si dimer, as the direct pathway has an overall energy barrier of 6.4 kcal/mol. In addition, compared to the dissociation channel through the formation of an intermediate binding at $C^\alpha$, the [2 + 2]- and [4 + 2]-like additions of pyrrole on Si(100) are not favorable, either kinetically or thermodynamically.

Compared to addition pathways of thiophene and furan, the selection of the dissociation channel for pyrrole stems from the low barriers for both N−H dissociation and the subsequent isomerization.[53] Definitely, thiophene and furan do not exhibit dissociation or isomerization reaction pathways. Pyrrole could possibly bind to a Si≡Si dimer via a pericyclic addition pathway; however, it is not favorable either kinetically or thermodynamically. Thus, pyrrole exhibits a distinctly different reaction channel on Si(100) in contrast to furan and thiophene. In fact, the observed [4 + 2]-like and [2 + 2]-like adducts of N-methylpyrrole on Si(111)-7×7 confirm the necessity of the N−H bond for favoring the dissociation channel in five-membered aromatic molecules with one heteroatom and demonstrate a strategy for shaping the reaction channel by using protection groups, such as the methyl in N-methylpyrrole.[71]
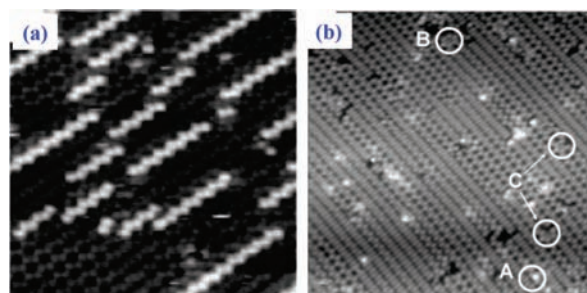


**Figure 9.** (a) Occupied state STM image of Ge(100) with the chemisorbed thiophene. (From ref 74.)[74] (b) Occupied state STM image of Ge(100) with the chemisorbed pyrrole. (From ref 76.)

## 4.3. Thiophene and Pyrrole on Ge(100)

Interestingly, thiophene chemisorbs onto Ge(100) through the formation of a Ge···S dative bond at a coverage lower than 0.25 monolayer (ML) and through the [4 + 2]-like addition at higher coverage at room temperature.[63,72−74] In contrast to the [4 + 2]-like addition of thiophene on Si(100), the [4 + 2]-like addition reaction on Ge(100) has a higher activation barrier for the transition states,[73] as the major contribution to the barrier, the energy difference between the buckled and symmetric dimers of Ge(100) (6.9 kcal/mol), is larger than that for Si(100) (3.2 kcal/mol).[75] Alternatively, dative bonding is barrierless, suggesting that Ge···S dative bonding is kinetically favorable.[73] Thus, dative-bonded thiophene is formed at low coverage. At high coverage, the [4 + 2]-like addition similar to the formation of 2,5-dihydrothiophene on Si(100) is found on Ge(100).

Interestingly, the dative-bonded thiophene molecules form a molecular chainlike structure along the direction of dimer rows at low coverage (Figure 9a).[73,74] The $\pi-\pi$ stacking interaction enhances the stability of the molecular chain of dative bonded thiophene from the point of thermodynamics. A similar molecular chainlike structure is also observed in chemisorbed pyrrole on Si(111)-7×7.[58] This suggests that the intermolecular $\pi-\pi$ interaction plays a similar role in the formation of this chainlike structure. On the other hand, the Ge≡Ge dimer pinned by the dative-bonded thiophene molecule possibly retards the dynamic flipping of its adjacent unreacted Ge≡Ge dimer. Thus, the relatively slower atomic

flipping of the adjacent Ge≡Ge dimer compared to other unreacted dimers located far from the reacted one makes this dimer more easily accessible for the incoming gas phase thiophene molecule.

Pyrrole dissociates on Ge(100) without [4 + 2]-like or [2 + 2]-like additions.[53,76,77] STM studies revealed three dissociation pathways for this molecule.[76,77] In the first dissociation pathway, pyrrole is chemically bound to two dangling bonds of two adjacent dimers in a dimer row on Ge(100) through both Ge−N and Ge−C covalent bonds via the dissociation at both N−H and $C^\alpha$−H of one molecule. Molecular aromaticity is still retained upon dissociation in this pathway. Therefore, it appears as a bright protrusion in the STM image (A in Figure 9b). The product of this pathway retains molecular aromaticity. In the second and third pathways, pyrrole forms tilted species through N−H dissociation; the dissociated pyrrolyl interacts with two adjacent Ge≡Ge dimer rows through both a strong Ge−N bond and a relatively weak Ge−$C^\beta$ interaction. The only difference between the second and third pathways is the bonding of the dissociated hydrogen atom. In the second pathway, the hydrogen atom diffuses out of the region of interest; therefore, the bonded pyrrolyl-like product is present as a complete hexagonal flower-like bright protrusion in the STM image (B in Figure 9b). However, in the third pathway the dissociated hydrogen atom bonds to the other Ge atom of the Ge≡Ge dimer interacting with the dissociated pyrrolyl, making the product observed as a flower-like image with a dark site contributed from the bonded hydrogen atom (C in Figure 9b). Notably, all three pathways involve at least two Ge≡Ge dimers for each molecule as the arrangement of two adjacent dimers makes them accessible to one molecule simultaneously. The aromaticity of the products from the second and third pathways is weakened to some extent because the molecular $C^\beta$ atom interacts with the Ge atom of the adjacent dimer row. DFT calculations show the first pathway forms the most stable product.[78]

Pyrrole does not react with Ge(100) through [4 + 2]- or [2 + 2]-like addition. Similar to the higher barrier for the transition state of [4 + 2]-like addition of thiophene on Ge(100) compared to that on Si(100), it is expected that the energy barrier for [4 + 2]-like addition of pyrrole on Ge(100) is higher than that on Si(100). DFT calculation[78] shows that [4 + 2]-like addition is not favorable thermodynamically and kinetically, in contrast to N−H dissociation via initial attachment to the $C^\alpha$ atom. Recent theoretical studies[53] show that N−H dissociation on Ge(100) forms a product bonded to Ge(100) through a Ge−N bond with an adsorption energy of −34.3 kcal/mol, through a direct dissociation pathway with an energy barrier of 14.9 kcal/mol (Figure 7a) or through an alternative barrierless dissociation channel (Figure 7b).

## 4.4. Electronic and Structural Factors of the Semiconductor Surfaces for the Selection of Reaction Channels

Thiophene forms a dative bond on Ge(100) but not on Si(100) because [4 + 2]-like addition on Ge(100) is unfavorable due to the higher energy barrier mainly contributed by the larger energy difference between the buckled and symmetric Ge≡Ge dimers.[79−81] On the other hand, the strong electronic affinity in terms of a larger amount of transferred electron density in the formation of buckled Ge≡Ge dimer than that in the Si≡Si dimer makes the
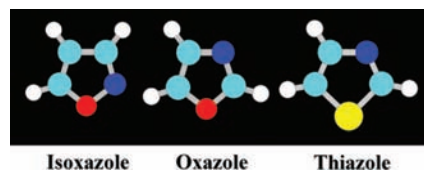


**Figure 10.** Molecular structures of three representative five-membered aromatic molecules (isoxazole, oxazole, and thiazole) consisting of two different heteroatoms in each of them. The yellow, red, and blue balls represent sulfur, oxygen, and nitrogen atoms, respectively.

buckled-down Ge atom more electron-deficient and therefore forms a relatively more stable dative-bonded product.

Interestingly, pyrrole carries out N−H dissociation on both Si(100) and Ge(100), as the N−H bond of the molecule can dissociate through an alternative pathway in which the electron-deficient substrate atom is initially attached to the electron-rich $C^\alpha$ atom of pyrrole rather than the nitrogen atom. An additional five-membered ring transition state is involved for transferring the initial binding at the $C^\alpha$ to the N atom.[53,69] This transition state has a lower energy than the first one. In the first transition state, the adsorption of pyrrole at the $C^\alpha$ atom is facilitated in this aromatic molecule due to its capability for delocalizing the π-electron on the aromatic ring. Thus, the first transition state has a lower barrier. The overall process of the alternative dissociation pathway (Figure 7b) is barrierless. However, for pyrrolidine and 3-pyrroline, a transition state formed via initial attachment at the carbon atom could be highly unstable, as it results in a pentavalent carbon due to the absence of electronic delocalization in the nonaromatic rings. Thus, the two nonaromatic molecules cannot process N−H dissociation through the alternative pathway in terms of an initial binding at the carbon atom adjacent to the nitrogen atom. For a potential direct dissociation pathway for pyrrolidine and 3-pyrroline on Ge(100), the barriers are 10.2 and 8.2 kcal/mol higher than the same barriers on Si(100), suggesting that the N−H dissociation on Ge(100) is suppressed.[53] Thus, the two molecules adopt a kinetically favorable pathway on Ge(100), formation of dative bonds. However, they follow a thermodynamically favorable pathway on Si(100), N−H dissociation, though the formation of dative bonds on Si(100) for these molecules is also barrierless.

Furan dimerizes on Si(111)-7×7 but not on Si(100) and Ge(100), as a reasonable arrangement of reactive sites accessible for a subsequent coupling of two monosigma bonded intermediates is absent on the (100) surfaces. Alternatively, it bonds to Si(100) through a [4 + 2]-like addition reaction.

## 5. Five-Membered Aromatic Molecules Containing Two Different Heteroatoms

Isoxazole, oxazole, and thiazole are three representative five-membered ring aromatic molecules containing two different heteroatoms (Figure 10). They can be considered as aromatic molecules formed by replacing two carbon atoms of benzene with an oxygen or sulfur atom, and one carbon atom of benzene with a nitrogen atom. The oxygen/sulfur atom and the nitrogen atom contribute two and one electrons, respectively, for the formation of an aromatic π-conjugation of $4n+2$ electrons in the ring. In the three molecules, each nitrogen atom has $sp^2$ hybridization and contributes one electron of the unhybridized 2p orbital into the formation of
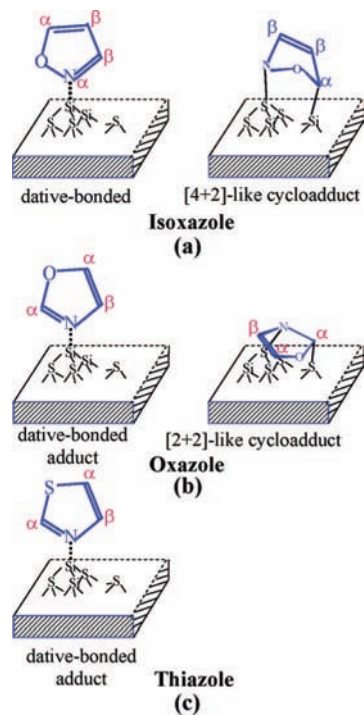
**Figure 11.** Binding modes of isoxazole, oxazole, and thiazole on Si(111)-7×7 at low temperature.

the six electron π-conjugation. The lone pair localized in one $sp^2$ hybridized orbital of the nitrogen atom can be donated to form a dative bond. Thus, the electronic structure of the nitrogen atom in each of the three five-membered ring aromatic molecules is different from that of the nitrogen in pyrrole. Compared to the two heteroatoms separated by carbon in oxazole and thiazole, the two heteroatoms in isoxazole are adjacent. The different geometric arrangement of heteroatoms in oxazole and isoxazole results in a different distribution of electron density on the aromatic ring. In addition, the different heteroatoms in oxazole and thiazole also induce a slightly different distribution of electron density.

Isoxazole has two heteroatoms with different electronic structures. Similar to pyridine, the lone pair of the nitrogen atom in isoxazole does not participate in the formation of the aromatic π-conjugation, though the lone pair is slightly withdrawn by its neighboring oxygen atom. Therefore, the nitrogen atom of isoxazole has an electron density higher than those of the oxygen atom and all the carbon atoms of this molecule. It can act as an electron donor to form a dative bond with an electron-deficient adatom of Si(111)-7×7.[82] Oxazole is an isomer of isoxazole. The difference between the two isomers is the geometry of the nitrogen atom on the five-membered ring. For isoxazole, the nitrogen atom is adjacent to the oxygen atom. However, it is separated by one carbon atom from the oxygen atom in oxazole. The electron-withdrawing effect of oxygen for the nitrogen atom in oxazole is weaker than that for the case of isoxazole. Therefore, the nitrogen atom of oxazole has an electron density similar to that of pyridine, implying the capability for a significant donation of electron density. Similar to oxazole, thiazole also exhibits the capability of donating electron density to form a Si···N dative bond. These molecules exhibit different pathways on Si(111)-7×7 as shown in Figure 11.

The lone pair in an unhybridized p orbital of the oxygen atom of oxazole, which contributes to the formation of

aromatic π-conjugation, in fact plays a different role in the formation of the aromatic π-conjugation than the two electrons in the two p orbitals of two carbon atoms of a pyridine molecule. To some extent, oxazole may be considered as a hybrid of furan and pyridine. In fact, oxazole can be chemically attached to Si(111)-7×7 through both the covalent addition channel similar to thiophene[55] and furan,[57] as well as the dative-bond addition similar to pyridine.[83] Oxazole carries out the addition reaction at low temperature through a [2 + 2]-like addition at N and $C^\alpha$ atoms, instead of a [4 + 2]-like addition. This is determined by its characteristic electronic structure. It is understandable if we consider this addition reaction as a stepwise reaction mechanism as schematically shown in Figure 12. The attack of a nitrogen atom on an adatom forms an intermediate with a lower energy (Figure 12b) than other possible intermediates because the nitrogen atom and silicon adatom are electron-rich and electron-deficient, respectively, and geometrically the adatom is at a favorable outward position in contrast to the inward rest atom. In addition, the interaction of the radical of an electron-rich rest atom with a $C^\alpha$ atom with lower electron density due to the electron-withdrawing effect of its adjacent oxygen atom (Figure 12c) will facilitate the subsequent formation of a Si−C σ bond. Therefore, [2 + 2]-like addition is a kinetically favorable pathway for oxazole at low temperature. However, a [4 + 2]-like addition at two $C^\alpha$ atoms is not kinetically favorable for oxazole due to a high barrier for an initial binding at the $C^\alpha$ atom, in contrast to an initial binding at the N atom in the [2 + 2]-like addition. For pyridine, [2 + 2]-like addition is not kinetically favorable over [4 + 2]-like addition, as both transition states are formed through an initial binding at the N atom. Thus, pyridine is chemisorbed on Si(111)-7×7 through a thermodynamically favorable [4 + 2]-like addition mechanism at $C^1$ and $C^4$ in addition to the formation of a Si···N dative bond.

For isoxazole, an isomer of oxazole, its electron-rich nitrogen atom can form an intermediate with the electron-deficient adatom of Si(111)-7×7. Its $C^\alpha$ atom has lower electron density than the $C^\beta$ atom due to the strong electron-withdrawing effect of the oxygen atom on its adjacent $C^\alpha$ atom. It can interact with the radical of the rest atom of this surface, forming a Si−C σ bond.[82] Thus, the low electron density and favorable geometric arrangement of the $C^\alpha$ atom of isoxazole makes [4 + 2]-like addition thermodynamically and kinetically favorable (Figure 11b).

The chemisorption of thiazole on Si(111)-7×7 (Figure 11c) is different from the simultaneous dative-bonded addition and [4 + 2]-like or [2 + 2]-like addition for isoxazole and oxazole at low temperature (Figure 11a and b). This difference can be understood in the contrast of their electronic structures. For both isoxazole and oxazole, the $C^\alpha$ atom has the low electron density due to the electron-withdrawing effect of the electronegative oxygen atom. Thus, for isoxazole the binding between the electron-rich N atom and the electron-deficient $C^\alpha$ atom and the adatom-rest atom pair of Si(111)-7×7 (Figure 11b) is thermodynamically and kinetically favorable; for oxazole the attachment of the electron-rich N atom and the electron-deficient $C^\alpha$ to the adatom-rest atom pair is kinetically favorable at low temperature. Compared to isoxazole and oxazole, the $C^\alpha$ atom of thiazole has a relatively high electron density due to the absence of a strong electron-withdrawing effect from the sulfur atom with a relatively lower electronegativity than the oxygen atom. Thus, referring to the [2 + 2]-like addition of oxazole
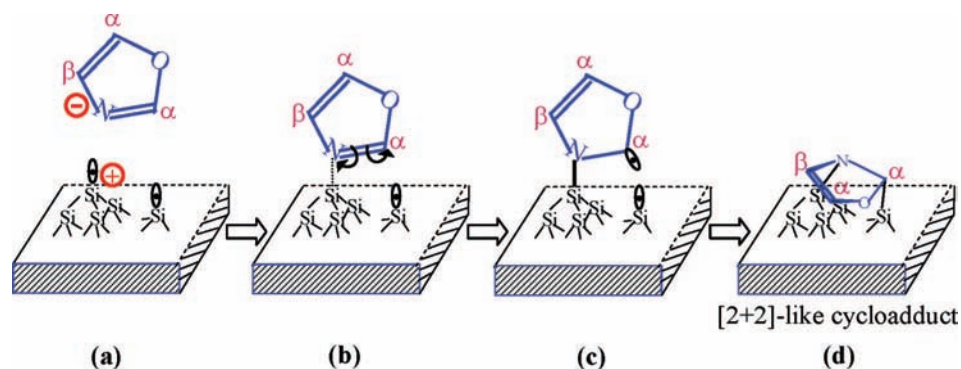
**Figure 12.** Schematic showing the pathway for the formation of the [2 + 2]-like adduct of oxazole on Si(111)-7×7 at low temperature.
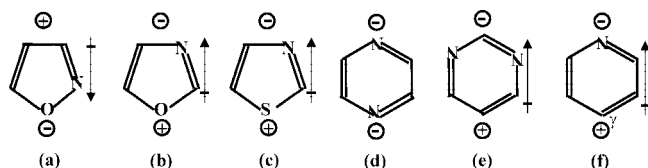


**Figure 13.** Polarity of isoxazole (a), oxazole (b), thiazole (c), pyrazine (d), pyrimidine (e), and pyridine (f).
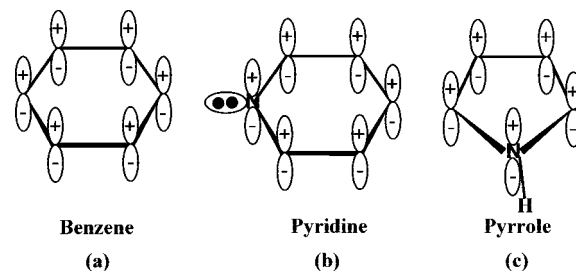


**Figure 14.** Overlap of all parallel p orbitals and the formation of the aromatic $\pi$ conjugation of benzene (a), pyridine (b), and pyrrole (c).

at low temperature (Figure 11b), for thiazole a chemical binding between the nitrogen atom and the $C^\alpha$ atom of thiazole and the adatom−rest atom pair to form a [2 + 2]-like adduct is neither kinetically nor thermodynamically favorable. Alternatively, dative-bond addition between the electron-rich nitrogen atom of thiazole and the electron-deficient adatom site is kinetically favorable at low temperature (Figure 11c). Therefore, the dative-bonded thiazole is the major product at low temperature.

Molecular polarity is an additional factor affecting the formation of dative bonds with the silicon surface. All three of the molecules discussed here have a strong molecular polarity as shown in Figure 13a, b, and c. A more detailed discussion in section 11 indicates that molecular polarity could be a necessary factor for the formation of dative bonds between aromatics and semiconductor surfaces.

Overall, the competition and selectivity of these reaction channels of each multiheteroatom aromatic system are clearly dominated by the distribution of electronic density on the molecular ring, the geometric arrangement of heteroatoms on the ring, the contribution of heteroatoms for the formation of aromatic $\pi$-conjugation, the electronegativity of the heteroatoms, and the molecular polarity.

## 6. Six-Membered Heteroatom Aromatic Molecules

### 6.1. Competition and Selectivity for Dative and Covalent Binding of Pyridine on Si(100), Si(111)-7×7, and Ge(100)

Pyridine is a tertiary amine with an aromatic ring. Compared to pyrrole, the nitrogen atom of pyridine has significantly different electronic density and structure though the nitrogen atoms of both molecules are $sp^2$ hybridized. In pyridine, the $sp^2$ hybridization of the nitrogen atom is different from that of pyrrole. For pyrrole, the three $sp^2$-hybridized orbitals are equivalent, forming two N−C bonds and one N−H bond (Figure 14c). The lone pair of the unhybridized p orbital participates in the aromatic $\pi$ conjugation, forming the sextet of pyrrole. In pyridine, the nitrogen atom is inequivalently $sp^2$ hybridized (Figure 14b). The

remaining unhybridized p orbital of the nitrogen atom has only one electron which combines with the other five p orbitals of the carbon atoms to form an aromatic sextet. Two $sp^2$ orbitals with one electron in each orbital form two sigma bonds with two $C^\alpha$ atoms. Notably, one $sp^2$ orbital has a lone pair which does not participate in the aromatic $\pi$-conjugation system. Thus, compared to the nitrogen atom of pyrrole, the nitrogen atom of pyridine is electron rich. More importantly, the lone pair on the nitrogen atom of pyridine is localized on this atom (Figure 14b). Thus, the lone pair could be donated to the electron-deficient adatom of the Si(111)-7×7 or the buckled down atoms of Si=Si or Ge=Ge dimers to form a dative bond.

In fact, pyridine can form dative-bonded adducts with these three semiconductor surfaces at ~110 K, which is distinctly different from the formation of Si−N or Ge−N covalent bonds on the three surfaces through dissociation of the N−H bond of pyrrole. Pyridine forms both the dative-bonded adduct and the [4 + 2]-like adduct on Si(111)- 7×7[83] and Si(100)[84−86] at low temperature. At room temperature, the dative-bonded pyridine desorbs or partially converts into the [4 + 2]-like adduct.[83−85] There is no dative-bonded adduct of pyridine formed on the two silicon single crystal surfaces at room temperature. However, pyridine forms a nearly complete dative-bonded monolayer on Ge(100) at room temperature,[86−88] which suggests a new approach to synthesis of ordered organic monolayers modifying and functionalizing semiconductor surfaces. The difference in reaction mechanisms of pyridine on silicon and germanium surfaces reflects the trend of increased electron affinity along the periodic table from Si(100) to Ge(100).

The reasons for the absence of a [4 + 2]-like addition for pyridine on Ge(100) could be both thermodynamic and kinetic. From the viewpoint of thermodynamics, the relatively weak Ge−N $\sigma$ bond in contrast to the Si−N $\sigma$ bond results in a lower adsorption energy for [4 + 2]-like addition on

Ge(100) than on Si(100). The weak Ge−N bond stems from the large strain in the [4 + 2]-like adduct due to the larger Ge−Ge bond length of the Ge≡Ge dimer. In addition, the larger energy difference between the buckled Ge≡Ge dimer and the symmetric Ge≡Ge dimer[75] results in a higher energy barrier for the transition state of the [4 + 2]-like addition pathway on Ge(100) than on Si(100); therefore, from the point of kinetics, pyridine prefers the dative-bonding pathway on Ge(100), which is barrierless.

## 6.2. Reaction Mechanisms of Six-Membered Aromatic Molecules Containing Two Heteroatoms on Si(100) and Si(111)-7×7

Pyrazine (Figure 13d) is a six-membered aromatic molecule containing two nitrogen atoms at two opposite ends of the aromatic ring. Recent studies show that pyrazine can be chemically bound to Si(100) and Si(111)-7×7 via a [4 + 2]-like addition through binding the two *para*-nitrogen atoms to a Si≡Si dimer on Si(100)[89−91] or a pair of adjacent adatom-rest atoms on Si(111)-7×7.[92] This indicates that the carbon atoms of the ring are not directly involved in any chemical binding with the two surfaces. The two nitrogen atoms of this molecule do not have the same electronic structure and distribution as that of pyridine. However, there is no Si···N dative bond observed for this molecule.

Pyrimidine (Figure 13e) is an isomer of pyrazine. Compared to pyrazine, the two nitrogen atoms are not at opposite positions on the aromatic ring. It has two nitrogen atoms at α and γ positions which have electronic structure similar to that of pyridine. Interestingly, pyrimidine forms a [4 + 2]-like adduct on Si(111)-7×7[93] but a dative-bonded product on Ge(100).[94] The absence of the [4 + 2]-like addition on Ge(100) could be for the same reasons as the absence of the [4 + 2]-like adduct for pyridine on Ge(100).

Notably, the observation of the dative-bonded pyrimidine and the absence of a dative-bonded product for pyrazine on semiconductor surfaces is possibly related to the polarity of the aromatic molecules (Figure 13). The contribution of molecular polarity in the formation of dative bonds with semiconductor surfaces will be discussed in section 11.

## 7. Substituted Aromatic Molecules

Studies of the chemical binding of substituted aromatic molecules to semiconductor surfaces have been carried out with both experimental techniques and theoretical approaches. The studied molecules include chlorobenzene,[95−103] dibromobenzene,[103] N-methylpyrrole,[53,104] toluene,[105] p-xylene,[105] m-xylene,[105] o-xylene,[105] styrene,[106−112] benzoquinone,[113] phenylacetylene,[108,114−117] benzonitrile,[118−122] phenol,[123−125] benzenethiol,[126] 1,4-benzenedithiol,[126] aniline,[66,127−129] 1,4-phenylenediamine,[130] benzoic acid,[128] 4-nitrobenzoic acid,[131] o-benzoquinone,[113] phenylazide,[132,133] benzylazide,[132,134] nitrobenzene,[135] and 1-hexylnaphthalene.[136] In some substituted aromatic molecules, the substituted functional groups significantly shape the reaction channel for their chemical binding on semiconductor surfaces. These substituted aromatic molecules can be categorized on the basis of participation of their functional group in reaction with semiconductor surfaces. The first category comprises molecules reacting only through the phenyl ring; the second is formed of the molecules binding to the surface only through the substituent group; the third category is molecules reacting through both the phenyl ring and the substituent group.

Chlorobenzene is one example of the first category. Due to the inertness of the halogen atom, it bonds to Si(111)-7×7 through a [4 + 2]-like addition mechanism via breaking the aromatic π-conjugation of the phenyl ring.[97] Definitely, the formed product loses its aromaticity. However, the C−Cl bond of chlorobenzene can be selectively broken upon photoirradiation, forming a phenyl radical.[99] This phenyl radical subsequently forms a Si−C bond with an adatom. The single-sigma bonded benzyl on Si(111)-7×7 preserves the original aromaticity of chlorobenzene. Thus, the photoirradiation-assisted selective dissociation is a promising strategy for shaping molecular reaction channels on semiconductor surfaces. Similar to chlorobenzene, N-methylpyrrole can be chemisorbed on Si(111)-7×7 through both [4 + 2]-like and [2 + 2]-like additions, forming multiple products.[71] Toluene,[105] p-xylene,[105] m-xylene,[105] and o-xylene[105] are chemically bonded to Si(100) with a binding mechanism similar to that of benzene. In addition, the C−H bond of the substituted groups of these four methyl-substituted benzene molecules can partially dissociate. On the basis of DFT calculation, benzoquinone was predicted to undergo [4 + 2] and/or [2 + 2]-addition reactions through the unsaturated C≡C bond(s) of the phenyl ring.[113] This is due to the restriction of the geometry of two facing carbonyl groups in a benzoquinone molecule.

Many substituted functional groups such as C≡N, C≡C, N₃, N=O, OH, SH, and NH₂ are reactive for the binding sites of these clean semiconductor surfaces. Some of these substituents can bond to the surface without perturbing the phenyl ring. For example, benzonitrile[118−122] and phenylacetylene[108,114−117] bond to Si(100) and Si(111)-7×7 through a [2 + 2]-like addition at the nitrile and acetylene groups and therefore form a benzoamine-like and styrene-like structure on the surface, respectively. For phenol,[123−125] benzenethiol,[126] aniline,[66,127−129] and 1,4-phenylenediamine,[130] the substituent OH, SH, and NH₂ dissociate on the semiconductor surface and therefore form a phenyl ring-covered organic monolayer. The aromaticity of this category of substituted aromatic molecule remains upon chemical binding of these substituted functional groups. For phenylazide,[132,133] binding to Si(100) occurs through a 1,3-addition followed by nitrogen elimination. However, benzylazide chemisorbs on Si(100) through the favorable 1,2-addition as opposed to 1,3-addition.[132,134] The two adjacent carbonyl groups enforce a *cis* conformation. In contrast to dissociation of these substituent groups, the two adjacent carbonyl groups in an o-benzoquinone molecule are theoretically predicted to react with a Si≡Si dimer through a [4 + 2]-addition mechanism.[113] This [4 + 2] cycloaddition at the two adjacent carbonyl groups is thermodynamically favorable. The adsorption energy of such a [4 + 2]-addition is almost twice that of [2 + 2]-addition at a carbonyl for this molecule. This is understandable since this reaction forms an aromatic ring in the [4 + 2]-addition. In addition, similar to 1,3-butadiene, the [4 + 2]-addition at the two carbonyl groups is kinetically favorable compared to the [2 + 2]-addition.[113]

For some substituted aromatic molecules, the functional groups react with the semiconductor surface, as does the associated phenyl ring. For example, the ethylenyl group of styrene and its conjugated phenyl ring both react with an adatom and adjacent rest atom pair, forming a 5-ethylidene-1,3-cyclohexadiene-like skeleton on Si(111)-7×7.[108] Definitely, the product of this category of aromatic molecule loses its original aromaticity upon adsorption.
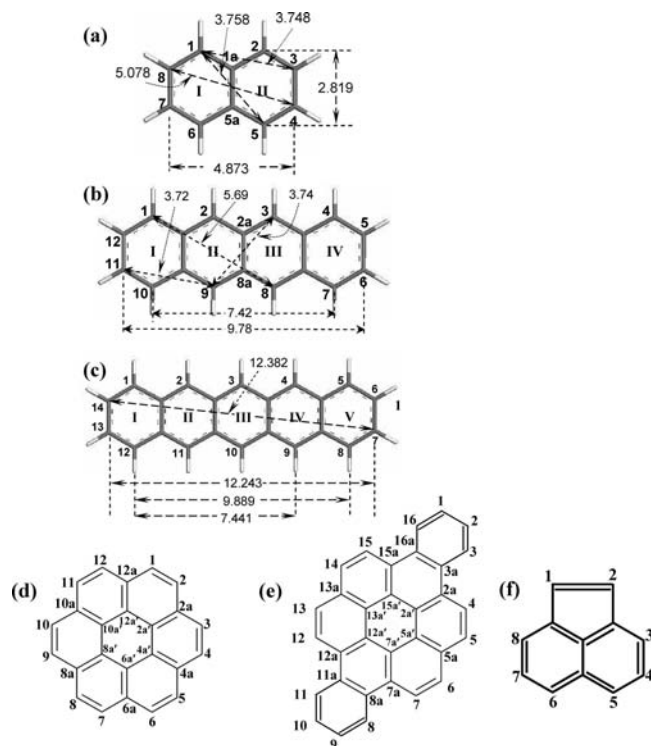
**Figure 15.** Molecular structures of naphthalene (a), tetracene (b), and pentacene (c), coronene (d), dibenzo[*a,j*]coronene (e), and acenaphthylene (f).

## 8. Polycyclic Aromatic Hydrocarbon Systems

The chemical attachment and growth of thin films of polycyclic aromatic hydrocarbons comprised of one or more fused benzene rings on semiconductor surfaces has attracted much attention, as some acene-series hydrocarbons have been successfully employed for device fabrication. This class of molecules exhibits promising characteristics for the development of new semiconductor devices such as organic field effect transistors (OFETs) due to the relatively high carrier mobility of the organic layer. This category of molecule includes naphthalene, tetracene, pentacene, coronene, dibenzo[*a,j*]coronene, and acenaphthalene as shown in Figure 15. The carbon atoms of these molecules are labeled in Figure 15. These labels will be frequently cited in this section. These molecules exhibit diverse reaction mechanisms on semiconductor surfaces, mainly determined by the electronic and geometric structures of molecules and semiconductor surfaces. Particularly, understanding the intrinsic connection between reaction mechanisms and electronic and geometric structures is extremely important for a controllable growth of organic thin films of those molecules for applications in the development of semiconductor devices, since the charging mobility depends strongly on the molecular orientation, packing, and interaction of the molecules at the device interface.

## 8.1. Polycyclic Aromatic Hydrocarbons on Si(100) and Ge(100)

Naphthalene, consisting of two fused benzene rings, can be considered as the basic system of the acene-series of molecules. Its adsorption and binding configuration were studied with infrared reflection absorption spectroscopy (IRAS) and DFT calculation.[137,138] Similar to benzene, the adsorption of naphthalene on Si(100) exhibits a strong
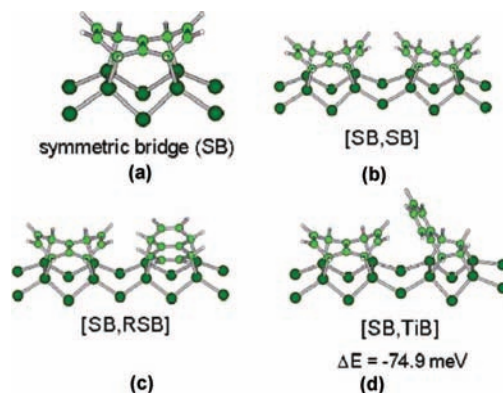


**Figure 16.** Possible binding configurations of naphthalene on Si(100). (From ref 137.)

coverage dependence.[137,138] At low exposure, naphthalene adsorbs on two adjacent dimers in a dimer row with the configuration of a symmetric bridge (Figure 16a), which is the most energetically favorable configuration. In this mode, $C^1$, $C^2$, $C^5$, and $C^6$ carbon atoms of the molecule are bound to the dangling bonds of two adjacent dimers to form four Si−C sigma bonds. However, both MIR-IRAS and DFT calculations suggest that the binding model of the symmetric bridge is not the energetically most stable configuration at high exposure due to the steric repulsion between the hydrogen atoms of the two adjacent molecules in a dimer row, as shown in Figure 16b. Alternatively, the rotated symmetric bridge model (RSB, the model on the right side of Figure 16c) or the tight bridge model (TiB, the model on the right half of Figure 16d) is energetically favorable due to a smaller steric repulsion with its adjacent molecule in a dimer row (Figures 16c and 17d). Thus, the binding of naphthalene at high exposure results in multiple configurations including a symmetric bridge, a rotated symmetric bridge, and a tight bridge (Figure 16).

There are no results reported on the detailed binding configuration of anthracene on the clean Si(100) surface, though its chemical adsorption on Si(111) has been studied.[139]

The chemical binding of tetracene on Si(100) was studied recently.[140,141] Both STM studies and theoretical calculations revealed two binding configurations (A and B in Figure 17a), in which Si−C covalent bonds are formed. For both of the two configurations A and B, tetracene is flat lying on the surface. In configuration A, the long axis of the bonded molecule is perpendicular to the dimer row. Two carbon atoms in each of the inner aromatic rings ($C^2$, $C^3$, $C^8$, and $C^9$) bond to two underlying Si=Si dimers, forming four Si−C bonds (left-bottom panel of Figure 17c). This binding is described as a so-called [2 + 8 + 2] addition.[140,141] In the formed products, rings I and IV maintain aromaticity upon chemical binding to Si(100). In configuration B, the molecular long axis is parallel to the dimer row. Only the two central carbon atoms ($C^{2a}$ and $C^{8a}$) participate in the chemical binding with one underlying Si=Si dimer, forming two Si−C sigma bonds (site B in Figure 17c). Due to the rehybridization of the two bonded carbon atoms, the two sides of the $C^{2a}$−$C^{8a}$ bond are significantly bent from the original planar structure. In configuration B (the right-bottom structure in Figure 17c), rings I and II (or rings III and IV) contain eight π-electrons. Thus, this product loses its original aromaticity. Although a third adsorbate (type C in Figure 17b) is indicated by the empty state STM image,[140,141] its binding configuration is still uncertain.
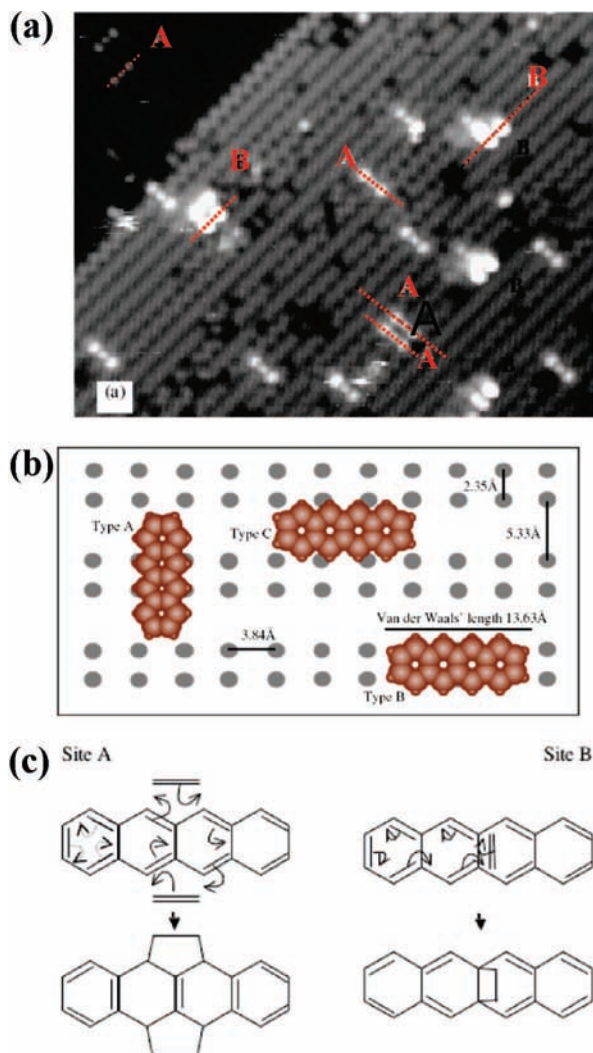
**Figure 17.** (a) Occupied state STM image of tetracene on Si(100). Two types of bright features can be distinguished. Feature A is a tetracene molecule perpendicular to the Si dimer rows, while B corresponds to a tetracene molecule on top of the Si dimer rows. (b) Schematic of the adsorption sites for tetracene on Si(100) based on STM images: type A, the molecular long axis is perpendicular to the dimer rows; types B and C, the molecular long axis is parallel to the dimer rows. (c) Mechanisms of molecular addition reaction at binding sites A and B. (From ref 140.)

Pentacene is a planar molecule containing five fused benzene rings. The chemisorption of this molecule on Si(100) and the growth of thin films on this substrate have been well studied by using several experimental techniques and theoretical calculations.[142−150] These investigations show that pentacene chemisorbs on Si(100) with Si−C covalent bonds through an addition reaction mechanism,[142−144,146] though a limited amount of dissociation through breaking C−H bonds was also observed.[145] STM studies[151] show that the plane of the adsorbates is parallel to the silicon surface. Four major binding configurations were revealed as shown in Figure 18. They include A1 (on top of the dimer row), IB (in between two adjacent Si dimer rows), and B1 and B2 (perpendicular to a Si dimer row). In addition, four minor configurations which occupied ∼5% of the surface were also observed. Figure 19 represents the STM images and the calculated adsorption structures of the four major binding sites. DFT calculations[143,151] show that the binding energies of A1, IB, B1, and B2 are 104.5, 67.1, 127.8, and 100.7 kcal/mol, respectively. Studies of the near edge X-ray absorption fine
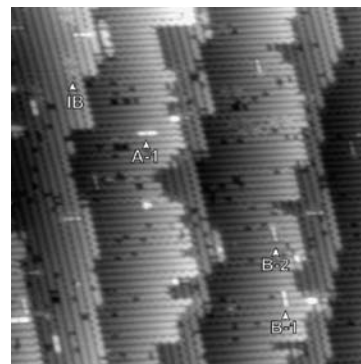


**Figure 18.** Large-scale STM image of Si(100) with chemisorbed pentacene. (From ref 151.)

structure (NEXAFS) spectra at the carbon K-edge[144] show that the chemisorbed molecules are flat-lying on the surface and the physisorbed molecules have an upright molecular orientation. In multilayer thin films, molecules are weakly physisorbed via van der Waals interactions and the angle between the molecular plane and the Si(100) surface is 76 ± 2°.

Different from the above three acenes consisting of more than one fused benzene ring arranged linearly, coronene contains seven fused benzene rings which are arranged as a hexagonal structure (Figure 15d). The free molecule has $D_{6h}$ symmetry. It adopts a $\gamma$ packing containing herringbone and stacking geometries[152] to form a 3-D crystal structure. The 3-D coronene is an important photoilluminator for green light. It is also a new material with promising applications in semiconductor device technologies. Thus, its surface chemistry on Si(100) has been investigated.[153] On a clean Si(100) surface, it forms a major product (with a population of ∼75%) of on-top binding mode (Figure 20a) and two minor modes formed in between two adjacent dimer rows (Figure 20b and c). For the adsorption site on-top of a dimer row, it forms four Si−C sigma bonds with two adjacent dimers in a dimer row. The two minor modes are called type-C-assisted adsorption, which involves dissociation of one water molecule near the two binding configurations.

Figure 20a shows STM images and binding configurations of the on-top binding mode. Four carbon atoms at the two ends of the molecule along any $C_3$ axis of this molecule ($C^1$, $C^2$, $C^7$, and $C^8$), as shown in Figure 20a2 and a3, participate in this binding. DFT calculations suggest that the adsorption energy of this tetrasigma on-top binding mode formed along dimer rows is 24.6 kcal/mol.[153] In this binding configuration, due to the rehybridization of the four carbon atoms ($C^1$, $C^2$, $C^7$, and $C^8$) in the front and back benzene rings of coronene, the bonded molecule loses its original planarity and forms a saddle-like structure. In this adsorbate two separated naphthalene-like structures have aromaticity. The two minor adsorption sites (Figure 20b and c) are defect-assisted sites. Figure 20b2 and b3 are structural modes of one binding configuration associated with the dissociation of one water molecule. The adsorption energy of this mode is calculated to be 24.2 kcal/mol, which is similar to that of the on-top binding mode.[153] In this mode, the molecule also forms four Si−C sigma bonds with Si(100). Compared to the on-top binding mode, these bonds involve dangling bonds of two adjacent dimer rows. The third binding mode (Figure 20c) is also associated with a type-C defect and two adjacent dimer rows. Its binding energy is 32 kcal/mol from a DFT calculation.[153] For all three binding modes, the formation of
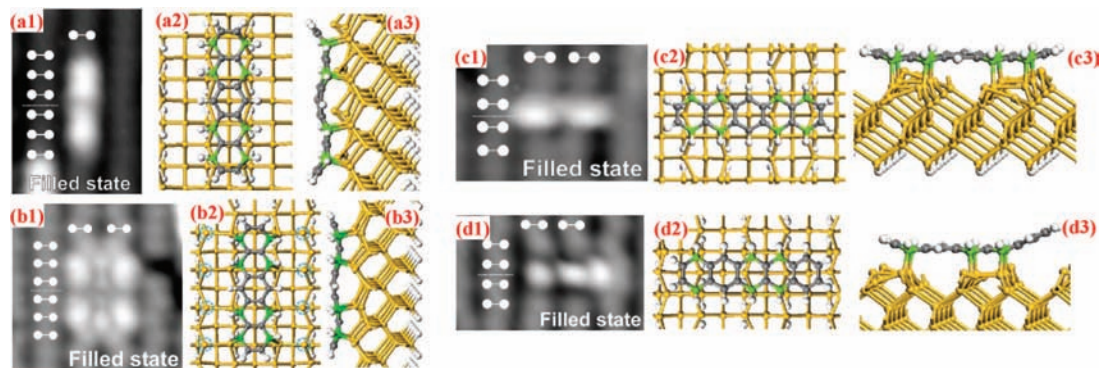
**Figure 19.** Comparison of experimental STM images of pentacene on silicon (100) with the computed adsorption sites. a1, b1, c1, and d1 are experimental STM images of binding configurations of A1, IB, B1, and B2, respectively. a2, b2, c2, and d2 are the top views of the calculated binding configurations. a3, b3, c3, and d3 are side views of the calculated binding configurations. (From ref 151.)
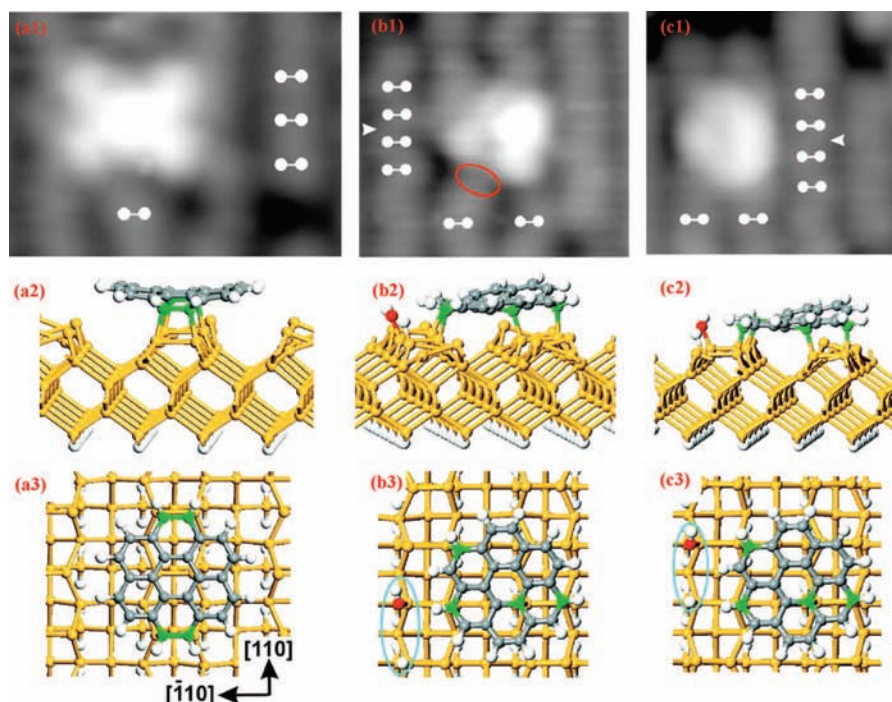


**Figure 20.** STM images and calculated binding configurations of coronene on Si(100). (a1) STM images of the on-top binding mode. (a2 and a3) Side view and top view of the theoretically calculated atomic configurations of coronene adsorbed with the on-top mode. (b1) One STM image of the minority species of adsorbed coronene on a defect-assisted adsorption site in between dimer rows. (b2 and b3) Side view and top view of the theoretically calculated atomic configurations of coronene adsorbed on a defect-assisted adsorption site in between dimer rows. (c1) One STM image of the minority species of adsorbed coronene on another defect-assisted adsorption site in between dimer rows. (c2 and c3) Side view and top view of the theoretically calculated atomic configurations of coronene adsorbed on another defect-assisted adsorption site in between dimer rows. Compared to the binding configuration in part b, the binding site of the OH group is different in this binding configuration (c). (From ref 153.)

four Si–C sigma bonds results in the loss of $\pi$ character in some phenyl rings and thereby makes the molecule adopt a nonplanar structure. Compared to the adsorbate formed on defect-free sites (Figure 20a), only one naphthalene-like structure remains in the minor modes (Figure 20b and c) and makes the two defect-assisted adsorbates to have aromaticity to some extent.

Dibenzo[$a,j$]coronene is another polyaromatic molecule (Figure 15e). It can be considered as a derivative of coronene or of pentacene. This molecule exhibits quite different binding chemistry on Si(100). Three binding configurations (*I*, *II*, and *III*) were revealed with STM and electronic structure calculations.[154] Figure 21a shows the filled state STM image and the calculated structure of this binding configuration *I*. In this configuration (*I*), six covalent chemical bonds are formed between carbon atoms (four $C^2$ and

two $C^4$ atoms) in the phenyl rings on the two ends of the molecular long axis and Si atoms on the substrate with a binding energy of 26.2 kcal/mol. STM studies show this is the dominant binding configuration. Figure 21b presents the filled state STM image and calculated binding configuration of the binding structure *II*. It also forms six Si–C sigma bonds at four $C^2$ and two $C^4$ atoms with a binding energy of 37.5 kcal/mol. Compared to structure *I*, the higher binding energy of structure *II* could result from less strain due to bending of the molecule along the long molecular axis than that of structure *I*. Another structural factor for the relatively high binding energy in configuration *II* is the outward convex profile along the short molecular axis in configuration *II*, in contrast to an outward convex profile along the long molecular axis in binding configuration *I*. The filled state STM image and the calculated binding structure of config-
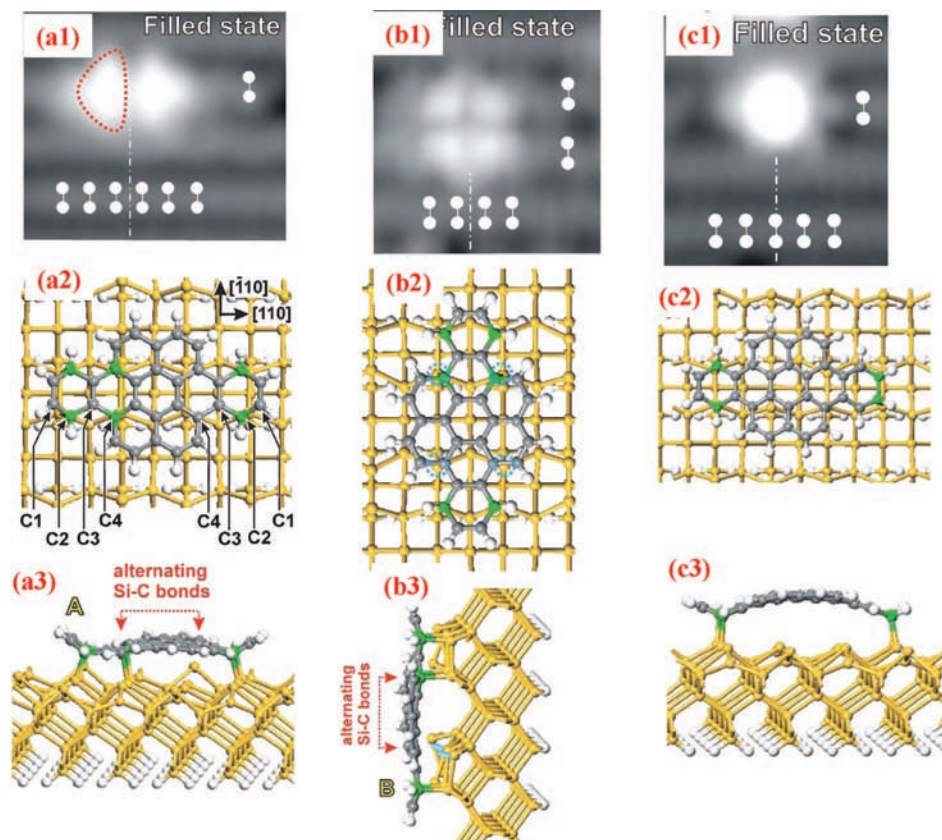
**Figure 21.** STM images and calculated binding configurations of dibenzo[$a,j$]coronene on Si(100). (a1) Filled state STM image of binding configuration *I*. (a2 and a3) Top view and side view of the theoretically calculated structure of binding configuration *I*. (b1) Filled state STM image of binding configuration *II*. (b2 and b3) Top view and side view of the theoretically calculated structure of binding configuration *II*. (c1) Filled state STM image of binding configuration *III*. (c2 and c3) Top view and side view of the theoretically calculated structure of binding configuration *III*. (From ref 154.)

uration *III* are shown in Figure 21c. Different from configurations *I* and *II*, this structure forms only four Si−C bonds at two $C^1$ and two $C^2$ atoms in configuration *III*. Thus, the molecule in this configuration has a much smaller binding energy of 17.7 kcal/mol in contrast to configurations *I* and *II*.

Compared to the above five molecules consisting of fused benzene rings, acenaphthylene includes two fused benzene rings and one cyclopentadienyl ring (Figure 15f). To some extent, it is a fusion of a naphthalene molecule and a cyclopentadienyl ring. It can be considered as a precursor of a more extended fullerene or nanotube. Thus, the experimental studies[155] and DFT calculations[156] of the adsorption of this molecule on Si(100) could provide clues for understanding chemisorption and immobilization of extra large aromatic organic systems such as buckyballs ($C_{60}$) and carbon nanotubes. Both STM and FT-IR studies[155] revealed a high selectivity in chemical binding of this molecule on Si(100). The 1,2-alkene group of the cyclopentadienyl ring ($C^1$ and $C^2$ in Figure 15f) chemically binds to a Si=Si dimer, therefore forming a monolayer with the naphthalene structure perpendicular to the surface. The DFT calculations[156] on the basis of several potential binding configurations show that the product formed through a [2 + 2]-like reaction at the 1,2-alkene unit is the most thermodynamically stable with an adsorption energy of ∼37 kcal/mol. In addition, the formation of this product is also kinetically favorable. Selected isotopic labeling studies using FTIR[155] show that the aromaticity of this molecule is preserved upon chemical binding (Figure 22). The homogeneous monolayer formed on Si(100) is a stable, uniform organic monolayer with a
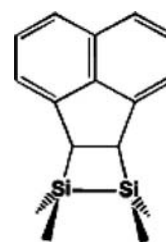


**Figure 22.** Binding configuration of acenaphthylene on Si(100) through a [2 + 2]-like addition at a 1,2-alkene group to form a four-membered $Si_2C_2$ ring. (From ref 155.)

single aromatic product, which may be used as a good precursor for the formation of an ordered and monodispersed organic multilayer architecture. It is a model system for developing a strategy to chemically bind more complex π-systems to semiconductor surfaces for further functionalization and modification.

## 8.2. Polycyclic Aromatic Hydrocarbons on Si(111)-7×7

### 8.2.1. Naphthalene on Si(111)-7×7

Naphthalene is two linearly fused benzene rings. Both STM studies and DFT calculations[157] suggest that naphthalene chemisorbs on Si(111)-7×7 mainly through the formation of two covalent bonds between $C^1$ and $C^6$ of ring I or the equivalent $C^2$ and $C^5$ of ring II and a neighboring adatom and rest atom pair. Figure 23a is the STM image of the chemisorbed naphthalene on Si(111)-7×7. Figure 23b1, b2, b3, and b4 schematically present the four different binding
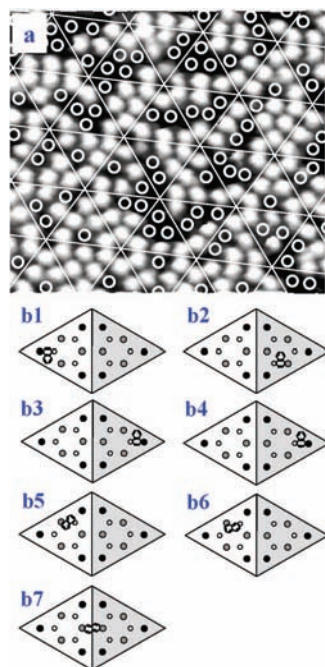
**Figure 23.** (a) STM image of Si(111)-7×7 exposed to 0.09 L of naphthalene. The superimposed white lines mark out individual half unit cells, and each circle indicates a missing adatom. Parts b1, b2, b3, b4, b5, b6, and b7 correspond to binding configurations A1, A2, A3, A4, B, C, and D of naphthalene on Si(111)-7×7.



**Figure 24.** (a) Aromatic sextet of a free naphthalene represented by the circle in ring I. This aromatic sextet is shared via movement of two $\pi$ electrons (symbolized by the arrow) according to Clar's sextet concept. (b) Disigma reaction at ring II of naphthalene on Si(111)-7×7 through binding configuration A produces one sextet in the resulting structure. Sigma binding at both rings I and II of naphthalene results in configurations B in part c, C in part d, and D in part e on Si(111)-7×7, which contains conjugated double bonds but no sextet.

sites of naphthalene with disigma binding at the $C^1$ and $C^6$ atoms of the same ring. The four possible binding sites (Figure 23b1, b2, b3, and b4) correspond to configuration A in Figure 24. In addition, three minor disigma models involve $C^1$ and $C^5$ in configuration B, corresponding to Figure 23b5, $C^1$ and $C^3$ in configuration C, corresponding to Figure 23b6, and $C^4$ and $C^8$ in configuration D, corresponding to Figure 23b7, respectively. DFT calculation shows that disigma binding configuration A at $C^1$ and $C^6$ (Figure 23b1, b2, b3, and b4) and disigma binding configurations B (Figure 23b5), C (Figure 23b6), and D (Figure 23b7) have binding energies of 29.1, 27.9, 28.2, 29.9, 13.5, 18.0, and 25.3 kcal/mol, respectively. Binding configuration A has an asymmetric folded structure with an isolated benzene ring not involved in the surface binding. This unreacted aromatic ring has a planar structure so as to enhance the overlapping of the $\pi$-orbital and in turn its aromaticity. On the other hand, theoretical calculations suggest that disigma addition at the ring fused carbon atoms ($C^{1a}$ and $C^{5a}$) with an adatom–rest atom pair on Si(111)-7×7 is thermodynamically unfavorable. A possible explanation for the inertness of the ring fused carbon atoms could be their high steric rigidity due to their strong covalent binding with three adjacent carbon atoms in contrast to the nonfused carbon atoms binding to two neighboring carbon atoms and one hydrogen atom.

Calculations show that configuration A has a higher adsorption energy than the other three binding modes B, C, and D. The difference in adsorption energy of these binding configurations can be well understood by utilizing Clar's sextet concept.[158,159] Figure 24 shows the aromatic $\pi$-conjugation in a free naphthalene molecule and the bonded adsorbates with different configurations. Obviously, only configuration A maintains one aromatic sextet. The preservation of the resonance energy due to the aromatic sextet in configuration A definitely contributes to its extra stability in contrast to other configurations. On the other hand, from the
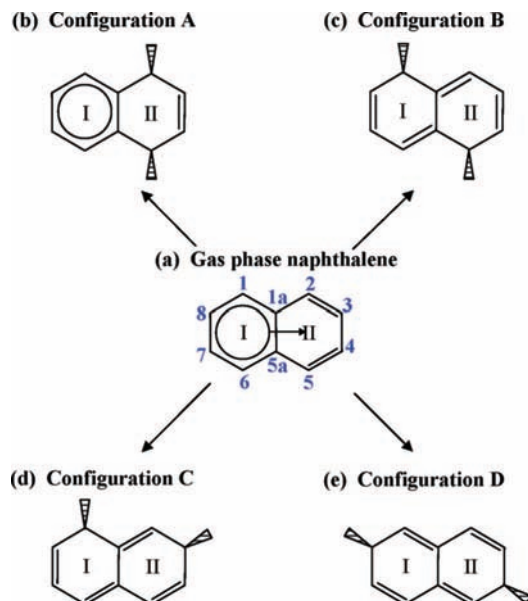
view of kinetics, the existence of one or more binding configurations depends on the relative formation activation barriers. Although there is no kinetic data available in experimental studies and theoretical calculations, it is expected that the formation of configurations B, C, and D would have a high activation barrier due to the energy required for the extended conjugation of the aromatic $\pi$ system to form a twisted or deformed structure. Thus, it is proposed that configuration A is the major product of naphthalene chemisorption on Si(111)-7×7.

Statistical studies of several large-scale STM images of the reacted Si(111)-7×7 surface show that the most reactive site is the center adatom on the faulted half unit cell.[157,160] The reactivity of the corner adatom of faulted halves and that of the center adatom of the unfaulted half are comparable. At high exposure, the corner adatoms of faulted halves have a lower reactivity in contrast to that at low exposure. Overall, the multiple reactive sites of the Si(111)-7×7 have different reactivities for naphthalene, similar to the case for benzene, as discussed in section 3.2. This suggests that naphthalene, with a larger size than benzene, does not significantly modify the reactivity of the various reactive sites on Si(111)-7×7.

### 8.2.2. Anthracene on Si(111)-7×7

The adsorption and growth of anthracene thin films on Si(111)-7×7 was studied using photoemission electron microscopy (PEEM).[139] The binding configuration of this molecule was not studied, but the molecular orientation in the thin film deposited on Si(111)-7×7 was examined. In the monolayer, molecules are lying flat. However, for the second layer in terms of the first physisorbed layer, molecules are standing up on the chemisorbed monolayer due to the absence of strong interactions between the physisorbed layer and the chemisorbed layer.
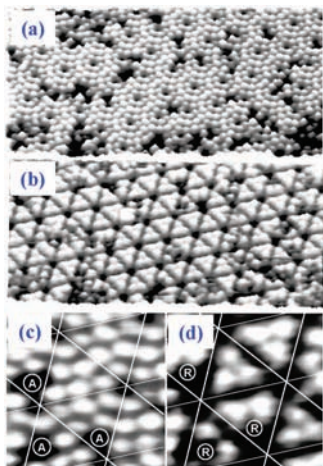
**Figure 25.** STM images of unoccupied states (a) and occupied states (b) of the chemisorbed tetracene on Si(111)-7×7. The corresponding high resolution images are shown in parts c and d. The image in part b is obtained by scanning the same area of image a with negative bias. The image in part d is obtained by scanning the *same* area of images c with negative bias. The high resolution images show simultaneous disappearance of adatoms (labeled A in part c) and rest atoms (labeled R in part d) that are adjacent to each other. This is a clear evidence for the participation of both adatom and rest atom in binding with tetracene.

### 8.2.3. Tetracene on Si(111)-7×7

Compared to naphthalene, tetracene has a more complicated structure and more categories of nonfused carbon atoms. Figure 25 shows the STM images of Si(111)-7×7 following exposure to tetracene molecules.[161,162] Both experimental and theoretical studies show that the most reactive carbon atoms of tetracene for [4 + 2]-like addition with Si(111)-7×7 are the *meso* carbons of the inner rings (namely $C^2$ and $C^9$ or the equivalent $C^3$ and $C^8$) in Figure 15b. Again, this can be rationalized qualitatively with Clar's sextet definition.[158,159] A free tetracene molecule (gas phase) is a $\pi$ system sharing a single aromatic sextet having six $\pi$ electrons (Figure 26a). Figure 26a shows the sextet of tetracene represented as a circle in the ring, which is mobile within the molecule through the movement of two $\pi$ electrons as symbolized by the arrow. Notably, an addition reaction at an inner ring forms a product with two sextets (rings I and III) located on both sides of the reacted ring (Figure 26b), whereas a reaction at the outer ring (ring I or IV) results in only one sextet which is shared among the remaining three unreacted rings (Figure 26c). Therefore, the binding at the inner ring ($C^2$ and $C^9$) is the major reaction channel due to its high binding energy. This binding forms a symmetric butterfly structure (configuration A in Figure 26b). Such a structure enhances the overlap of the $\pi$-orbitals and in turn the aromaticity on both sides of the reacted ring (Figure 26b). It is proposed that tetracene uses the fused carbon atoms ($C^{2a}$ and $C^{8a}$) to bind to a Si=Si dimer of Si(100) on the basis of STM studies.[140,141] However, DFT calculations show that such binding at $C^{2a}$ and $C^{8a}$ with an adatom and its adjacent rest atom on Si(111)-7×7 is definitely not thermodynamically favorable.[161] This is consistent with theoretical studies on the binding of naphthalene on Si(111)-7×7,[157] which shows that disigma covalent binding at two fused carbon atoms is thermodynamically unfavorable. The fused carbons are much more rigid and are expected to be more resistant toward transformation from the planar $sp^2$ to the tetragonal $sp^3$ hybridization.
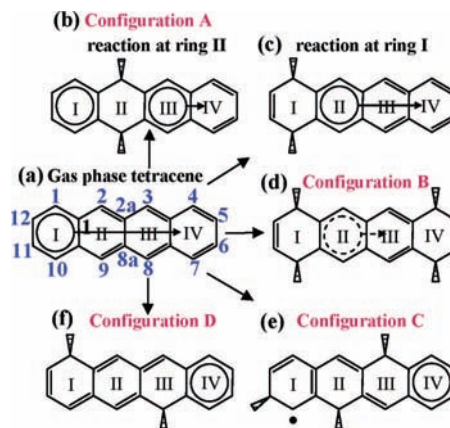


**Figure 26.** (a) Sharing of an aromatic sextet (represented by the circle in ring I) within a free tetracene molecule via movement of two $\pi$ electrons (symbolized by the arrow) according to Clar's sextet concept. Disigma reactions at ring II (b) and ring I (c) of tetracene produce two and one sextet in the resulting structures, respectively. (d) Loss of aromatic sextet due to nonplanar structure in configuration B of tetracene on Si(111)-7×7. (e) Tetracene in configuration C contains a radical site and possibly a sextet at ring IV. (f) Reactions at rings I and III in configuration D result in isolation of a sextet to ring IV.

In contrast to benzene[43] and naphthalene,[157] each half unit cell of Si(111)-7×7 only accommodates one tetracene due to the large size of this molecule. In principle, the disigma binding mode at $C^2$–$C^9$ or $C^3$–$C^8$ (configuration A in Figure 26) only results in the disappearance of one adatom in each half unit cell. However, in some half unit cells, two center adatoms disappear simultaneously as observed in STM images (Figure 27a). Such an observation is due to tetracene bonded to Si(111)-7×7 with the structure indicated as configuration B (Figure 26d). DFT calculation[161] shows that the binding configuration B stems from the binding of $C^1$–$C^{10}$ of ring I and $C^4$–$C^7$ of ring IV to two adjacent pairs of center adatom–rest atoms as the separation between $C^1$ and $C^4$ on tetracene (7.42 Å) is comparable to the separation of 7.68 Å between two adjacent center adatoms.[163,164] The calculated adsorption energy of the binding mode (configuration B) is ~54.6 kcal/mol, which is larger than that of the disigma binding mode (configuration A) at $C^1$–$C^{10}$ or $C^4$–$C^7$ by ~11.9–14.2 kcal/mol due to the formation of four Si–C sigma bonds. Figure 27b schematically shows the tetrasigma binding mode (configuration B) of this molecule on half a unit cell.

Notably, it can be observed from Figure 27a,ii that the three neighboring adatoms (marked by the crosses) on an unfaulted half unit cell have greater brightness as compared to the adatoms in the other unfaulted half unit cells that have not been reacted. This increase of charge density on the three adatoms indicates a transfer of charge from the neighboring reacted rest atoms (labeled with two small circles) to the three brighter adatoms (marked with three crosses). This electron transfer is schematically shown in Figure 27c. This is clear evidence for the direct participation of the two rest atoms in reaction with tetracene instead of only a $\pi$ electron interaction between $\pi$-conjugated molecules and dangling bonds on adatoms of Si(111)-7×7. Such a movement of electrons through the backbonds into other adatoms which do not participate in this reaction facilitates the reaction of the rest atoms, via removal of their excess charges to the unreacted adjacent adatoms. The electron transfer from rest atoms to their adjacent unreacted adatoms during the reaction with tetracene (Figure 27c) is opposite to that from adatom
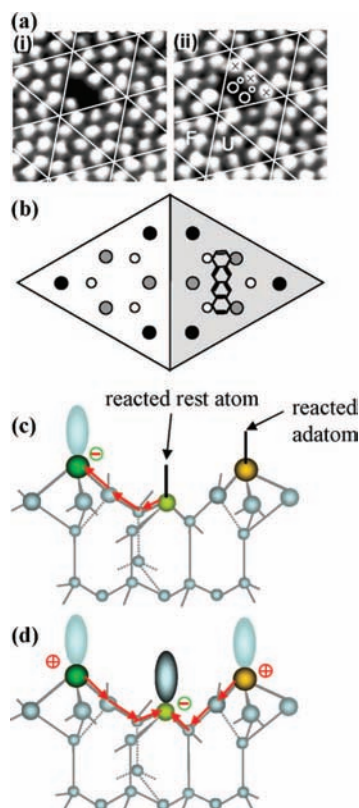
**Figure 27.** STM images (a) and schematic diagram (b) of configuration B of tetracene on Si(111)-7×7. Images i and ii of (a) were obtained at $V_s$ = 1.5 and −1.5 V, respectively, with F and U denoting the faulted and unfaulted half unit cells. (c) Schematic diagram showing electron transfer from a reacted rest atom to its adjacent unreacted adatom. (d) Schematic diagram showing electron transfer from adatom to rest atom during reconstruction for the formation of a clean Si(111)-7×7.

to rest atom during the 7×7 reconstruction of a clean surface (Figure 27d).

An aromatic sextet is formed between rings I and III in the product of binding mode B (Figure 26d). However, the tetrasigma binding configuration shows that rings II and III deviate slightly from the planar structure due to the rehybridization of $C^1$, $C^{10}$, $C^4$, and $C^7$ from $sp^2$ to $sp^3$. This deformation would impede the efficient overlap of the $\pi$-orbitals within the sextet and thereby cause a loss in aromaticity.

Other binding modes such as binding modes C and D were proposed in Figure 26e and f. For example, three C−Si covalent bonds can be formed between $C^{11}$, $C^3$, and $C^9$ in configuration C of Figure 26e and the Si dangling bonds at positions 3, 6, and 1 of Si(111)-7×7 (Figure 28a), respectively. In addition, $C^1$ and $C^8$ of configuration D could bind to two adjacent adatoms at the border of a faulted and an unfaulted half unit cell. However, STM cannot exclusively assign a particular feature to the two binding modes since other binding modes possibly could produce a similar feature.

DFT calculation[161] shows that the tetrasigma bonded molecule (configuration B) located on the unfaulted half unit-cell is slightly more stable than that on the faulted half. This is consistent with Brommer's concept.[165] Based on Brommer's concept of local softness and electronegativity with regard to the relative reactivities of the dangling bonds on Si(111)-7×7, electron donating species prefer to react with the center adatoms on the faulted as compared to the unfaulted half cell. However, the opposite behavior, that is
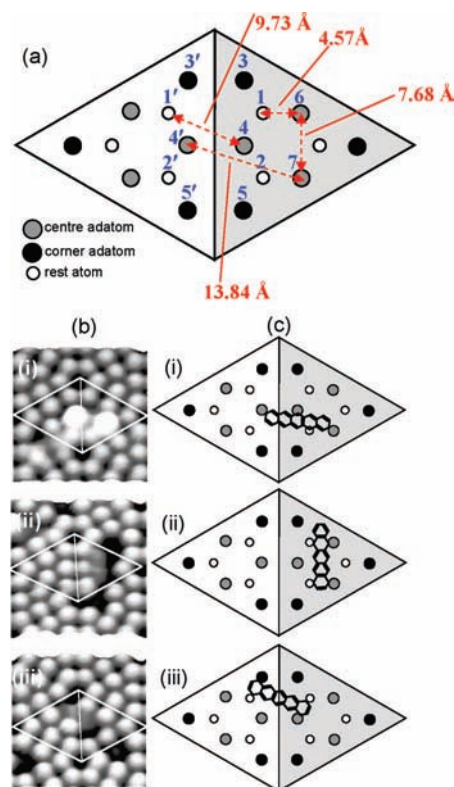
**Figure 28.** (a) Dimensions, in units of angstrom, between various dangling bonds within a single unit cell (whose two different halves are distinguished by the shaded and unshaded triangles) of Si(111)-7×7. Some of the adatoms and rest atoms are labeled, and their locations on the different halves of the unit cell are differentiated by the primed and unprimed labels. (b) STM images ($V_s$ = 2.0 V). (c) Schematics i, ii, and iii showing the configurations of pentacene on a Si(111)-7×7 unit cell for type A, B, and C binding modes, respectively.

the reaction with the unfaulted center adatom, is expected to be observed for electron accepting species. The calculated Mulliken charge difference[161] obtained by subtracting the charge on an isolated tetracene molecule from those adsorbed with binding configuration B on the unfaulted half unit cell shows a charge transfer of ∼0.79 electrons from substrate to adsorbate. This indicates that tetracene is an electron acceptor with respect to Si(111)-7×7.

### 8.2.4. Pentacene on Si(111)-7×7

Although benzene, naphthalene, and tetracene exhibit different binding configurations, all of them have a major binding configuration utilizing two facing carbon atoms on the same phenyl ring, such as $C^2$ and $C^5$ of naphthalene or $C^2$ and $C^9$ of tetracene bound to one adatom−rest atom pair. Compared to these molecules, however, pentacene exhibits a significantly different binding configuration.[166,167] The formation of the unique binding configurations of pentacene possibly results from its larger size. Based on STM results and DFT calculations,[166] three binding configurations (Figures 28c and 29), each involving four C−Si covalent bonds, were revealed by identifying the orientation of pentacene with respect to the underlying substrate. Parts i, ii, and iii of Figure 28b are the observed images of pentacene on Si(111)-7×7 at room temperature corresponding to the three binding configurations A, B, and C in Figure 29. As shown in Figure 29b, configuration A involves a unique engagement of two pairs of adatoms and rest atoms on the surface with four carbon atoms of pentacene ($C^4$, $C^6$, $C^{13}$, and $C^{10}$). This
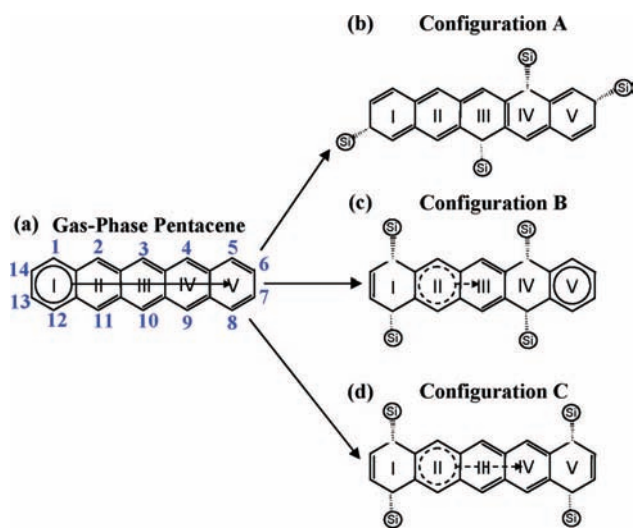
**Figure 29.** (a) Sharing of an aromatic sextet (represented by the circle in ring I) within pentacene via movement of two $\pi$ electrons (symbolized by the arrow) according to Clar's sextet concept. (b) Pentacene in configuration A contains conjugated double bonds but no sextet. (c) Presence of a sextet at ring V of pentacene in configuration B. (d) Aromaticity loss at rings II, III, and IV due to the twisted structure of pentacene in configuration C.

product contains the C=C bonds, but its aromaticity is completely lost. Another configuration B binds to two center adatom–rest atom pairs within a half unit cell (Figures 28b,ii, c,ii, and 29c). The third configuration C is a twisted pentacene structure where the molecule terminally bridges at two oppositely oriented adatom–rest atom pairs that span across the faulted and unfaulted halves of a unit cell (Figures 28b,iii, 28c,iii, and 29d). Each configuration has a few possible binding energies since it may bond to Si(111)-7×7 through a few different binding geometries in terms of the different combination of surface dangling bonds used to attach the molecule.[166] For configurations A, B, and C, they are 57.9–58.6 kcal/mol, 66.6–75.1 kcal/mol, and 50.5–53.9 kcal/mol, respectively.[166]

The three binding configurations result in the adsorbed pentacene species having different electronic structures. STM studies suggest that for configuration A one of the bright spots was located at position 7 of one 7 × 7 unit cell and the other bright spot would appear at either position 4′ or 5′ on the other half of the unit cell (Figure 28b,i and a). These two adatom positions are separated by a distance of 13.84 Å.[163,164] However, in configuration B, the bound molecule appears as a dark feature in the STM image (Figure 28b,ii). The dark feature occupies only half of the 7 × 7 unit cell. Similar to configuration B, pentacene in configuration C also appears as a dark feature, but it straddles the border between the faulted and unfaulted half unit cell (Figure 28b,iii). DFT calculation suggests that $C^{12}$ and $C^1$ of ring I and $C^9$ and $C^4$ of ring IV in configuration B form four C–Si sigma bonds with two adjacent pairs of center adatom–rest atoms at surface dangling bonds 7, 2, 6, and 1 (Figure 28a), respectively. In configuration C, the dark feature in the STM image straddles the faulted and unfaulted halves of the 7 × 7 unit cell and covers a center adatom on one half and a corner adatom on the other half (Figure 28b,iii). Theoretical studies suggest that configuration C involves the formation of covalent bonds between $C^1$ and $C^{12}$ of ring I and $C^5$ and $C^8$ of ring V with two adatom–rest atom pairs located on different halves of a unit cell at surface dangling bonds 3′, 1′, 1, and 4 (Figure 28a), respectively.

Similar to tetracene on Si(111)-7×7, the chemically bound pentacene molecules adopt an orientation nearly parallel to the surface. However, due to the rehybridization of some carbon atoms from $sp^2$ to $sp^3$ and the twist or tilting of some rings, the aromaticity could be weakened or lost. The variation in molecular structure and aromaticity definitely directly contributes to the binding energy. Again, a qualitative approach to compare the binding configuration is to make use of Clar's sextet concept.[158,159] From this concept, only one ring within a free pentacene molecule can be assigned to three conjugated double bonds without duplication and, thus, be considered as an aromatic sextet. The qualitative analysis for the free tetracene molecules and the three binding configurations is shown in Figure 29. In configuration A (Figure 29b), the unique orientation of the four surface dangling bonds participating in the reaction results in a complete loss of the aromatic sextet in the product, though several conjugated double bonds can still be observed. In configuration B (Figure 29c), the two disigma reactions at rings I and IV form the product and thereby isolate the sextet to ring V. In addition, it seems a sextet at ring II can be identified. However, the slight deviation of rings V and II from planarity would impede the efficient overlap of the $\pi$-orbitals within the sextet and therefore cause a loss of aromaticity of configuration B to some extent, though the product of configuration B is aromatic due to at least the existence of aromatic ring V. Compared to configuration A, configuration B has higher stability, as the resonance energy of the aromatic sextet of rings II and V contributes to the stability of the formed adsorbate of configuration B. For configuration C, it seems that a sextet could be shared among rings II, III, and IV in the product. However, the significantly twisted structure of this configuration prevents the proper overlap of the $\pi$ orbitals from taking place and hence destroys the aromatic sextet, which is consistent with the lower binding energy of configuration C in contrast to configuration B.

## 9. Extra Large Aromatic Systems

Fullerene is the third allotrope of elemental carbon.[168–170] Fullerenes are a group of large molecules consisting entirely of carbon atoms. They may exist in the form of a hollow sphere, an ellipsoid, or a tube. Fullerene molecules with the shape of a ball or an ellipsoid are called buckyballs. The ones with the form of a tube are called carbon nanotubes. Their structure, various mechanical, chemical, and physical properties, including their surface chemistry and immobilization on metal, semiconductor, and insulator surfaces, have been extensively studied in recent years due to promising applications in a wide spectrum of technological areas such as new generation semiconductor device technology. Similar to acene-series molecules, fullerenes exhibit aromaticity, as they contain fused benzene rings. Here, these molecules are categorized as extra large aromatic systems. Fullerenes tend to react as electrophiles. In addition, a relief of spatial strain of the bonded carbon atoms with $sp^2$ hybridization by rehybridizing into $sp^3$ is a driving force for the addition reaction between C=C bonds of fullerene and reactive sites of semiconductor surfaces.

The simplest and also the most extensively studied fullerene is $C_{60}$, consisting of 12 pentagonal rings and 20 hexagonal rings as shown in Figure 30. As each fullerene molecule consists of a large number of carbon atoms with different binding nature, their binding chemistry on semi-
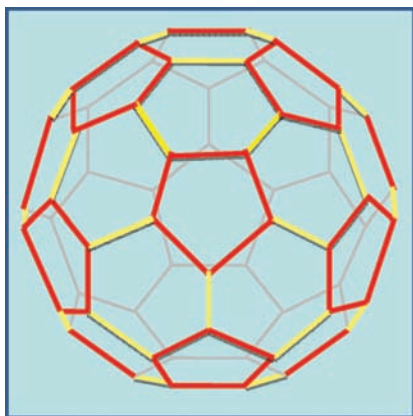
**Figure 30.** Structure of a $C_{60}$ molecule consisting of 20 six-membered rings and 12 five-membered rings. All carbon atoms are $sp^2$ hybridized. Bonds marked with yellow and red are C=C and C—C bonds, respectively.
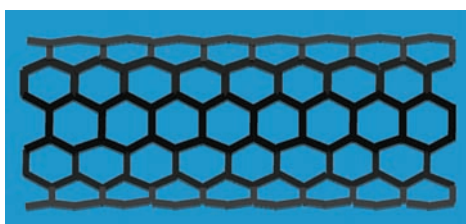


**Figure 31.** Structural model of single-walled carbon nanotubes.

conductor surfaces is quite complicated. Their surface chemistry, particularly their interfacial binding, has been extensively investigated with various experimental techniques including STM,[171−182] PES,[178,183−187] HREELS,[178,186,188] NEXAFS,[185] FT-IR, Raman spectroscopy,[189] and theoretical calculations.[172,190−196] Several surface phenomena such as interfacial charge transfer, chemical reaction, orientational ordering, surface reconstruction, and relaxation upon adsorption of fullerene molecules have been revealed. In addition, the manipulation of fullerene molecules on semiconductor surfaces and on prefunctionalized semiconductor surfaces,[172,173,197−201] and the surface chemistry of heterofullerenes such as $C_{59}Si$,[202] $C_{59}N$,[203] and $C_{60}F_x$[204] were also extensively studied. However, in this section our focus is the electronic and structural factors in the chemical binding of extra large aromatic systems on clean semiconductor surfaces, primarily on Si(100) and Si(111)-7×7. $C_{60}$ will be used as a model molecule to address the chemical binding of fullerenes on semiconductor surfaces.

Carbon nanotubes are another important category of fullerene. Generally, carbon nanotubes have a diameter of a few angstroms to a few nanometers or larger, but their length can be as long as a few millimeters (Figure 31). They can be considered as rolled graphene sheets. They are categorized as single-walled nanotubes (SWNTs) and multiwalled nanotubes (MWNTs). Here the chemisorption of SWNTs will be used as a model for the surface chemistry of carbon nanotubes on semiconductor surfaces.

## 9.1. $C_{60}$ on Si(100)

STM studies[172−182] show $C_{60}$ is adsorbed at the trough between two adjacent dimer rows along the [110] direction without preference to step edge, suggesting a strong bonding between this molecule and Si(100) surface dangling bonds (Figure 32a[179]). The binding chemistry was extensively
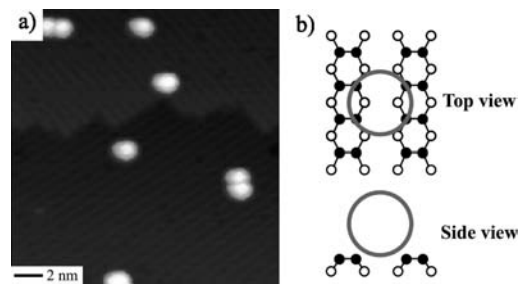


**Figure 32.** (a) STM image of Si(100) with the chemisorbed $C_{60}$ molecules. (b) Top view and side view of the schematics for the chemisorbed $C_{60}$ bonded with four Si=Si dimers between two adjacent dimer rows. (From ref 179.)

studied by PES[178,183−187] and HREELS.[178,186,188] The bonding states between $C_{60}$ and a clean Si(100) surface are clearly identified at 2.4 eV in the valence band spectra.[178,186] The shift of binding energy of the molecular orbital and the C 1s core-level spectra indicate a significant charge transfer from the silicon surface to $C_{60}$ molecules. Similar to the calculated charge transfer (0.79 eV) from Si(111)-7×7 to the chemisorbed tetracene,[161] these studies suggest that buckyball is an electron acceptor. At low coverage, $C_{60}$ molecules adsorb predominately at a four-dimer site in the trough between two adjacent dimer rows (Figure 32b). At a coverage of 1 ML, 75% of $C_{60}$ molecules are physisorbed and 25% chemisorbed.[185] NEXAFS studies further show that the character of chemisorption of $C_{60}$ on Si(100) is covalent and LUMO+1 contributes to this binding.[185] At 1.0 ML, the adsorbed molecules form a thin film with a C(4×4) and (4×3) superlattice on the Si(100) surface.[179] At higher coverage such as 5 ML, the molecules in the multilayer of this film have the same packing as those of bulk $C_{60}$.[179] The $C_{60}$ molecule in each layer has weak van der Waals interactions with their adjacent layers, and the molecules adopt a hexagonal stacking mode similar to the bulk $C_{60}$.

Calculations using *ab initio* total energy minimization studied the possible structures of $C_{60}$ on Si(100).[194,195] These calculations show that the $C_{60}$ molecule bonds to Si(100) through breaking four C=C bonds. One $\pi$ electron from each broken C=C bond forms a Si—C bond with a dangling bond of this silicon surface. The second $\pi$ electron from each broken C=C bond forms a new $\pi$ bond within the molecular cage. Rebonding takes place within the $C_{60}$ molecule so that no extra $\pi$-radical is left upon breaking four C=C bonds and forming four Si—C bonds. The four Si—C bonds are primarily covalent with some charge transfer, consistent with experimental findings.

Notably, the binding energy for $C_{60}$ and Si(100) is ~47.6−66.8 kcal/mol.[194] The aromaticity of $C_{60}$ is expected to remain upon chemical binding on Si(100). Thus, the chemical binding of four surface silicon atoms to a small portion of the whole $C_{60}$ molecule does not significantly change its original aromaticity.

## 9.2. $C_{60}$ on Si(111)-7×7

Extensive studies have been carried out on the adsorption of $C_{60}$ molecules on Si(111)-7×7.[171,177,178,182,186,187] Compared to Si(100), the adsorption of $C_{60}$ on Si(111)-7×7 exhibits more complicated behavior. This stems from the fact that Si(111)-7×7 consists of multiple surface sites with different electronic and geometric structures. STM studies[171] show there exist two types of binding configurations (Figure 33a) at a low coverage (<1 ML). One is called a "large" molecule
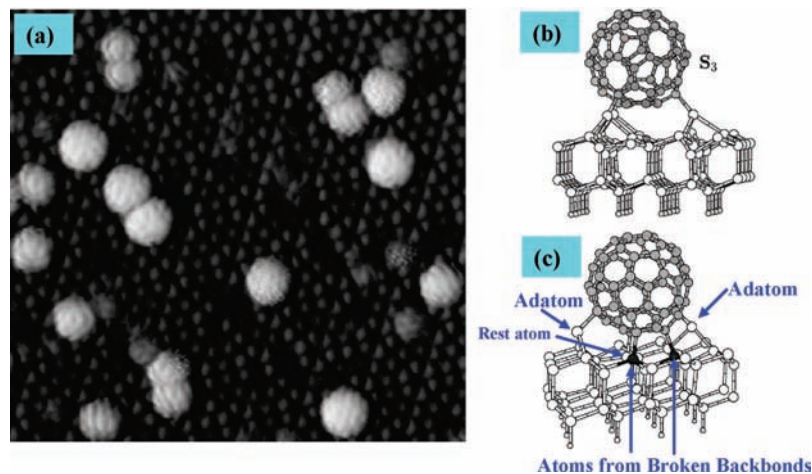
**Figure 33.** (a) STM image of Si(111)-7×7 with chemisorbed $C_{60}$ molecules. (From ref 171.) (b) One binding configuration of $C_{60}$ on Si(111)-7×7, labeled as S3, in which the molecule maintains the 3-fold symmetry of the substrate. This binding configuration corresponds to the so-called "large" molecule in STM images. (From ref 196.) (c) The most stable structure revealed in calculations. In this binding mode, two of the adatoms have broken their bonds with corresponding pedestal atoms highlighted as bold features. Thus, two extra Si—C bonds are formed with $C_{60}$. It corresponds to the "small" molecule in the STM image. (From ref 196.)

which has an apparent height of ~0.6 nm and width of ~2.0 nm in the STM image and appears more round and fuzzy. The other is called a "small" molecule which has a height of ~0.5 nm and width of ~1.5 nm in the STM image. The "small" molecule presents a more discernible internal structure and a large variety of shapes. DFT calculations[196] suggest two binding modes for the observed "large" and "small" molecules (Figure 33b and c).

The calculated structure of the "large" molecule bonds to three adatoms of this surface as shown in Figure 33b. Upon relaxation, the carbon atoms remain in their original positions and the molecule preserves a spherical shape. However, the height of this molecule over the substrate decreases from 5.9 to 5.35 Å. Notably, the three adatoms bonded to the $C_{60}$ molecule move up significantly toward the $C_{60}$ molecule by ~1.0 Å. The rest atom close to the molecule and pedestal atoms move down by 0.61 Å and up by 0.08 Å, respectively. This relaxation increases the binding energy to 94.4 kcal/mol.

Figure 33c is the binding configuration of the "small" molecule from theoretical simulation. Its height over the substrate is only 4.56 Å. The molecule occupies almost a bridge position between two adatoms. One Si—Si backbond of each adatom is broken to form an extra Si—C bond with the $C_{60}$ molecule. Thus, the "small" molecule is bonded to the surface through five Si—C bonds, including two with adatoms, two with silicon atoms formed by breaking the Si—Si backbonds of the two adatoms, and one with the rest atom. This relaxed structure has a higher binding energy of 151.4 kcal/mol.

Obviously, the structural relaxation substantially impacts the adsorption energy of $C_{60}$ at different sites. In addition, this calculation shows a significant charge transfer from the silicon surface to $C_{60}$ upon chemisorption, consistent with the charge transfer revealed by HREELS[178,186] and valence bond spectroscopy.[178,186] The calculated charge transfer is 0.94−1.13e,[196] depending on different binding sites. A similar charge transfer from Si(111)-7×7 to tetracene[161] and Si(100) to $C_{60}$[178,186] has also been observed. This charging of the $C_{60}$ molecule stems from the hybridization of the molecular orbital and surface state instead of an occupation of the initially unoccupied state of the $C_{60}$ molecules. NEXAFS studies[185] show that 75% of the molecules physisorb and 25%

chemisorb on Si(111)-7×7 at 1.0 ML as on the Si(100) surface. At a higher exposure, intermolecular interactions play an important role in the adsorption.

## 9.3. Carbon Nanotubes on Si(100)

Carbon nanotubes can exhibit either metallic or semiconducting behavior depending on the diameter and helicity of the tube. It is a very promising material to be applied to electronic and optoelectronic devices. However, one crucial technological problem to be solved before applying them in the semiconductor industry is the integration with conventional semiconductor platforms. Although some experimental studies have been carried out for the parallel assembly of carbon nanotubes to hydrogen-passivated silicon surfaces,[184,197,198,205] and perpendicular assembly of carboxylic acid-functionalized carbon nanotubes on HO-passivated silicon surfaces,[206] the interfacial chemistry between carbon nanotubes and clean semiconductor surfaces is not clear so far. In fact, there is no experimental result reported on the interfacial chemistry between carbon nanotubes and silicon surfaces.

Theoretical calculations[190−192] investigated the nature of the interfacial interactions between carbon nanotubes and Si(100) and the modification of electronic properties through the chemical binding of carbon nanotubes. For the chemical binding of metallic nanotubes on Si(100), a (6,6) carbon nanotube with a diameter of 8.2 Å consisting of 72 atoms was selected as a model to study.[191] The trench site (binding between adjacent dimer rows) and on-top site (on the top of a silicon dimer row) were considered. The most stable configuration is the trench site without tilting (the long axis of the carbon tube is parallel to the direction of the dimer row). Figure 34a is the calculated binding configuration of the nanotube. The binding energy per unit length of the carbon nanotube is calculated to be 5.9 kcal/mol per angstrom. Upon this binding, the relative tilting between two adjacent dimers in a dimer row is reduced to 9° from the original 19° at alternate dimers on a clean Si(100) surface. This adsorption-induced distortion implies the formation of Si—C chemical bonds at the interface of the carbon nanotubes and the dimer row. The binding energy of the carbon nanotube on the trench site is decreased to 3.57 kcal/mol per Å if the aligned angle between the long axis of the tube
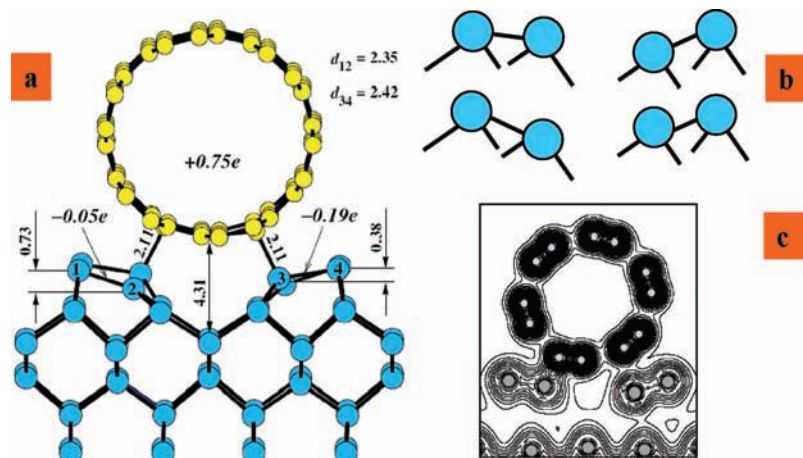
**Figure 34.** (a) Calculated equilibrium geometry of the adsorbed carbon nanotube on the Si(100) surface which is the most stable structure formed through aligning the long-axis of SWNTs parallel to the direction of the dimer row. The distances are in angstroms, and the charge transferred from the carbon nanotube (positive) to the surface (negative) is indicated in units of electrons per unit cell. Blue and yellow balls represent silicon and carbon atoms, respectively. (b) Schematic of a (4×2) reconstruction on the Si(100) surface. (c) Total charge density contour plots for the adsorbed carbon nanotubes on Si(100) with a binding geometry shown in Figure 34a. (From ref 191.)

and the dimer row is 15°. This tilting binding does not result in a significant structural distortion of the carbon nanotube and the silicon surface dimer except a longer Si−C bond length of 3.0 Å.

Mulliken population analyses[191] show 0.75 electron per unit cell of the carbon nanotube is transferred to the Si dimer which forms C−Si bonds with the nanotube. The unit cell in this calculation was defined as a (2 × 4) unit cell of a clean Si(100) surface (Figure 34b). The charge on these dimers is increased by 0.19 electron per unit cell. The dimers which do not form any chemical bond with the nanotube also get 0.05 electron per unit cell from the nanotube. The charge transfer from the nanotube to Si dimers is consistent with the empty states of the buckled-down silicon atoms. Figure 34a shows the charge transfer between carbon nanotubes and Si=Si dimers of Si(100). Notably, the charge transfer from carbon nanotubes to Si(100) is opposite to the charge transfer from Si(111)-7×7 to tetracene[161] and from Si(111)-7×7 to $C_{60}$.[186,196] DFT calculations show that the formation of C−Si covalent bonds stems from hybridization of the unoccupied 3p states of the buckled-down silicon atoms of a Si−Si dimer and the occupied 2p states of the carbon atoms. In addition, the calculated total charge density plot (Figure 34c) for the trench site binding configuration clearly shows the formation of Si−C bonds between buckled-down silicon atoms of Si−Si dimers and the nearest carbon atoms of the nanotube. Overall, upon chemical binding the metallic character is enhanced due to the formation of Si−C bonds at the interface and the significant electron transfer from carbon nanotubes to the buckled-down silicon atoms, which creates an electronic channel along the nanotube/silicon interface. This indicates that the chemical binding and the resulting electron transfer between nanotube and Si(100) is a promising strategy for the development of a new silicon-based nanoelectronic technology.

Compared to metallic nanotubes on Si(100), semiconducting nanotubes exhibit different adsorption behavior.[190] Figure 35 presents the difference in binding configurations of semiconducting nanotubes (12,4 and 8,4) (Figure 35a and c) and metallic nanotubes (9,3) (Figure 35b and d) on Si(100). The analyses of Voronoi and Hirshfield deformation density charge[190,207] show that the charge is transferred from the semiconducting nanotube to the silicon surface, which is similar to the charge transfer for metallic nanotubes[191] on silicon. The magnitude of the transferred charge is larger for the configuration parallel to the dimer trench (Figure 35a and b) in contrast to the one perpendicular to the dimer trench (Figure 35c and d). *Ab-initio* calculations[190] show that the band gap of the hybrid system consisting of semiconducting nanotube and the Si(100) single crystal is significantly reduced in contrast to the case of the free nanotube and free Si(100). This dramatic reduction of the semiconductor gap for the hybrid could stem from the modification of the band structure through surface relaxation and charge transfer to the silicon surface upon chemically binding the carbon nanotubes. The calculated Si−C bond length at the interface of semiconducting nanotube/semiconducting Si(100) is larger than that of the metallic nanotube/semiconducting Si(100) hybrid system, suggesting a lower adsorption energy for semiconducting nanotubes.

Overall, these calculations show significant difference in the adsorption structure and electronic structure, and charge transfer between the metallic nanotube/Si(100) and semiconducting nanotube/Si(100) hybrid systems. This difference could be a strategy to shape the electronic properties of the surface in the development of new silicon-based molecular devices.

## 10. Graphene

Graphene is a huge aromatic system that conducts both electricity and heat in two dimensions. Besides its electronic properties, graphene exhibits several other unusual attributes. It can be considered as a building block of zero-dimensional fullerenes and three-dimensional nanotubes. It has been known conceptually for more than half a century[208−210] and was presumed not to exist as a separate entity. However, a free-standing graphene was prepared 4−5 years ago.[211,212] Since then, it has attracted tremendous interest because it might perform as an atomically thin and robust component for a wide spectrum of nanoelectronics and nano-electro-mechanical devices, and as a building block of various new materials.

Although its electronic and mechanical properties were studied recently,[211−218] its binding on solid surfaces has not been studied because this material is relatively new. However, its binding chemistry on both inert and reactive surfaces, particularly on semiconductor surfaces, is quite important
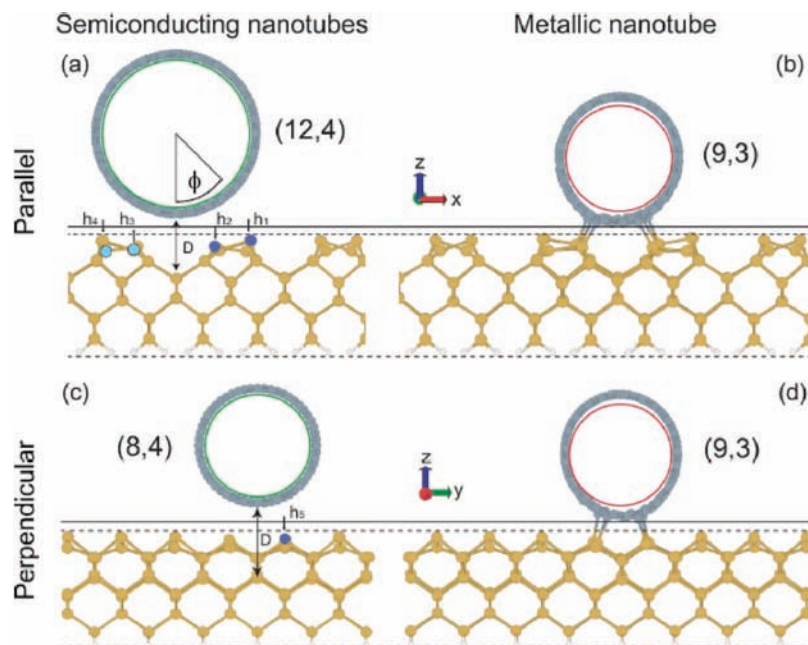
**Figure 35.** Binding configurations of semiconducting nanotubes (a and c) and metallic nanotubes (b and d) on Si(100). In parts a and b the long-axis of the carbon nanotubes is parallel to the dimer row. In parts c and d the long axis is perpendicular to the dimer row. (From ref 190.)

for transplanting its unique electronic and mechanical properties to existing silicon-based device technology. It is also important for development of new devices and materials. Thus, we assume that the binding of graphene on semiconductor surfaces will be studied soon, though as yet there are no results to report.

## 11. Aromatic Systems on Partially Hydrogenated Semiconductor Surfaces in Vacuum

The partial hydrogenation of semiconductor surfaces has become an important approach to the modification of surface reactivity and toward nanopatterning. In this section hydrogenation refers to passivation of reactive sites on clean semiconductor surfaces with hydrogen atoms through physical or/and chemical methods under vacuum conditions. Controllable hydrogenation of semiconductor surfaces usually changes surface electronic structures and reactivity. The subsequent controllable removal of hydrogen atoms bonded on a fully hydrogenated semiconductor surface may create reactive sites and therefore provide platforms which make organic reactions selectively occur on a surface.

### 11.1. Formation of a Partially Hydrogenated Semiconductor Surface

A fully hydrogenated surface can be prepared by thermal cracking of hydrogen molecules and the following adsorption of hydrogen atoms on clean semiconductor surfaces,[16] or with hydrogen plasma for some semiconductor surfaces such as diamond (100).[219] The procedure of the first method is quite simple. A hot tungsten wire can be used to thermally dissociate hydrogen molecules in the experimental chamber. The formed hydrogen atoms react with clean semiconductor surfaces. The clean semiconductor surfaces are usually simultaneously heated to a certain temperature during hydrogen cracking and atomic deposition. Experimental parameters including the temperature of the tungsten filament, the sample–filament distance, the temperature of the semiconductor surface, the pressure of hydrogen in the chamber,
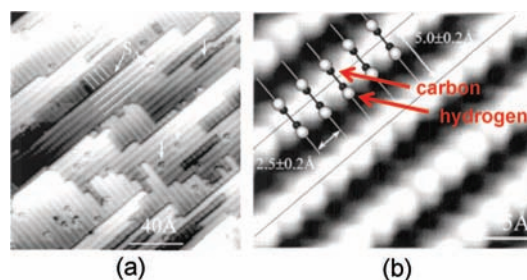


**Figure 36.** STM images (occupied states) of the hydrogenated diamond C(100)-(2×1) surface: (a) large area; (b) small area with high resolution showing the assignment of STM features of the hydrogenated semiconductor surface. (From ref 219.)

and the time of deposition can be adjusted. The surface structure and formation of hydrides on the hydrogenated semiconductor surface can be identified with reflection high energy electron diffraction (RHEED) and HREELS. This method can be used to form fully hydrogenated Si(100), Ge(100), and Si(111) surfaces. Another method is treatment of the surface with hydrogen plasma. This approach requires relatively complicated instrumentation. It is used to generate hydrogenated surfaces if the thermal cracking of hydrogen molecules does not work. In fact, it is the major method for hydrogenation of diamond surfaces.[219] Briefly, microwave heating of hydrogen gas at a relatively high pressure generates a hydrogen plasma which is in contact with the sample surfaces for hydrogenation. Figure 36 represents STM images of a hydrogenated diamond surface prepared with hydrogen plasma.[219]

The fully hydrogenated surface can be generated with the above routes. To selectively create reactive sites on hydrogenated semiconductor surfaces, several methods have been developed to partially desorb hydrogen atoms bonded on the semiconductor surface. These methods are electron stimulated desorption (ESD), photon stimulated desorption (PSD), and thermal desorption. The advantage of ESD is that the energy of electrons impacting the surfaces is adjustable. In fact, an STM tip has been used as an electron beam source

at an atomic scale, selectively removing one or more hydrogen atoms in ESD (also called feedback controlled lithography FCL[220]). This method has advanced many potential techniques such as nanopatterning and lithography at an atomic scale.[220] PSD can be carried out by lasers or with synchrotron radiation. The synchrotron-based PSD has the advantage of tunable energy windows and spatial resolution of the photon beam for selective excitation of chemical bonds. By controlling the intensity and size of the beam and using different patterning of multiple beams, PSD and ESD can create surface active sites with a specific pattern. Compared to PSD and ESD, thermal desorption is a relatively simple method. However, it is not a localized technique. A complicated surface restructuring may accompany the partial desorption of hydrogen atoms in the route of thermal desorption. The kinetics of this process can be studied with STM or TPD.

## 11.2. Electronic Structures of Partially Hydrogenated Semiconductors

Generally, the electronic structures of hydrogen-passivated semiconductor surfaces exhibit different surface states and band gaps compared to clean semiconductor surfaces. For a clean Ge(111)-2×8 surface, surface states of the rest atoms and adatoms are at ∼16.3 and ∼33.3 kcal/mol below the Fermi level, respectively.[221,222] A monohydride (Ge−H) can be formed at sample temperatures >150 °C, whereas GeH₂ and GeH₃ are formed at low temperatures <100 °C.[223] A new surface state was observed at ∼119 kcal/mol below the Fermi level, corresponding to the formation of a Ge−H bond in a monohydride-covered surface. In the low coverage regime, adsorption takes place on the rest atom sites and not on the adatom sites;[224] STM studies show that local electron density is transferred from a rest atom to the nearest-neighbor adatoms at low coverage.[224]

For partially hydrogenated Si(100), isolated dangling bonds were observed.[225] A surface state at ∼16.7 kcal/mol below the Fermi level as well as one at ∼23.8 kcal/mol was identified in the valence band spectra.[225] This state may be attributed to the isolated silicon dangling bonds on the partially hydrogenated Si(100).

Diamond surfaces have received much attention recently due to their exceptional physical properties including high thermal stability, biocompatibility, and large band gap. Hydrogenated diamond surfaces have such properties as well. Compared to the conversion from clean silicon and germanium surfaces to hydrogen-passivated surfaces, two rather amazing features are seen upon hydrogenation of diamond surfaces. Compared to the rapid oxidation of hydrogenated silicon surfaces formed in vacuum upon exposure to ambient conditions, the hydrogenated diamond surfaces are very stable in air for many weeks.[226,227] In addition, diamond surfaces are changed into conducting p-type semiconductor surfaces upon hydrogenation because the surface bonded hydrogen atoms play the role of a dopant by being directly responsible for the hole accumulation layer, forming shallow electron acceptors.[228]

## 11.3. Reactivity of Partially Hydrogenated Semiconductors

As mentioned above, hydrogen atoms bonded on such semiconductor surfaces can be removed by a localized technique such as ESD and PSD or a nonlocalized technique
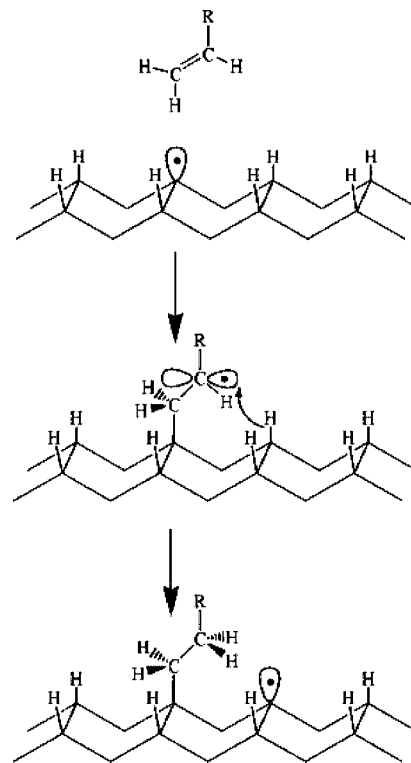


**Figure 37.** Mechanism for formation of a molecular chain through self-directed growth of molecular nanostructures on silicon. Formation of a carbon-centered radical subsequently abstracts a hydrogen atom from an adjacent dimer along a dimer row, creating a new Si radical. This reaction can form a phenyl-terminated molecular chain on this surface by using styrene. (From ref 230.)

such as thermal desorption. The regenerated dangling bonds or active sites exhibit reactivity which in many cases is different from that of clean semiconductor surfaces. Reactions of organic and inorganic molecules on such partially hydrogenated semiconductor surfaces have been studied. The particular interests are the local manipulation of hydrogen atoms and the subsequent promotion of surface reactivity at these selective sites[229] as well as the growth of nanopatterned materials through certain surface reaction mechanisms.[230−232] Here the reactions of aromatic molecules on partially hydrogenated surfaces are reviewed.

For these partially hydrogenated semiconductor surfaces, a few aromatic systems on such surfaces were studied. They form chains of aromatic molecules on partially hydrogenated Si(100) through radical generation and a hydrogen abstraction mechanism. Active sites can be created by using feedback controlled lithography, which was first demonstrated by Lyding.[233,234] The generation of a dangling bond on Si(100) through initial desorption of a hydrogen atom by applying a pulse to a specific site has been creatively used to self-propagate the attachment of organic molecules along a dimer-row. This approach was successfully used to grow 1-D organic wires with a diameter on the molecule scale. The first example was the formation of one-dimensional aromatic chains on Si(100) reported by Wolkow et al.[230] Figure 37 schematically shows the mechanism for the formation of a molecular chain along the direction of dimer rows of Si(100) terminated with hydrogen atoms.[230] A bias is applied to a specific hydrogen atom, desorbing this hydrogen atom and generating a dangling bond. The adsorption of a styrene molecule on this single dangling bond creates a radical on the vinyl group. This vinyl group subsequently picks up one
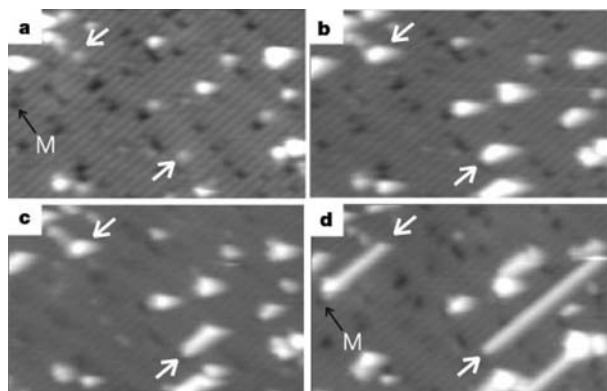
**Figure 38.** Sequence of STM images showing the growth of styrene lines on a H-terminated Si(100) surface at different exposures of styrene. The white and black arrows denote the dangling-bond sites starting to grow styrene lines and the defects terminating propagation of a molecular chain, respectively: (a) 3 L; (b) 28 L; (c) 50 L; (d) 105 L. (From ref 230.)



**Figure 39.** (a) STM image of CuPc molecules adsorbed on clusters of dangling bonds of partially hydrogenated Si(100). Molecule #1 possesses a 4-fold symmetry, whereas molecule #2 possesses a radial symmetry. Molecule #1 exhibits the expected 16 Å diameter, whereas molecule #2 perturbs the surface over a diameter of ∼35 Å. (b) STM image of an isolated $NH_3$-reacted CuPc molecule. The arrow suggests that a rotation about this axis would sweep out a circle with the observed diameter of ∼30 Å. (From ref 220.)
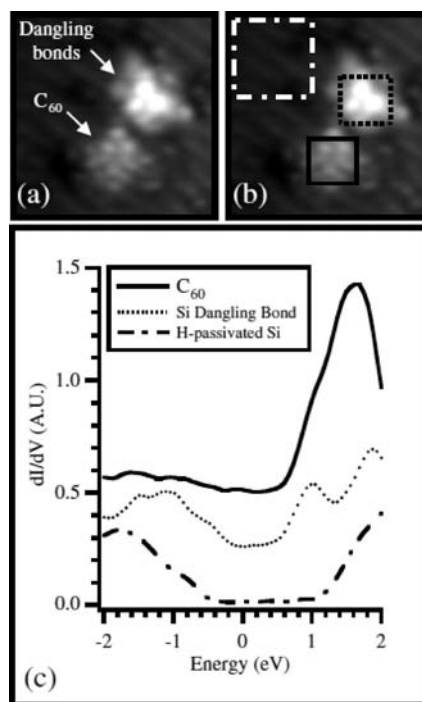


**Figure 40.** (a) STM image of an isolated C60 molecule and a cluster of Si dangling bonds. (b) STM image showing locations where the STM spectroscopy was performed at every pixel within this image. (c) The spectra of three different locations in part b obtained by averaging spectra of all of the pixels in the location. (From ref 220.)

hydrogen atom from an adjacent dimer terminated with hydrogen atoms, creating another dangling bond site on this dimer. Such alternating creation of a dangling bond on a silicon dimer and a radical on a vinyl group will continue and terminate at a defect site on this dimer row. Figure 38 represents the STM images for the growth of an aromatic chain on hydrogen-terminated Si(100) at different exposures of styrene.[230] Recently, such a radical generation and hydrogen absorption mechanism was successfully applied to develop an interconnected one-dimensional inorganic and organic nanostructure on Si(100).[235]

The adsorption of several large molecules with aromatic groups on partially hydrogenated Si(100) was studied. For a complicated organic molecule, in fact, a group of isolated dangling bonds created with FCL is required for adsorption. Several aromatic systems including biphenyl,[236] copper phthalocyanine[220,237] (CuPc), 1,4″-paraterphenyldimethylac-etone, and $C_{60}$[220] can assemble onto such a template with multiple dangling bonds. Diphenyl can be selectively ad-sorbed into a group of dangling bonds with four or more adjacent dangling bonds on two or three neighboring dimers.[236] Notably, the dynamics of the adsorbed molecules are modified by the presence of the bonded hydrogen atoms around these dangling bonds. CuPc is attached to the surface through the Cu atom or through formation of a $\pi$ bond with a pyrrole group. CuPc molecules are adsorbed on clusters of Si dangling bonds through two binding modes. As shown in Figure 39a, molecule #1 has a size of ∼16 Å with a nearly 4-fold symmetry compared to the large size of ∼35 Å with radial symmetry of molecule #2. The match of measured size of CuPc on this surface to its size in its free state suggests a site-specific adsorption. In fact, molecule #1 binds to a dangling bond of a hydrogenated silicon surface through a Si···Cu $\pi$-binding. Molecule #2 is adsorbed to dangling bonds through a weak interaction with one of the outer benzene rings, which supports the measured large size (35 Å) and its rational freedom. The assignment of the binding geometry of molecule #2 is supported by the STM feature of ammonia-reacted CuPc on such a Si(100) surface. Before sublimation of CuPc onto a partially hydrogenated Si(100), the CuPc source is exposed to ammonia; this treatment forms ammonia-reacted CuPc. The measured size of the ammonia-reacted CuPc adsorbed on the surface is ∼30 Å (Figure 39b). Such a large size suggests a weak interaction between an
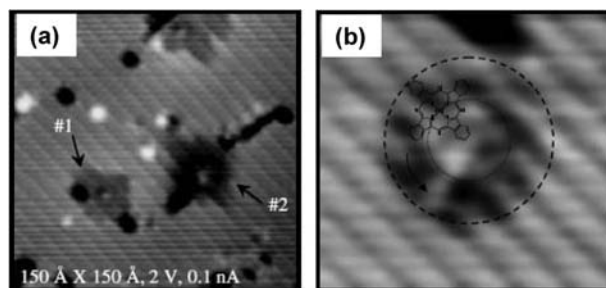
outer benzene ring and the surface and a rotational freedom for the adsorbed molecule.[238]

The geometric and electronic structures of $C_{60}$ on a cluster of dangling bonds on hydrogenated Si(100) have been well studied. $C_{60}$ is adsorbed on a group of dangling bonds. Figure 40a represents the STM image of an adsorbed $C_{60}$ and a cluster of created dangling bonds. Figure 40c shows the measured density of states of three different areas of Figure 40b including $C_{60}$, Si-dangling bonds, and an H-terminated surface.[220] Clearly, a new surface state is observed at ∼30.1 kcal/mol above the Fermi level, which is attributed to the lowest unoccupied state of the adsorbed $C_{60}$. This difference suggests that the intramolecular electronic structure is sensitive to the localized substrate structure.[220]

## 12. Aromatic Systems on Hydrogenated or Halogenated Semiconductor Surfaces in Solution

As discussed above, the functionalization of clean or hydrogenated semiconductor surfaces in vacuum has been used to develop organic monolayers or even multilayers with well controlled surface structure and chemistry. On the other hand, organic reactions in solution on hydrogenated and halogenated semiconductor surfaces allow us to synthesize complicated organic structures on semiconductor surfaces. Such semiconductor-based advanced organic layers are crucial in the development of sophisticated surfaces with a wide spectrum of applications in the design of sensor, nanopatterning, immobilization of biomolecules, and surface-related microreactors. We note that many excellent studies on the functionalization of porous silicon and germanium surfaces have been carried out in the Buriak group.[17,239,240] However, this section will focus on the organic functionalization on flat semiconductor wafers instead of porous semiconductor materials.

### 12.1. Formation of Hydrogenated or Halogenated Semiconductor Surfaces

Most functionalization of semiconductor surfaces with organic reactions in solution was carried out on silicon surfaces, though several studies have been reported on germanium surfaces.[241–244] The starting platforms for such functionalization in solution are silicon or germanium wafers with a layer of native oxide. The first step is the removal of native oxide and subsequent formation of hydrogen-terminated surfaces. In most cases, the formed surface is fully covered with hydrogen. In general, dilute HF or $NH_4F$ is used to etch surface oxides and form a hydrogen-terminated semiconductor surface.[245,246] The surface flatness and smoothness can be identified with the sharpness of vibrational peaks of $\nu(Si-H)$ at $\sim 2080$ cm$^{-1}$ or $\nu(Ge-H)$ at $\sim 2100$ cm$^{-1}$. Multiple silicon hydrides such as SiH, $SiH_2$, and $SiH_3$ can be formed, determined by reaction conditions which are widely adjustable.[245–247]

In a few cases, halogenated surfaces (Si−Cl and Si−Br) are used as reactants for organic modification. They can be obtained by treating hydrogenated silicon surfaces with $PCl_5$ at 80−100 °C[248] or N-bromosuccinimide at 60 °C[249] through radical initiation from benzoyl peroxide. In addition, $Cl_2$ or $CCl_3Br$ can initiate the conversion from hydrogenated silicon surfaces into halogenated-silicon surfaces.[249–251] A chlorinated germanium surface can be prepared by a reaction with gaseous HCl or 10% aqueous HCl on Ge(111) wafers pretreated with $H_2O_2$ and oxalic acid.[241,252]

### 12.2. Functionalization of Hydrogenated or Halogenated Semiconductor Surfaces

Driven by the wide spectrum of applications, several different approaches for formation of organic structures on silicon surfaces in solution have been developed. They are radical-initiated hydrosilylation, thermal-driven hydrosilylation, photomediated hydrosilylation, metal complex-catalyzed hydrosilylation, electrochemical grafting, Grignard-related hydrosilylation, and mechanical carving and simultaneous hydrosilylation in solution. In addition, chlorinated germanium surfaces can be functionalized by using ethyl Grignard reagents. Moreover, reactions similar to thermal-driven hydrosilylation can be used to hydrogermylate hydrogenated germanium surfaces. Figure 41 briefly represents these reaction mechanisms.[17] The following is a brief description and comparison of these approaches. A detailed description can be found in the original literature.

For radical-initiated hydrosilylation, hydrosilylation of a hydrogenated silicon surface inserts an unsaturated bond, which is generally a terminal group, into a Si−H or Ge−H bond, forming an alkenyl or alkyl monolayer through Si−C or Ge−C covalent bonds.[253,254] Generally, a diacyl peroxide is used as radical initiator which decomposes and forms an alkyl radical and $CO_2$. This alkyl radical can abstract a hydrogen atom from the silicon surface, forming a silicon radical. This silicon radical can rapidly react with an unsaturated bond of an organic molecule and therefore form a radical on the $\beta$-carbon of the immobilized organic chain. This carbon-based radical can abstract a hydrogen atom from its adjacent Si−H bond or from another molecule. Figure 41a represents the reaction mechanism of this radical-initiated hydrosilylation.[254]

In the absence of radical initiator, hydrosilylation through homolytic cleavage of Si−H bonds can occur at a temperature higher than that for radical-initiated hydrosilylation. The high temperature, generally 150−200 °C, promotes homolytic cleavage of Si−H to generate silicon radicals on silicon surfaces.[255–264] Such a radical on a silicon atom can react with an unsaturated bond with the same reaction mechanism as that of radical-initiated hydrosilylation (Figure 41a). The organic layers formed through thermal-driven hydrosilylation are thermally stable up to $\sim 350$ °C in vacuum.[255] This method has been used to functionalize both hydrogenated Si(100) and Si(111). In most cases, half of the hydrogen atoms on the hydrogenated silicon surface can be converted into organic chains with radical-initiated hydrosilylation and thermal-driven hydrosilylation.

Besides radical initiation and thermal cleavage, photolysis is an alternative source to break Si−H bonds to generate silicon radicals for further reaction with unsaturated bonds of organic molecules.[251,264–269] Compared to homogeneous contact between a silicon surface and a radical initiator in solution and the possible damage to other parts of a silicon device wafer in thermal-driven hydrosilylation, photoinitiated hydrosilylation can controllably functionalize a local area required for specific applications. The general procedure is an irradiation of a hydrogenated semiconductor surface with light in the presence of alkenes or alkynes. Both ultraviolet[184,251,265,266] and white light[268–270] can be used for this purpose. By using masks with different sizes, shapes, or/and multiple beams with certain pattern and spot size, semiconductor surfaces can be selectively functionalized for technological purposes.[271] As shown in Figure 42, the Si(111) wafer was selectively functionalized[271] using this approach. Notably, styrene- and phenylacetylene-terminated monolayers have been developed on hydrogenated Si(111) through photomediated hydrosilylation. The preserved phenyl group protrudes away from the surface on the functionalized silicon surfaces.[15,251,265–269]

Transition metal complexes can catalyze hydrosilyation at liquid−solid interfaces. Similar to the catalysis of Pt(0) complexes for hydrosilylation of alkenes with silanes in organic reactions in solution,[272] Pt(0) complexes can catalyze hydrosilylation at the liquid−solid interface between unsaturated organic molecules and a hydrogenated silicon wafer in solution as represented in Figure 41b. Notably, the transition-metal complex can catalyze oxidation of the silicon surface
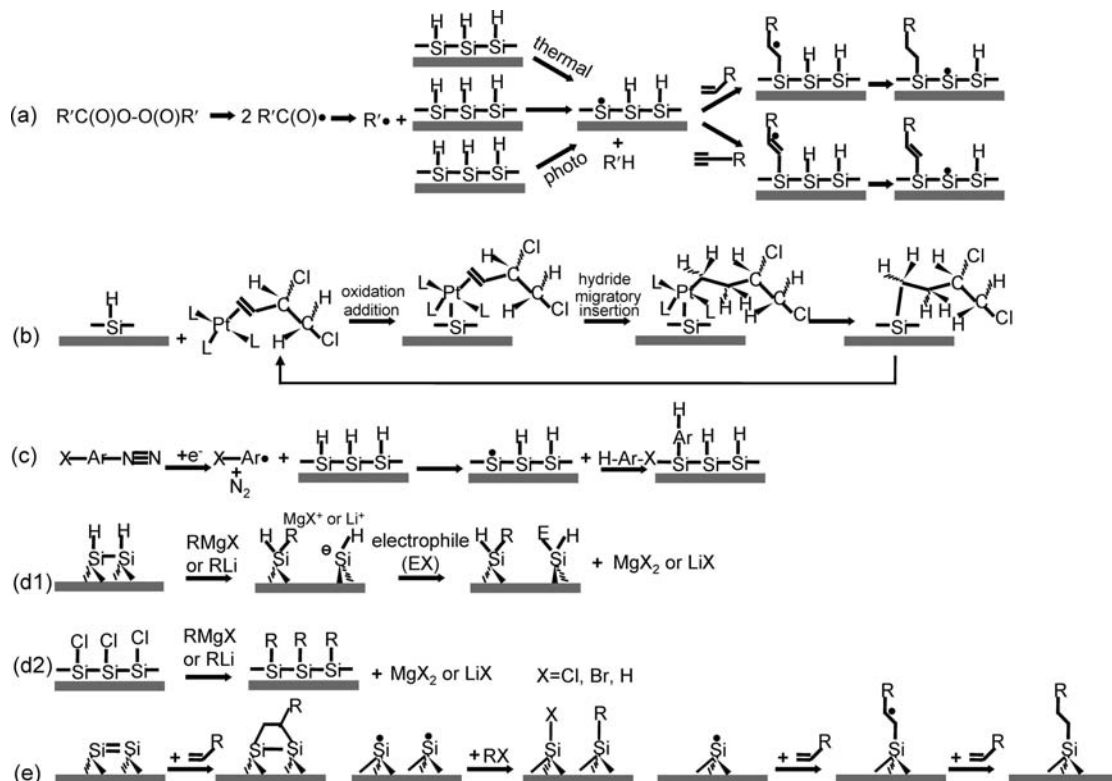
**Figure 41.** Reaction mechanisms for organic functionalization of hydrogenated and halogenated semiconductor surfaces in solution: (a) radical-initiated hydrosilylation, thermal-driven hydrosilylation, and photomediated hydrosilylation; (b) metal complex-catalyzed hydrosilylation; (c) electrochemical grafting; (d) Grignard-related hydrosilylation and halogenosilylation; and (e) mechanical carving and simultaneous hydrosilylation in solution. (After ref 17.)
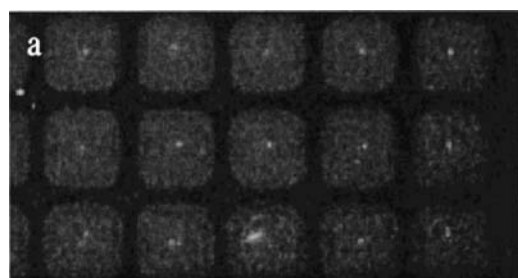
**Figure 42.** SEM image of a hydrogenated Si(111) wafer upon selective functionalization through photochemical hydrosilylation on exposed holes. The dark grid in this image is the gold grid with a width of 10 $\mu$m. (From ref 271.)

as well. Actually, to avoid this accompanying problem of oxidation, Lewis acid-catalyzed or mediated hydrosilyation is an alternative route.[273-275] Lewis-acid hydrosilylation has been successfully used to functionalize the hydrogenated Si(111) surface at a relatively high temperature such as 100 °C.[273]

Compared to the oxidation of silicon surfaces during catalysis by transition metal complexes for hydrosilyation at the liquid−solid interface, electrochemistry-based functionalization avoids the problem of oxidation during the process of hydrosilylation, because an electron-rich cathode is inactive for nucleophilic attack by water. As demonstrated in Figure 41c, aryl radicals can be produced by applying a negative potential of about 1 V in an HF solution containing the bromobenzene diazonium salt.[276] The aryl radical can abstract a bonded hydrogen atom to form a silicon radical. Another aryl radical can bond with the silicon radical through a Si−C covalent linkage. Such an electrochemistry approach has been successfully applied to grow a robust phenyl
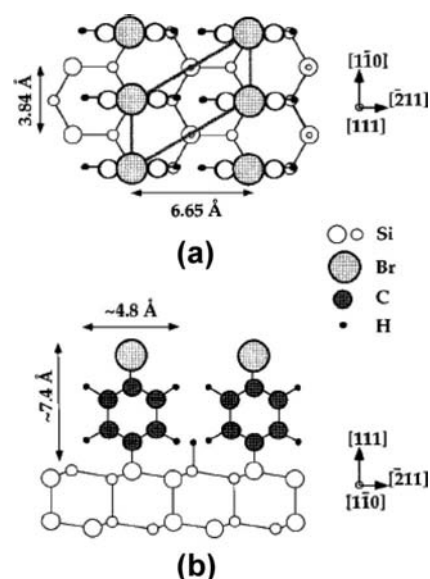
**Figure 43.** (2 × 1) structure in a monolayer of bromoaryl layers on Si(111) formed from 4-Br benzenediazonium salts on hydrogenated Si(111) through the electrochemical method in solution: (a) top view; (b) side view. (From ref 276.)

monolayer on hydrogenated Si(111) surfaces by electrochemically reducing 4-NO$_2$ and 4-Br benzenediazonium salts on H-terminated Si(111) electrodes.[276,277] The coverage of the formed phenyl monolayer is ∼50%. Figure 43 schematically shows the 2 × 1 structure of the phenyl monolayer formed on hydrogenated Si(111) in solution.

The transmetalation reaction is another approach to form Si−C bonds on Si surfaces.[278] Figure 41d1 represents the mechanism. The formation of Si−C bonds results from the

attack of the weak Si−Si bonds by a carbanion nucleophile. With a similar mechanism (Figure 41d2), hydrogenated- or halogenated-Si(111) can be functionalized.[248,249,279−283] Monolayers of several aromatic systems including oligothiophenes[249] and 5-(N-pyrrolyl)phenyllithium reagents[281] have been developed on Si(111) with this method.

All of the above approaches involve the use of hydrogenated or halogenated silicon wafers as starting materials. A simple and quite effective surface functionalization is a combination of physical removal of native oxide and instant chemical functionalization in solution. The mechanical removal of natural oxide creates dangling bonds (or silicon radicals) which may exhibit reactivity similar to that of a Si=Si dimer formed under UHV conditions.[284−286] Figure 41e represents three different reactions possibly occurring on this surface. More descriptions of this method can be found in a nice review[17] and in the original literature. In this method, precise control of mechanical removal can be developed into a technique to selectively functionalize silicon surfaces to form organic nanopatterns on semiconductor surfaces.

Two approaches have been developed for functionalization of germanium surfaces. One starts from a halogenated germanium surface. Alkyl Grignard reagent reacts with the halogenated surface and forms an alkyl-terminated germanium surface.[287] The other method is hydrogermylation of the hydrogenated germanium surface.[288] This route is similar to hydrosilylation, in which an unsaturated C−C bond is inserted into the Ge−H bond.

## 12.3. Formation of Organic Multilayers on Semiconductor Surfaces through Chemical Reactions

Because organic monolayers formed through dry chemistry in vacuum and wet chemistry in solution are quite robust, they have been used as substrates to immobilize second organic layers through chemical reactions, or biomolecules such as DNA through formation of strong chemical bonds or weak noncovalent interactions. The immobilization of biomolecules is beyond the focus of this review. The formation of the second organic layers on the first layer through organic reactions will be briefly introduced here for completeness.

Several routes for the formation of organic multilayers through chemical reactions in solution were well developed. They included C−H bond activation of terminal methyl groups,[289] amide and sulfonamide bond formation,[290−292] ester hydrolysis,[256] ester reduction and cleavage,[292] ester formation,[292] hydroboration of olefins,[274,275] and polymerization.[293] These routes were nicely reviewed by Buriak.[17]

Many organic reactions only occur in solution since they involve solvent-mediated electron/proton transfer or participation of a third molecule such as a catalyst. Thus, formation of multilayer organic architectures through chemical reactions under vacuum conditions remains a great challenge. A few strategies have been creatively developed for the formation of organic multilayers under vacuum conditions. Bent et al. successfully designed a layer-by-layer growth through a urea coupling reaction
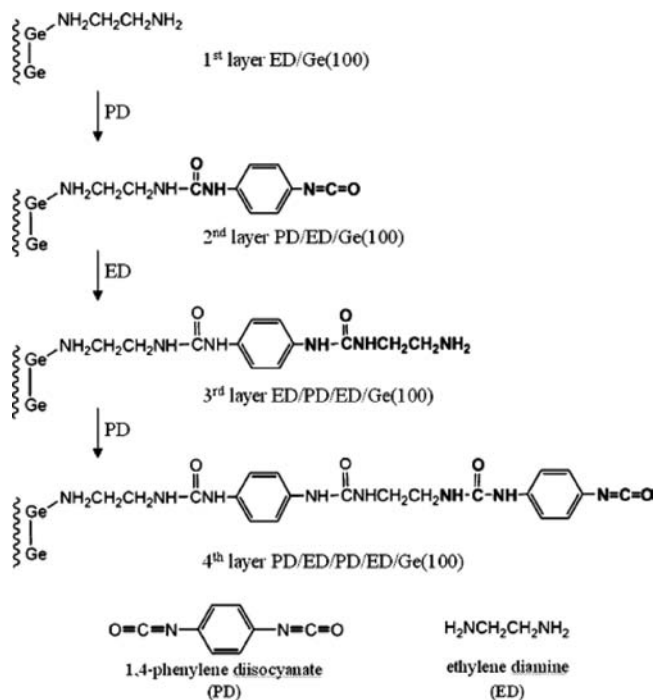


**Figure 44.** Layer-by-layer growth of an organic multilayer through interlayer chemical reactions on Ge(100) in vacuum. (From ref 294.)

between ethylenediamine and 1,4-phenylene diisocyanate on Ge(100) in vacuum at room temperature.[294] Figure 44 represents the layer-by-layer growth of an organic multilayer through interlayer chemical reaction on Ge(100) in vacuum. Ethylenediamine reacts with Ge(100), forming a monolayer with an amine group protruding into vacuum. This amine group subsequently reacts with 1,4-phenylene diisocyanate, leading to a spontaneous urea coupling reaction between the surface-bound amine and the highly reactive isocyanate functional group. Bent et al. have demonstrated that such a method can grow at least four layers of organic molecules on Ge(100) through repeated urea coupling. This elegant layer-by-layer growth provides a strategy for formation of organic multilayers with controllable thickness on semiconductor interfaces under vacuum conditions.

Xu et al. recently developed a photochemistry-grafted organic multilayer on Si(111)-7×7 in vacuum.[122] Figure 45 schematically presents the formation of the covalently bonded second layer in vacuum. The first organic layer with protruding C−Cl groups was formed through OH dissociation on a Si(111)-7×7 surface. The C−Cl bonds of the robust organic monolayer were then cleaved by a 193 nm photon, producing radicals on the terminal C atoms of the adsorbed molecules, which subsequently react with the cyano groups of the physisorbed benzonitrile molecules near to the formed radicals. This reaction forms a benzoimine-like second layer with radicals on the carbon atoms of the cyano groups. This generated carbon-based radicals abstract nearby H atoms, creating silicon-based radicals on the adjacent silicon atom. The formation of this multilayer organic architecture demonstrated that a combination of organic reactions and photochemistry on the semiconductor surfaces is an important approach to the development of organic architectures in vacuum, since photons can be readily used in vacuum.
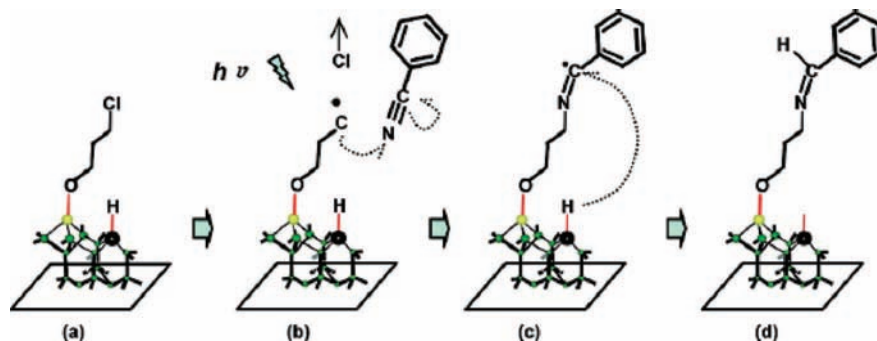
**Figure 45.** Schematic of the formation of the covalently bonded second layer in vacuum.

## 13. Overall Interpretation of the Reaction Mechanism of Aromatic Systems on Semiconductor Surfaces

Based on the mechanistic studies of the chemical binding of various aromatic molecules on clean and passivated semiconductor surfaces reviewed above, these aromatic systems can be broadly classified as heteroaromatic and nonheteroaromatic systems. The heteroaromatic molecules studied include thiophene, furan, pyrrole, oxazole, isoxazole, thiazole, pyridine, pyrazine, pyrimidine, and the substituted heteroatom aromatic molecules. Nonheteroaromatic molecules include benzene, naphthalene, tetracene, pentacene, coronene, acenaphthalene, graphene, $C_{60}$ and carbon nanotubes, and their derivatives. For the first category of aromatic molecule, heteroatoms play an important role in choosing the reaction channel and in shaping the binding configuration. However, for the second category of aromatic molecule, the geometric and electronic structures of the reactive sites of the semiconductor surfaces play a more important role in determining the reaction mechanism.

For heteroatom aromatic molecules, there are several interacting complicated electronic and structural factors which affect the molecular reaction channel on semiconductor surfaces. Among them, the electronic and structural factors of the heteroatoms in terms of the hybridization of the atomic orbital, the electron contribution to the aromatic ring, and the atomic geometric arrangement on the aromatic ring are crucial. Figure 46 shows the hybridization of heteroatoms of the first category of aromatic molecule. Obviously, the equivalent $sp^2$ hybridization of electrons on the N 2p orbital of pyrrole does not allow donation of electron density to an electron-deficient surface silicon atom. This is why it cannot form a dative bond with Si(100), Si(111)-7×7, and Ge(100). The N, O, and S atoms in all other molecules in Figure 46 have the possibility to form a dative bond due to the availability of one lone pair in an inequivalent $sp^2$ hybridized orbital of these heteroatoms. Thus, in principle, the nitrogen atoms of isoxazole, oxazole, thiazole, pyridine, and pyrimidine, and the sulfur atom of thiophene and thiazole can transfer electron density to semiconductor surfaces, forming dative bonds. However, for the same molecule, such as thiophene, a dative bond is formed with Ge(100), but not with Si(100), suggesting the importance of the electronic structure of the surface reactive site as well. In fact, even for the same molecule on the same semiconductor surface, such as isoxazole (or oxazole and thiazole) on Si(111)-7×7, an adatom of this surface forms a dative bond with the nitrogen atom but not with its oxygen atom, even though the oxygen or sulfur atom has a lone pair. Thus, the competition and selectivity of reaction channels
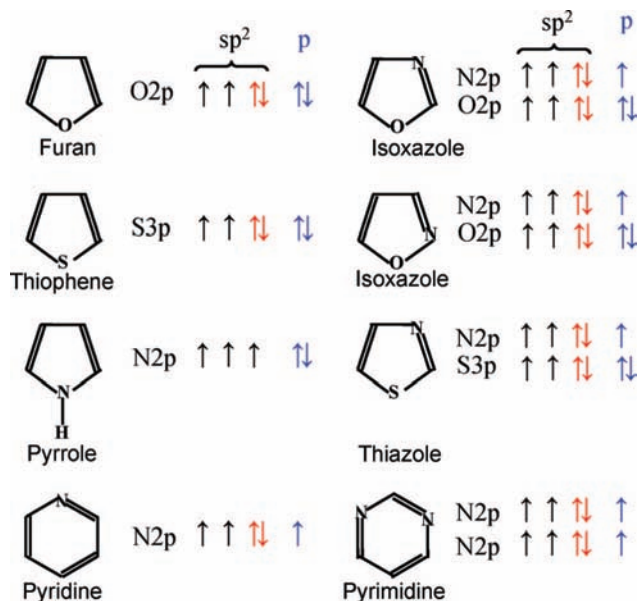


**Figure 46.** Hybridization of electrons on N 2p, O 2p, and S 3p orbitals of the heteroatoms of heteroatom aromatic molecules reviewed in this article. The red arrows show the lone pair in an $sp^2$ hybridized orbital which is localized and therefore could be donated for the formation of dative bonds with a semiconductor surface. The blue arrows show the contribution of electrons on p orbitals in the formation of $4n + 2$ aromatic $\pi$ conjugation.

in an aromatic molecule containing multiple heteroatoms is quite complicated, in contrast to the case of heteroatom molecules containing only one heteroatom. In general, the binding mechanisms of heteroatom aromatic molecules are more complicated than those of nonheteroatom aromatic molecules. The difference in reaction mechanism between oxazole and thiazole demonstrates that the electronegativity of the heteroatom is another factor in determining the reaction channel for heteroatom aromatic systems. The difference in reaction channel between oxazole and isoxazole suggests that the arrangement of heteroatoms in the molecule is also a factor in determining the reaction pathway. Thus, these differences show that the variation of molecular structure is an approach to shaping chemical binding on the semiconductor surfaces. This is an advantage in the use of organic molecules for the modification and functionalization of semiconductor surfaces, since the molecular structure and functional group in organics can be varied controllably.

Molecular polarity could be another factor for some heteroatomic aromatic molecules in determining the reaction channel on semiconductor surfaces. Pyrazine is a six-membered aromatic ring molecule with two symmetrically arranged nitrogen atoms (Figure 13d). Similar to the role of the nitrogen atom of isoxazole, oxazole, thiazole, and

pyridine in the formation of aromatic $\pi$ conjugation, each nitrogen atom in pyrazine contributes only one electron for the formation of the aromatic $\pi$ sextet. Thus, each of the two nitrogen atoms in pyrazine has a high electron density due to their localized lone pairs. However, pyrazine does not form a dative bond with the Si(111)-7×7 and Si(100) surfaces. This is possibly because the nonpolar pyrazine does not allow electron-rich nitrogen atoms to transfer electron density to the electron-deficient surface silicon atoms of Si(111)-7×7 and Si(100). This understanding is further supported by the formation of a dative bond between pyrimidine (Figure 13e), an isomer of pyrazine with polarity, on Ge(100). Thus, it is expected that polar pyrimidine forms a dative bond with Si(100) and Si(111)-7×7. In addition, the understanding of the role of the molecular dipole is consistent with the formation of dative bonds between oxazole, isoxazole, thiazole, and Si(111)-7×7. All of these molecules have a strong dipole moment. Thus, molecular polarity is a necessary factor, in addition to the availability of a localized lone pair for the formation of dative bonding between heteroatom aromatic molecules and semiconductor surfaces.

The simplest molecule in the second broad category of aromatic molecule considered here is benzene. Its six atoms exhibit equivalent reactivity for surface reactive sites. Compared to the equivalence in reactivity and electron density of all six carbon atoms in benzene, the fused and nonfused carbon atoms in acenes exhibit quite different reactivity. Compared to the fused carbon atoms in the acene-series molecules, the nonfused carbon atoms have much higher reactivity in the formation of Si−C bonds with semiconductor surfaces, due to less steric strain in the bonding of the nonfused carbon atoms. Thus, the nonfused carbon atom is easily rehybridized into sp$^3$ in contrast to the very rigid fused carbon atom structure. For large acene-series molecules, the selection of reaction channel is mainly determined by the availability of the combined reactive site (such as two pairs of adjacent adatom−rest atoms for pentacene), which matches the molecular structure. Compared to the heteroatom aromatic molecules, the distribution of electron density on the nonheteroatom aromatic ring is not so important a factor in determining molecular reaction channel and binding configuration. In addition, compared to small five-membered and six-membered aromatic molecules, a large charge transfer from Si(100) to tetracene and $C_{60}$ and from carbon nanotubes to Si(100) is clearly observed for large aromatic molecules. This is possibly due to the availability of molecular conjugated $\pi$-orbitals upon chemical binding, which can transfer electrons to or accept electrons from semiconductor surfaces. In addition, the multiple reactive sites with different geometric and electronic structures make it more complicated. From the view of promising applications, the complicated reaction mechanisms offer diverse approaches to fine-tuning the chemical and physical properties of semiconductor surfaces by chemical binding of organic materials controllably.

Compared to the participation of the aromatic group in reactions between organic molecules and clean semiconductor surfaces *in vacuum*, in many cases aromatic systems or molecules with aromatic groups do not directly participate in the functionalization reaction *in solution*. This mainly results from the high resonance energy due to the formation of a large $\pi$ bond delocalized on an aromatic group. Thus, generally C=C or C≡C groups instead of the aromatic group

are used as the functional group to react with hydrogenated or halogenated semiconductor surfaces. Thus, in solution, aromatic groups are generally preserved in the formed organic monolayers. Such protruding aromatic groups can be well used as linkers for further syntheses of multilayer organic architectures on semiconductor surfaces, or for immobilization of biomolecules such as DNA, useful in the development of biosensing technology.

## 14. Summary

Molecular chemical binding on reactive sites of semiconductor surfaces is an important approach to shaping chemical, physical, and mechanical properties of semiconductor surfaces, and integrating functions of organic materials into inorganic semiconductor-based devices for a wide spectrum of technological needs. The aromatic system is one of the most important building blocks for a great number of organic materials. The chemical binding and reaction mechanisms of various aromatic molecules from the simplest benzene to the extra large buckyballs and carbon nanotubes on different semiconductor surfaces were reviewed on the basis of recent extensive experimental and theoretical studies. In general, aromatic molecules could be chemically bound to semiconductor surfaces through one or more of several possible reaction pathways, including [4 + 2]-like and [2 + 2]-like additions, dative bonding, and dissociative reaction. Systematic studies from simplest benzene to extra large carbon buckyballs and nanotubes show that the selection of the reaction channel for aromatic systems is determined by the interplay of structural and electronic factors of the aromatic molecules and geometric and electronic factors of the surface reactive sites. The electronic and structural factors of aromatic molecules include the distribution of electron density on the molecule determined by the geometric arrangement of the carbon atoms and particularly the heteroatoms on the ring, the electronegativity of the heteroatoms, and the electronic contribution of the heteroatoms to the formation of aromatic $\pi$ conjugation, as well as the overall molecular polarity. The intrinsic connection between electronic and structural factors and molecular reaction mechanisms in the modification and functionalization of various semiconductor surfaces with aromatic systems was established in this review.

## 15. Acknowledgments

## 16. References

(1) Somorjai, G. A. *Introduction to Surface Chemistry and Catalysis*; John Wiley & Sons, Inc.: 1993.
(2) Yates, J. T. *Science* **1998**, *279*, 335.
(3) Barteau, M. A. *Chem. Rev.* **1996**, *96*, 1413.
(4) Ma, Z.; Zaera, F. *Surf. Sci. Rep.* **2006**, *61*, 229.
(5) Tao, F.; Bernasek, S. L. *Chem. Rev.* **2007**, *107*, 1408.
(6) Tao, F.; Bernasek, S. L. *J. Am. Chem. Soc.* **2005**, *127*, 12750.
(7) Bratlie, K. M.; Montano, M. O.; Flores, L. D.; Paajanen, M.; Somorjai, G. A. *J. Am. Chem. Soc.* **2006**, *128*, 12810.
(8) Bratlie, K. M.; Flores, L. D.; Somorjai, G. A. *Surf. Sci.* **2005**, *599*, 93.
(9) Richter, C. A.; Hacker, C. A.; Richter, L. J.; Vogel, E. M. *Solid-State Electron.* **2004**, *48*, 1747.
(10) Gu, J. H.; Yam, C. M.; Li, S.; Cai, C. Z. *J. Am. Chem. Soc.* **2004**, *126*, 8098.

(11) de Smet, L. C. P. M.; Stork, G. A.; Hurenkamp, G. H. F.; Sun, Q. Y.; Topal, H.; Vronen, P. J. E.; Sieval, A. B.; Wright, A.; Visser, G. M.; Zuilhof, H.; Sudholter, E. J. R. *J. Am. Chem. Soc.* **2003**, *125*, 13916.

(12) Pike, A. R.; Patole, S. N.; Murray, N. C.; Ilyas, T.; Connolly, B. A.; Horrocks, B. R.; Houlton, A. *Adv. Mater.* **2003**, *15*, 254.

(13) Nebel, C. E.; Rezek, B.; Shin, D.; Uetsuka, H.; Yang, N. *J. Phys. D: Appl. Phys.* **2007**, *40*, 6443.

(14) Rodriguez-Reyes, J. C. F.; Teplyakov, A. V. *Chem.—Eur. J.* **2007**, *13*, 9164.

(15) He, T.; Ding, H. J.; Peor, N.; Lu, M.; Corley, D. A.; Chen, B.; Ofir, Y.; Gao, Y. L.; Yitzchaik, S.; Tour, J. M. *J. Am. Chem. Soc.* **2008**, *130*, 1699.

(16) Mayne, A. J.; Riedel, D.; Comtet, G.; Dujardin, G. *Prog. Surf. Sci.* **2006**, *81*, 1.

(17) Buriak, J. M. *Chem. Rev.* **2002**, *102*, 1271.

(18) Wolkow, R. A. *Annu. Rev. Phys. Chem.* **1999**, *50*, 413.

(19) Filler, M. A.; Bent, S. F. *Prog. Surf. Sci.* **2003**, *73*, 1.

(20) Hamers, R. J.; Coulter, S. K.; Ellison, M. D.; Hovis, J. S.; Padowitz, D. F.; Schwartz, M. P.; Greenlief, C. M.; Russell, J. N. *Acc. Chem. Res.* **2000**, *33*, 617.

(21) Leftwich, T. R.; Teplyakov, A. V. *Surf. Sci. Rep.* **2008**, *63*, 1.

(22) Garratt, P. J., *Aromaticity*; McGraw-Hill: 1971.

(23) Davies, D. T. *Aromatic Heteroatom Chemistry*; Oxford University: 1992.

(24) Bent, S. F. *J. Phys. Chem. B* **2002**, *106*, 2830.

(25) Bent, S. F. *Surf. Sci.* **2002**, *500*, 879.

(26) Hovis, J. S.; Coulter, S. K.; Hamers, R. J.; D'Evelyn, M. P.; Russell, J. N.; Butler, J. E. *J. Am. Chem. Soc.* **2000**, *122*, 732.

(27) Wang, G. T.; Bent, S. F.; Russell, J. N.; Butler, J. E.; D'Evelyn, M. P. *J. Am. Chem. Soc.* **2000**, *122*, 744.

(28) Russell, J. N.; Butler, J. E.; Wang, G. T.; Bent, S. F.; Hovis, J. S.; Hamers, R. J.; D'Evelyn, M. P. *Mater. Chem. Phys.* **2001**, *72*, 147.

(29) Takayanagi, K.; Tanishiro, Y.; Takahashi, M.; Takahashi, S. *J. Vac. Sci. Technol. A* **1985**, *3*, 1502.

(30) Takayanagi, K.; Tanishiro, Y.; Takahashi, S.; Takahashi, M. *Surf. Sci.* **1985**, *164*, 367.

(31) Wang, Z. H.; Cao, Y.; Xu, G. Q. *Chem. Phys. Lett.* **2001**, *338*, 7.

(32) Lu, X.; Wang, X. L.; Yuan, Q. H.; Zhang, Q. *J. Am. Chem. Soc.* **2003**, *125*, 7923.

(33) Taguchi, Y.; Fujisawa, M.; Takaoka, T.; Okada, T.; Nishijima, M. *J. Chem. Phys.* **1991**, *95*, 6870.

(34) Fink, A.; Menzel, D.; Widdra, W. *J. Phys. Chem. B* **2001**, *105*, 3828.

(35) Craig, B. I. *Surf. Sci.* **1993**, *280*, L279.

(36) Jeong, H. D.; Ryu, S.; Lee, Y. S.; Kim, S. *Surf. Sci.* **1995**, *344*, L1226.

(37) Lopinski, G. P.; Fortier, T. M.; Moffatt, D. J.; Wolkow, R. A. *J. Vac. Sci. Technol. A* **1998**, *16*, 1037.

(38) Lopinski, G. P.; Moffatt, D. J.; Wolkow, R. A. *Chem. Phys. Lett.* **1998**, *282*, 305.

(39) Wolkow, R. A.; Lopinski, G. P.; Moffatt, D. J. *Surf. Sci.* **1998**, *416*, L1107.

(40) Hofer, W. A.; Fisher, A. J.; Lopinski, G. P.; Wolkow, R. A. *Surf. Sci.* **2001**, *482*, 1181.

(41) Kim, Y. K.; Lee, M. H.; Yeom, H. W. *Phys. Rev. B* **2005**, *71*, 115311.

(42) Taguchi, Y.; Fujisawa, M.; Nishijima, M. *Chem. Phys. Lett.* **1991**, *178*, 363.

(43) Cao, Y.; Wei, X. M.; Chin, W. S.; Lai, Y. H.; Deng, J. F.; Bernasek, S. L.; Xu, G. Q. *J. Phys. Chem. B* **1999**, *103*, 698.

(44) Kawasaki, T.; Sakai, D.; Kishimoto, H.; Akbar, A. A.; Ogawa, T.; Oshima, C. *Surf. Interface Anal.* **2001**, *31*, 126.

(45) Yong, K. S.; Yang, S. W.; Zhang, Y. P.; Wu, P.; Xu, G. Q. *Langmuir* **2008**, *24*, 3289.

(46) Tomimoto, H.; Sekitani, T.; Sumii, R.; Sako, E. O.; Wada, S.; Tanaka, K. *Surf. Sci.* **2004**, *566*, 664.

(47) Horn, S. A.; Patitsas, S. N. *Surf. Sci.* **2008**, *602*, 630.

(48) Petsalakis, I. D.; Polanyi, J. C.; Theodorakopoulos, G. *Isr. J. Chem.* **2005**, *45*, 111.

(49) Li, Y. C.; Wang, W. N.; Cao, Y.; Fan, K. N. *Acta Chim. Sin.* **2002**, *60*, 653.

(50) Tomimoto, H.; Takehara, T.; Fukawa, K.; Sumii, R.; Sekitani, T.; Tanaka, K. *Surf. Sci.* **2003**, *526*, 341.

(51) Cao, Y.; Yong, K. S.; Wang, Z. H.; Deng, J. F.; Lai, Y. H.; Xu, G. Q. *J. Chem. Phys.* **2001**, *115*, 3287.

(52) Cho, J. H.; Kim, K. S.; Morikawa, Y. *J. Chem. Phys.* **2006**, *124*.

(53) Wang, G. T.; Mui, C.; Tannaci, J. F.; Filler, M. A.; Musgrave, C. B.; Bent, S. F. *J. Phys. Chem. B* **2003**, *107*, 4982.

(54) Lu, X.; Lin, M. C. *Int. Rev. Phys. Chem.* **2002**, *21*, 137.

(55) Cao, Y.; Yong, K. S.; Wang, Z. Q.; Chin, W. S.; Lai, Y. H.; Deng, J. F.; Xu, G. Q. *J. Am. Chem. Soc.* **2000**, *122*, 1812.

(56) Lu, X.; Xu, X.; Wang, N. Q.; Zhang, Q.; Lin, M. C. *J. Phys. Chem. B* **2001**, *105*, 10069.

(57) Cao, Y.; Wang, Z. H.; Deng, J. F.; Xu, G. Q. *Angew. Chem., Int. Ed.* **2000**, *39*, 2740.

(58) Yuan, Z. L.; Chen, X. F.; Wang, Z. H.; Yong, K. S.; Cao, Y.; Xu, G. Q. *J. Chem. Phys.* **2003**, *119*, 10389.

(59) Isobe, N.; Shibayama, T.; Mori, Y.; Shobatake, K.; Sawabe, K. *Chem. Phys. Lett.* **2007**, *443*, 347.

(60) Qiao, M. H.; Cao, Y.; Tao, F.; Liu, Q.; Deng, J. F.; Xu, G. Q. *J. Phys. Chem. B* **2000**, *104*, 11211.

(61) Qiao, M. H.; Tao, F.; Cao, Y.; Li, Z. H.; Dai, W. L.; Deng, J. F.; Xu, G. Q. *J. Chem. Phys.* **2001**, *114*, 2766.

(62) Jeong, H. D.; Lee, Y. S.; Kim, S. *J. Chem. Phys.* **1996**, *105*, 200.

(63) Rousseau, G. B. D.; Dhanak, V.; Kadodwala, M. *Surf. Sci.* **2001**, *494*, 251.

(64) Lee, H. K.; Kim, K. J.; Kang, T. H.; Chung, J.; Kim, B. *Surf. Sci.* **2008**, *602*, 914.

(65) Qiao, M. H.; Cao, Y.; Deng, J. F.; Xu, G. Q. *Chem. Phys. Lett.* **2000**, *325*, 508.

(66) Cao, X. P.; Coulter, S. K.; Ellison, M. D.; Liu, H. B.; Liu, J. M.; Hamers, R. J. *J. Phys. Chem. B* **2001**, *105*, 3759.

(67) Kim, K.; Han, J.; Kang, T. H.; Ihm, K.; Jeon, C.; Moon, S.; Hwang, C. C.; Hwang, H. N.; Kim, B. *J. Electron Spectrosc. Relat. Phenom.* **2005**, *144*, 429.

(68) Qiao, M. H.; Tao, F.; Cao, Y.; Xu, G. Q. *Surf. Sci.* **2003**, *544*, 285.

(69) Luo, H. B.; Lin, M. C. *Chem. Phys. Lett.* **2001**, *343*, 219.

(70) Seino, K.; Schmidt, W. G.; Furthmuller, J.; Bechstedt, F. *Surf. Sci.* **2003**, *532*, 988.

(71) Tao, F.; Yuan, Z. L.; Chen, X. F.; Qiao, M. H.; Wang, Z. H.; Dai, Y. J.; Huang, H. G.; Cao, Y.; Xu, G. Q. *Phys. Rev. B* **2003**, *67*, 245406.

(72) Lee, H.; Jeon, S. M.; Kim, H. D.; Lim, D. K.; Jung, S. J.; Kim, S. *J. Phys.: Condens. Matter* **2008**, *20*, 135006.

(73) Jeon, S. M.; Jung, S. J.; Kim, H. D.; Lim, D. K.; Lee, H.; Kim, S. *J. Phys. Chem. B* **2006**, *110*, 21728.

(74) Jeon, S. M.; Jung, S. J.; Lim, D. K.; Kim, H. D.; Lee, H.; Kim, S. *J. Am. Chem. Soc.* **2006**, *128*, 6296.

(75) Kruger, P.; Pollmann, J. *Phys. Rev. Lett.* **1995**, *74*, 1155.

(76) Kim, D. H.; Choi, D. S.; Kim, A.; Bae, S. S.; Hong, S.; Kim, S. *J. Phys. Chem. B* **2006**, *110*, 7938.

(77) Kim, D. H.; Choi, D. S.; Kim, A.; Hong, S.; Kim, S. *Jpn. J. Appl. Phys. Part 1* **2006**, *45*, 2148.

(78) Kim, D. H.; Choi, D. S.; Hong, S.; Kim, S. *J. Phys. Chem. C* **2008**, *112*, 7412.

(79) Wolkow, R. A. *Phys. Rev. Lett.* **1992**, *68*, 2636.

(80) Weakliem, P. C.; Carter, E. A. *J. Chem. Phys.* **1992**, *96*, 3240.

(81) Kubby, J. A.; Griffith, J. E.; Becker, R. S.; Vickers, J. S. *Phys. Rev. B* **1987**, *36*, 6079.

(82) Tao, F.; Bernasek, S. L. *J. Am. Chem. Soc.* **2007**, *129*, 4815.

(83) Tao, F.; Lai, Y. H.; Xu, G. Q. *Langmuir* **2004**, *20*, 366.

(84) Tao, F.; Qiao, M. H.; Wang, Z. H.; Xu, G. Q. *J. Phys. Chem. B* **2003**, *107*, 6384.

(85) Miwa, J. A.; Eves, B. J.; Rosei, F.; Lopinski, G. P. *J. Phys. Chem. B* **2005**, *109*, 20055.

(86) Kim, H. J.; Cho, J. H. *J. Chem. Phys.* **2004**, *120*, 8222.

(87) Hong, S.; Cho, Y. E.; Maeng, J. Y.; Kim, S. *J. Phys. Chem. B* **2004**, *108*, 15229.

(88) Cho, Y. E.; Maeng, J. Y.; Kim, S.; Hong, S. Y. *J. Am. Chem. Soc.* **2003**, *125*, 7514.

(89) Huang, H. G.; Huang, J. Y.; Ning, Y. S.; Xu, G. Q. *J. Chem. Phys.* **2004**, *121*, 4820.

(90) Lu, X.; Xu, X.; Wu, J. M.; Wang, N. Q.; Zhang, Q. *New J. Chem.* **2002**, *26*, 160.

(91) Shimomura, M.; Ichikawa, D.; Fukuda, Y.; Abukawa, T.; Aoyama, T.; Kono, S. *Phys. Rev. B* **2005**, *72*.

(92) Huang, H. G.; Wang, Z. H.; Xu, G. Q. *J. Phys. Chem. B* **2004**, *108*, 12560.

(93) Huang, H. G.; Huang, J. Y.; Wang, Z. H.; Ning, Y. S.; Tao, F.; Zhang, Y. P.; Cai, Y. H.; Tang, H. H.; Xu, G. Q. *Surf. Sci.* **2007**, *601*, 1184.

(94) Lee, J. Y.; Jung, S. J.; Hong, S.; Kim, S. *J. Phys.Chem. B* **2005**, *109*, 348.

(95) Naumkin, F. Y.; Polanyi, J. C.; Rogers, D. *Surf. Sci.* **2003**, *547*, 335.

(96) Naumkin, F. Y.; Polanyi, J. C.; Rogers, D.; Hofer, W.; Fisher, A. *Surf. Sci.* **2003**, *547*, 324.

(97) Cao, Y.; Deng, J. F.; Xu, G. Q. *J. Chem. Phys.* **2000**, *112*, 4759.

(98) Chen, X. H.; Kong, Q.; Polanyi, J. C.; Rogers, D.; So, S. *Surf. Sci.* **1995**, *340*, 224.

(99) Jiang, G. P.; Polanyi, J. C.; Rogers, D. *Surf. Sci.* **2003**, *544*, 147.

(100) Li, Z. H.; Li, Y. C.; Wang, W. N.; Cao, Y.; Fan, K. N. *J. Phys. Chem. B* **2004**, *108*, 14049.

(101) Matta, C. F.; Polanyi, J. C. *Philos. Trans. R. Soc. London, Ser. A* **2004**, *362*, 1185.

(102) Sloan, P. A.; Palmer, R. E. *J. Phys.: Condens. Matter* **2006**, *18*, S1873.

(103) Dobrin, S.; Harikumar, K. R.; Polanyi, J. C. *Surf. Sci.* **2004**, *561*, 11.

(104) Tao, F.; Yuan, Z. L.; Chen, X. F.; Qiao, M. H.; Wang, Z. H.; Dai, Y. J.; Huang, H. G.; Cao, Y.; Xu, G. Q. *Phys. Rev. B* **2003**, *67*, 245406.

(105) Coulter, S. K.; Hovis, J. S.; Ellison, M. D.; Hamers, R. J. *J. Vac. Sci. Technol., A* **2000**, *18*, 1965.

(106) Schwartz, M. P.; Ellison, M. D.; Coulter, S. K.; Hovis, J. S.; Hamers, R. J. *J. Am. Chem. Soc.* **2000**, *122*, 8529.

(107) Hamers, R. J.; Hovis, J. S.; Coulter, S. K.; Ellison, M. D.; Padowitz, D. F. *Jpn. J. Appl. Phys., Part 1* **2000**, *39*, 4366.

(108) Tao, F.; Wang, Z. H.; Lai, Y. H.; Xu, G. Q. *J. Am. Chem. Soc.* **2003**, *125*, 6687.

(109) Zhang, Y. P.; Yang, L.; Lai, Y. H.; Xu, G. Q.; Wang, X. S. *Appl. Phys. Lett.* **2004**, *84*, 401.

(110) Hwang, Y. J.; Kim, A.; Hwang, E. Y.; Kim, S. *J. Am. Chem. Soc.* **2005**, *127*, 5016.

(111) Calzolari, A.; Di Felice, R. *J. Phys.: Condens. Matter* **2007**, *19*, 305017.

(112) Calzolari, A.; Ruini, A.; Molinari, E.; Caldas, M. J. *Phys. Rev. B* **2006**, *73*, 125420.

(113) Barriocanal, J. A.; Doren, D. J. *J. Am. Chem. Soc.* **2001**, *123*, 7340.

(114) Tao, F.; Qiao, M. H.; Li, Z. H.; Yang, L.; Dai, Y. J.; Huang, H. G.; Xu, G. Q. *Phys. Rev. B* **2003**, *67*, 115334.

(115) Kim, K. Y.; Song, B. K.; Jeong, S. M.; Kang, H. *J. Phys. Chem. B* **2003**, *107*, 11987.

(116) Zipoli, F.; Bernasconi, M. *J. Phys. Chem. B* **2006**, *110*, 23403.

(117) Pluchery, O.; Coustel, R.; Witkowski, N.; Borensztein, Y. *J. Phys. Chem. B* **2006**, *110*, 22635.

(118) Tao, F.; Wang, Z. H.; Chen, X. F.; Xu, G. Q. *Phys. Rev. B* **2002**, *65*, 115311.

(119) Tao, F.; Wang, Z. H.; Xu, G. Q. *J. Phys. Chem. B* **2002**, *106*, 3557.

(120) Qu, Y. Q.; Han, K. L. *J. Phys. Chem. B* **2004**, *108*, 8305.

(121) Rangan, S.; Gallet, J. J.; Bournel, F.; Kubsky, S.; Le Guen, K.; Dufour, G.; Rochet, F.; Sirotti, F.; Carniato, S.; Ilakovac, V. *Phys. Rev. B* **2005**, *71*, 165318.

(122) Cai, Y. H.; Shao, Y. X.; Xu, G. Q. *J. Am. Chem. Soc.* **2007**, *129*, 8404.

(123) Carbone, M.; Meloni, S.; Caminiti, R. *Phys. Rev. B* **2007**, *76*, 085332.

(124) Casaletto, M. P.; Carbone, M.; Piancastelli, M. N.; Horn, K.; Weiss, K.; Zanoni, R. *Surf. Sci.* **2005**, *582*, 42.

(125) Carbone, M.; Piancastelli, M. N.; Casaletto, M. P.; Zanoni, R.; Besnard-Ramage, M. J.; Comtet, G.; Dujardin, G.; Hellner, L. *Surf. Sci.* **1999**, *419*, 114.

(126) Baik, J.; Park, J.; Kim, M.; Ahn, J. R.; Park, C. Y.; An, K. S.; Hwang, C. C.; Hwang, H. N.; Kim, B. *J. Korean Phys. Soc.* **2007**, *50*, 690.

(127) Rummel, R. M.; Ziegler, C. *Surf. Sci.* **1998**, *418*, 303.

(128) Bitzer, T.; Alkunshalie, T.; Richardson, N. V. *Surf. Sci.* **1996**, *368*, 202.

(129) Tomimoto, H.; Sumii, R.; Shirota, N.; Yagi, S.; Taniguchi, M.; Sekitani, T.; Tanaka, K. *J. Vac. Sci. Technol., B* **2000**, *18*, 2335.

(130) Kugler, T.; Thibaut, U.; Abraham, M.; Folkers, G.; Gopel, W. *Surf. Sci.* **1992**, *260*, 64.

(131) Ihm, K.; Kang, T. H.; Han, J. H.; Moon, S.; Hwang, C. C.; Kim, K. J.; Hwang, H. N.; Jeon, C. H.; Kim, H. D.; Kim, B.; Park, C. Y. *J. Electron Spectrosc. Relat. Phenom.* **2005**, *144*, 397.

(132) Leftwich, T. R.; Teplyakov, A. V. *J. Phys. Chem. C* **2008**, *112*, 4297.

(133) Barriocanal, J. A.; Doren, D. J. *J. Vac. Sci. Technol.* **2000**, *18*, 1959.

(134) Bocharov, S.; Dmitrenko, O.; De Leo, L. P. M.; Teplyakov, A. V. *J. Am. Chem. Soc.* **2006**, *128*, 9300.

(135) De Leo, L. P. M.; Teplyakov, A. V. *J. Phys. Chem. B* **2006**, *110*, 6899.

(136) Rochefort, A.; Beausoleil, A. *Chem. Phys. Lett.* **2004**, *400*, 347–352.

(137) Okamura, K.; Ishii, H.; Kimura, Y.; Niwano, M. *Surf. Sci.* **2005**, *576*, 45.

(138) Okamura, K.; Hosoi, Y.; Kimura, Y.; Ishii, H.; Niwano, M. *Appl. Surf. Sci.* **2004**, *237*, 439.

(139) Buckanie, N. M.; Heringdorf, F. J. M. Z. *Surf. Sci.* **2007**, *601*, 1701.

(140) Rada, T.; Chen, Q.; Richardson, N. V. *J. Phys.: Condens. Matter* **2003**, *15*, S2749.

(141) Rada, T.; Chen, Q.; Richardson, N. *Phys. Status Solidi B* **2004**, *241*, 2353.

(142) Kasaya, M.; Tabata, H.; Kawai, T. *Surf. Sci.* **1998**, *400*, 367.

(143) Choudhary, D.; Clancy, P.; Bowler, D. R. *Surf. Sci.* **2005**, *578*, 20.

(144) Lee, H. K.; Han, J. H.; Kim, K. J.; Kang, T. H.; Kim, B. *Surf. Sci.* **2007**, *601*, 1456.

(145) Weidkamp, K. P.; Hacker, C. A.; Schwartz, M. P.; Cao, X. P.; Tromp, R. M.; Hamers, R. J. *J. Phys. Chem. B* **2003**, *107*, 11142.

(146) Hughes, G.; Roche, J.; Carty, D.; Cafolla, T.; Smith, K. E. *J. Vac. Sci. Technol., B* **2002**, *20*, 1620.

(147) Kasaya, M.; Tabata, H.; Kawai, T. *Surf. Sci.* **1998**, *406*, 302.

(148) Wakatsuchi, M.; Kato, H. S.; Yamada, T.; Kawai, M. *Jpn. J. Appl. Phys., Part 1* **2005**, *44*, 514.

(149) Tejima, M.; Kita, K.; Kyuno, K.; Toriumi, A. *Appl. Phys. Lett.* **2004**, *85*, 3746.

(150) Weidkamp, K. P.; Tromp, R. M.; Hamers, R. J. *J. Phys. Chem. C* **2007**, *111*, 16489.

(151) Suzuki, T.; Sorescu, D. C.; Yates, J. T. *Surf. Sci.* **2006**, *600*, 5092.

(152) Desiraju, G. R. *Chem. Commun.* **1997**, 1475.

(153) Suzuki, T.; Sorescu, D. C.; Jordan, K. D.; Levy, J.; Yates, J. T. *J. Chem. Phys.* **2006**, *124*, 054701.

(154) Suzuki, T.; Sorescu, D. C.; Jordan, K. D.; Yates, J. T. *J. Chem. Phys.* **2006**, *124*, 224708.

(155) Schwartz, M. P.; Halter, R. J.; McMahon, R. J.; Hamers, R. J. *J. Phys. Chem. B* **2003**, *107*, 224.

(156) Nunzi, F.; Sgamellotti, A.; Re, N. *J. Phys. Chem. B* **2004**, *108*, 10881.

(157) Yong, K. S.; Zhang, Y. P.; Yang, S. W.; Xu, G. Q. *Surf. Sci.* **2008**, *602*, 1921.

(158) Clar, E. *Polycyclic Hydrocarbons*; Academic Press: London, 1964; Vols. *1 and 2*.

(159) Clar, E. *The Aromatic Sextet*; Wiley: London, 1972.

(160) Yong, K. S. Ph.D. Thesis, National University of Singapore, 2007.

(161) Yong, K. S.; Zhang, Y. P.; Yang, S. W.; Wu, P.; Xu, G. Q. *J. Phys. Chem. A* **2007**, *111*, 12266.

(162) Schedel, T.; Frank, K. H.; Karlsson, U.; Koch, E. E. *Vacuum* **1990**, *41*, 652.

(163) Tong, S. Y.; Huang, H.; Wei, C. M.; Packard, W. E.; Men, F. K.; Glander, G.; Webb, M. B. *J. Vac. Sci. Technol., A* **1988**, *6*, 615.

(164) Huang, H.; Tong, S. Y.; Packard, W. E.; Webb, M. B. *Phys. Lett. A* **1988**, *130*, 166.

(165) Brommer, K. D.; Galvan, M.; Dalpino, A.; Joannopoulos, J. D. *Surf. Sci.* **1994**, *314*, 57.

(166) Yong, K. S.; Zhang, Y. P.; Yang, S. W.; Wu, P.; Xu, G. Q. *J. Phys. Chem. C* **2007**, *111*, 428.

(167) Hughes, G.; Carty, D.; Cafolla, A. A. *Surf. Sci.* **2005**, *582*, 90.

(168) Kawase, T.; Kurata, H. *Chem. Rev.* **2006**, *106*, 5250.

(169) Ajayan, P. M. *Chem. Rev.* **1999**, *99*, 1787.

(170) Thilgen, C.; Diederich, F. *Chem. Rev.* **2006**, *106*, 5049.

(171) Pascual, J. I.; Gomez-Herrero, J.; Rogero, C.; Baro, A. M.; Sanchez-Portal, D.; Artacho, E.; Ordejon, P.; Soler, J. M. *Chem. Phys. Lett.* **2000**, *321*, 78.

(172) Humphry, M. J.; Beton, P. H.; Keeling, D. L.; Fawcett, R. H. J.; Moriarty, P.; Butcher, M. J.; Birkett, P. R.; Walton, D. R. M.; Taylor, R.; Kroto, H. W. *J. Phys.: Condens. Matter* **2006**, *18*, S1837.

(173) Butcher, M. J.; Nolan, J. W.; Hunt, M. R. C.; Beton, P. H.; Dunsch, L.; Kuran, P.; Georgi, P.; Dennis, T. J. S. *Phys. Rev. B* **2003**, *67*, 125413.

(174) Wang, X. D.; Xue, Q. K.; Hashizume, T.; Shinohara, H.; Nishina, Y.; Sakurai, T. *Phys. Rev. B* **1994**, *49*, 7754.

(175) Chen, D.; Sarid, D. *Surf. Sci.* **1995**, *329*, 206.

(176) Shi, B. R.; Wang, X. S.; Huang, H. J.; Yang, S. H.; Heiland, W.; Cue, N. *J. Phys. Chem. B* **2001**, *105*, 11414.

(177) Wang, H. Q.; Zeng, C. G.; Li, Q. X.; Wang, B.; Yang, J. L.; Hou, J. G.; Zhu, Q. S. *Surf. Sci.* **1999**, *442*, L1024.

(178) Suto, S.; Sakamoto, K.; Kondo, D.; Wakita, T.; Kimura, A.; Kakizaki, A.; Hu, C. W.; Kasuya, A. *Surf. Sci.* **1999**, *438*, 242.

(179) Dunn, A. W.; Svensson, E. D.; Dekker, C. *Surf. Sci.* **2002**, *498*, 237.

(180) Wang, X. D.; Hashizume, T.; Shinohara, H.; Saito, Y.; Nishina, Y.; Sakurai, T. *Phys. Rev. B* **1993**, *47*, 15923.

(181) Yao, X. W.; Ruskell, T. G.; Workman, R. K.; Sarid, D.; Chen, D. *Surf. Sci.* **1996**, *367*, L85.

(182) Wang, X. D.; Hashizume, T.; Shinohara, H.; Saito, Y.; Nishina, Y.; Sakurai, T. *Jpn. J. Appl. Phys., Part 2* **1992**, *31*, L983.

(183) De Seta, M.; Sanvitto, D.; Evangelisti, F. *Phys. Rev. B* **1999**, *59*, 9878.

(184) Fleming, L.; Ulrich, M. D.; Efimenko, K.; Genzer, J.; Chan, A. S. Y.; Madey, T. E.; Oh, S. J.; Zhou, O.; Rowe, J. E. *J. Vac. Sci. Technol., B* **2004**, *22*, 2000.

(185) Kondo, D.; Sakamoto, K.; Takeda, H.; Matsui, F.; Amemiya, K.; Ohta, T.; Uchida, W.; Kasuya, A. *Surf. Sci.* **2002**, *514*, 337.

(186) Suto, S.; Sakamoto, K.; Kondo, D.; Wakita, T.; Kimura, A.; Kakizaki, A. *Surf. Sci.* **1999**, *428*, 85.

(187) Moriarty, P.; Upward, M. D.; Dunn, A. W.; Ma, Y. R.; Beton, P. H.; Teehan, D. *Phys. Rev. B* **1998**, *57*, 362.

(188) Suto, S.; Kasuya, A.; Ikeno, O.; Horiguchi, N.; Wawro, A.; Goto, T.; Nishina, Y. *Sci. Rep. Res. Inst., Tohoku Univ., Ser. A: Phys., Chem., Metall.* **1993**, *39*, 47.

(189) Drews, D.; Zahn, D. R. T. *Carbon* **1998**, *36*, 645.

(190) Barraza-Lopez, S.; Albrecht, P. M.; Romero, N. A.; Hess, K. *J. Appl. Phys.* **2006**, *100*, 124304.

(191) Orellana, W.; Miwa, R. H.; Fazzio, A. *Phys. Rev. Lett.* **2003**, *91*, 166802.

(192) Orellana, W.; Miwa, R. H.; Fazzio, A. *Surf. Sci.* **2004**, *566*, 728.

(193) Kawazoe, Y.; Kamiyama, H.; Maruyama, Y.; Ohno, K. *Jpn. J. Appl. Phys., Part 1* **1993**, *32*, 1433.

(194) Godwin, P. D.; Kenny, S. D.; Smith, R. *Surf. Sci.* **2003**, *529*, 237.

(195) Godwin, P. D.; Kenny, S. D.; Smith, R.; Belbruno, J. *Surf. Sci.* **2001**, *490*, 409.

(196) Sanchez-Portal, D.; Artacho, E.; Pascual, J. I.; Gomez-Herrero, J.; Martin, R. M.; Soler, J. M. *Surf. Sci.* **2001**, *482*, 39.

(197) Albrecht, P. M.; Lyding, J. W. *Small* **2007**, *3*, 146.

(198) Albrecht, P. M.; Lyding, J. W. *Appl. Phys. Lett.* **2003**, *83*, 5029.

(199) Su, M.; Li, Y.; Maynor, B.; Buldum, A.; Lu, J. P.; Liu, J. *J. Phys. Chem. B* **2000**, *104*, 6505.

(200) Martsinovich, N.; Hobbs, C.; Kantorovich, L.; Fawcett, R. H. J.; Humphry, M. J.; Keeling, D. L.; Beton, P. H. *Phys. Rev. B* **2006**, *74*, 085304.

(201) Moriarty, P.; Ma, Y. R.; Upward, M. D.; Beton, P. H. *Surf. Sci.* **1998**, *407*, 27.

(202) Zanella, I.; Fazzio, A.; da Silva, A. J. R. *J. Phys. Chem. B* **2006**, *110*, 10849.

(203) Butcher, M. J.; Jones, F. H.; Moriarty, P.; Beton, P. H.; Prassides, K.; Kordatos, K.; Tagmatarchis, N. *Appl. Phys. Lett.* **1999**, *75*, 1074.

(204) Fujikawa, Y.; Sadowski, J. T.; Kelly, K. F.; Nakayama, K. S.; Mickelson, E. T.; Hauge, R. H.; Margrave, J. L.; Sakurai, T. *Jpn. J. Appl. Phys., Part 1* **2002**, *41*, 245.

(205) Albrecht, P. M.; Barraza-Lopez, S.; Lyding, J. W. *Small* **2007**, *3*, 1402.

(206) Yu, J. X.; Shapter, J. G.; Quinton, J. S.; Johnston, M. R.; Beattie, D. A. *Phys. Chem. Chem. Phys.* **2007**, *9*, 510.

(207) Guerra, C. F.; Handgraaf, J. W.; Baerends, E. J.; Bickelhaupt, F. M. *J. Comput. Chem.* **2004**, *25*, 189.

(208) McClure, J. W. *Phys. Rev.* **1956**, *104*, 666.

(209) Wallace, P. R. *Phys. Rev.* **1947**, *71*, 476.

(210) Slonczewski, J. C.; Weiss, P. R. *Phys. Rev.* **1958**, *109*, 272.

(211) Novoselov, K. S.; Geim, A. K.; Morozov, S. V.; Jiang, D.; Zhang, Y.; Dubonos, S. V.; Grigorieva, I. V.; Firsov, A. A. *Science* **2004**, *306*, 666.

(212) Novoselov, K. S.; Geim, A. K.; Morozov, S. V.; Jiang, D.; Katsnelson, M. I.; Grigorieva, I. V.; Dubonos, S. V.; Firsov, A. A. *Nature* **2005**, *438*, 197.

(213) Geim, A. K.; Novoselov, K. S. *Nat. Mater.* **2007**, *6*, 183.

(214) Schedin, F.; Geim, A. K.; Morozov, S. V.; Hill, E. W.; Blake, P.; Katsnelson, M. I.; Novoselov, K. S. *Nat. Mater.* **2007**, *6*, 652.

(215) Pisana, S.; Lazzeri, M.; Casiraghi, C.; Novoselov, K. S.; Geim, A. K.; Ferrari, A. C.; Mauri, F. *Nat. Mater.* **2007**, *6*, 198.

(216) Novoselov, K. *Nat. Mater.* **2007**, *6*, 720.

(217) Lee, C.; Wei, X. D.; Kysar, J. W.; Hone, J. *Science* **2008**, *321*, 385.

(218) Bunch, J. S.; van der Zande, A. M.; Verbridge, S. S.; Frank, I. W.; Tanenbaum, D. M.; Parpia, J. M.; Craighead, H. G.; McEuen, P. L. *Science* **2007**, *315*, 490.

(219) Bobrov, K.; Mayne, A.; Comtet, G.; Dujardin, G.; Hellner, L.; Hoffman, A. *Phys. Rev. B* **2003**, *68*, 195416.

(220) Hersam, M. C.; Guisinger, N. P.; Lyding, J. W. *Nanotechnology* **2000**, *11*, 70.

(221) Aarts, J.; Hoeven, A. J.; Larsen, P. K. *Phys. Rev. B* **1988**, *37*, 8190.

(222) Bringans, R. D.; Hochst, H. *Phys. Rev. B* **1982**, *25*, 1081.

(223) Crowell, J. E.; Lu, G. Q. *J. Electron Spectrosc. Relat. Phenom.* **1990**, *54*, 1045.

(224) Klitsner, T.; Nelson, J. S. *Phys. Rev. Lett.* **1991**, *67*, 3800.

(225) Bobrov, K.; Comtet, G.; Dujardin, G.; Hellner, L. *Phys. Rev. Lett.* **2001**, *86*, 2633.

(226) Diederich, L.; Kuttel, O.; Aebi, P.; Schlapbach, L. *Surf. Sci.* **1998**, *418*, 219.

(227) Maier, F.; Ristein, J.; Ley, L. *Phys. Rev. B* **2001**, *64*, 165411.

(228) Hayashi, K.; Yamanaka, S.; Watanabe, H.; Sekiguchi, T.; Okushi, H.; Kajimura, K. *J. Appl. Phys.* **1997**, *81*, 744.

(229) Dujardin, G.; Rose, F.; Mayne, A. J. *Phys. Rev. B* **2001**, *63*, 235414.

(230) Lopinski, G. P.; Wayner, D. D. M.; Wolkow, R. A. *Nature* **2000**, *406*, 48.

(231) Yang, L.; Doren, D. J. *J. Phys. Chem. C* **2008**, *112*, 781.

(232) Takeuchi, N.; Selloni, A. *J. Phys. Chem. B* **2005**, *109*, 11967.

(233) Avouris, P.; Walkup, R. E.; Rossi, A. R.; Akpati, H. C.; Nordlander, P.; Shen, T. C.; Abeln, G. C.; Lyding, J. W. *Surf. Sci.* **1996**, *363*, 368.

(234) Abeln, G. C.; Hersam, M. C.; Thompson, D. S.; Hwang, S. T.; Choi, T.; Moore, J. S.; Lyding, J. W. *J. Vac. Sci. Technol., B* **1998**, *16*, 3874.

(235) Wang, Q. H.; Hersam, M. C. *J. Am. Chem. Soc.* **2008**, *130*, 12896.

(236) Mayne, A. J.; Soukiassian, L.; Commaux, N.; Comtet, G.; Dujardin, G. *Appl. Phys. Lett.* **2004**, *85*, 5379.

(237) Kato, K.; Kajiyama, H.; Heike, S.; Hashizume, T.; Uda, T. *Phys. Rev. Lett.* **2001**, *86*, 2842.

(238) Kaufhold, J.; Hauffe, K. *Ber. Bunsen-Ges. Phys. Chem.* **1965**, *69*, 168.

(239) Buriak, J. M. *Philos. Trans. R. Soc. London, Ser. A* **2006**, *364*, 217.

(240) Wang, D.; Buriak, J. M. *Langmuir* **2006**, *22*, 6214.

(241) Cullen, G. W.; Amick, J. A.; Gerlich, D. *J. Electrochem. Soc.* **1962**, *109*, 124.

(242) Amick, J. A.; Cullen, G. W.; Gerlich, D. *J. Electrochem. Soc.* **1962**, *109*, 127.

(243) Gerlich, D.; Cullen, G. W.; Amick, J. A. *J. Electrochem. Soc.* **1962**, *109*, 133.

(244) Choi, K.; Buriak, J. M. *Langmuir* **2000**, *16*, 7737.

(245) Higashi, G. S.; Chabal, Y. J.; Trucks, G. W.; Raghavachari, K. *Appl. Phys. Lett.* **1990**, *56*, 656.

(246) Higashi, G. S.; Becker, R. S.; Chabal, Y. J.; Becker, A. J. *Appl. Phys. Lett.* **1991**, *58*, 1656.

(247) Newton, T. A.; Boiani, J. A.; Hines, M. A. *Surf. Sci.* **1999**, *430*, 67.

(248) Bansal, A.; Li, X. L.; Lauermann, I.; Lewis, N. S.; Yi, S. I.; Weinberg, W. H. *J. Am. Chem. Soc.* **1996**, *118*, 7225.

(249) He, J.; Patitsas, S. N.; Preston, K. F.; Wolkow, R. A.; Wayner, D. D. M. *Chem. Phys. Lett.* **1998**, *286*, 508.

(250) Zhu, X. Y.; Boiadjiev, V.; Mulder, J. A.; Hsung, R. P.; Major, R. C. *Langmuir* **2000**, *16*, 6766.

(251) Terry, J.; Linford, M. R.; Wigren, C.; Cao, R. Y.; Pianetta, P.; Chidsey, C. E. D. *Appl. Phys. Lett.* **1997**, *71*, 1056.

(252) Lu, Z. H. *Appl. Phys. Lett.* **1996**, *68*, 520.

(253) Linford, M. R.; Fenter, P.; Eisenberger, P. M.; Chidsey, C. E. D. *J. Am. Chem. Soc.* **1995**, *117*, 3145.

(254) Chatgilialoglu, C. *Acc. Chem. Res.* **1992**, *25*, 188.

(255) Sung, M. M.; Kluth, G. J.; Yauw, O. W.; Maboudian, R. *Langmuir* **1997**, *13*, 6164.

(256) Sieval, A. B.; Demirel, A. L.; Nissink, J. W. M.; Linford, M. R.; van der Maas, J. H.; de Jeu, W. H.; Zuilhof, H.; Sudholter, E. J. R. *Langmuir* **1998**, *14*, 1759.

(257) Sieval, A. B.; Vleeming, V.; Zuilhof, H.; Sudholter, E. J. R. *Langmuir* **1999**, *15*, 8288.

(258) Sieval, A. B.; van den Hout, B.; Zuilhof, H.; Sudholter, E. J. R. *Langmuir* **2000**, *16*, 2987.

(259) Sieval, A. B.; van den Hout, B.; Zuilhof, H.; Sudholter, E. J. R. *Langmuir* **2001**, *17*, 2172.

(260) Sieval, A. B.; Linke, R.; Heij, G.; Meijer, G.; Zuilhof, H.; Sudholter, E. J. R. *Langmuir* **2001**, *17*, 7554.

(261) Bateman, J. E.; Eagling, R. D.; Worrall, D. R.; Horrocks, B. R.; Houlton, A. *Angew. Chem., Int. Ed.* **1998**, *37*, 2683.

(262) Boukherroub, R.; Morin, S.; Wayner, D. D. M.; Bensebaa, F.; Sproule, G. I.; Baribeau, J. M.; Lockwood, D. J. *Chem. Mater.* **2001**, *13*, 2002.

(263) Bateman, J. E.; Eagling, R. D.; Horrocks, B. R.; Houlton, A. *J. Phys. Chem. B* **2000**, *104*, 5557.

(264) Sano, H.; Maeda, H.; Matsuoka, S.; Lee, K. H.; Murase, K.; Sugimura, H. *Jpn. J. Appl. Phys.* **2008**, *47*, 5659.

(265) Terry, J.; Mo, R.; Wigren, C.; Cao, R. Y.; Mount, G.; Pianetta, P.; Linford, M. R.; Chidsey, C. E. D. *Nucl. Instrum. Methods Phys. Res., Sect. B* **1997**, *133*, 94.

(266) Terry, J.; Linford, M. R.; Wigren, C.; Cao, R. Y.; Pianetta, P.; Chidsey, C. E. D. *J. Appl. Phys.* **1999**, *85*, 213.

(267) Cicero, R. L.; Linford, M. R.; Chidsey, C. E. D. *Langmuir* **2000**, *16*, 5688.

(268) Stewart, M. P.; Buriak, J. M. *Angew. Chem., Int. Ed.* **1998**, *37*, 3257.

(269) Stewart, M. P.; Buriak, J. M. *J. Am. Chem. Soc.* **2001**, *123*, 7821.

(270) Imanishi, A.; Yamane, S.; Nakato, Y. *Langmuir* **2008**, *24*, 10755.

(271) Wojtyk, J. T. C.; Tomietto, M.; Boukherroub, R.; Wayner, D. D. M. *J. Am. Chem. Soc.* **2001**, *123*, 1535.

(272) Lewis, L. N. *J. Am. Chem. Soc.* **1990**, *112*, 5998.

(273) Boukherroub, R.; Morin, S.; Bensebaa, F.; Wayner, D. D. M. *Langmuir* **1999**, *15*, 3831.

(274) Buriak, J. M.; Allen, M. J. *J. Am. Chem. Soc.* **1998**, *120*, 1339.

(275) Buriak, J. M.; Stewart, M. P.; Geders, T. W.; Allen, M. J.; Choi, H. C.; Smith, J.; Raftery, D.; Canham, L. T. *J. Am. Chem. Soc.* **1999**, *121*, 11491.

(276) deVilleneuve, C. H.; Pinson, J.; Bernard, M. C.; Allongue, P. *J. Phys. Chem. B* **1997**, *101*, 2415.

(277) Hurley, P. T.; Ribbe, A. E.; Buriak, J. M. *J. Am. Chem. Soc.* **2003**, *125*, 11334.

(278) Fidelis, A.; Ozanam, F.; Chazalviel, J. N. *Surf. Sci.* **2000**, *444*, L7.

(279) Royea, W. J.; Juang, A.; Lewis, N. S. *Appl. Phys. Lett.* **2000**, *77*, 1988.

(280) Kim, N. Y.; Laibinis, P. E. *J. Am. Chem. Soc.* **1998**, *120*, 4516.

(281) Kim, N. Y.; Laibinis, P. E. *J. Am. Chem. Soc.* **1999**, *121*, 7162.

(282) Puniredd, S. R.; Assad, O.; Haick, H. *J. Am. Chem. Soc.* **2008**, *130*, 13727.

(283) Yu, H. B.; Webb, L. J.; Solares, S. D.; Cao, P. G.; Goddard, W. A.; Heath, J. R.; Lewis, N. S. *J. Phys. Chem. B* **2006**, *110*, 23898.

(284) Niederhauser, T. L.; Jiang, G. L.; Lua, Y. Y.; Dorff, M. J.; Woolley, A. T.; Asplund, M. C.; Berges, D. A.; Linford, M. R. *Langmuir* **2001**, *17*, 5889.

(285) Niederhauser, T. L.; Lua, Y. Y.; Sun, Y.; Jiang, G. L.; Strossman, G. S.; Pianetta, P.; Linford, M. R. *Chem. Mater.* **2002**, *14*, 27.

(286) Yang, L.; Lua, Y. Y.; Lee, M. V.; Linford, M. R. *Acc. Chem. Res.* **2005**, *38*, 933.

(287) He, J. L.; Lu, Z. H.; Mitchell, S. A.; Wayner, D. D. M. *J. Am. Chem. Soc.* **1998**, *120*, 2660.

(288) Sharp, I. D.; Schoell, S. J.; Hoeb, M.; Brandt, M. S.; Stutzmann, M. *Appl. Phys. Lett.* **2008**, *92*, 223306.

(289) Wagner, P.; Nock, S.; Spudich, J. A.; Volkmuth, W. D.; Chu, S.; Cicero, R. L.; Wade, C. P.; Linford, M. R.; Chidsey, C. E. D. *J. Struct. Biol.* **1997**, *119*, 189.

(290) Bitzer, T.; Richardson, N. V. *Appl. Surf. Sci.* **1999**, *145*, 339.

(291) Bitzer, T.; Rada, T.; Richardson, N. V. *J. Phys. Chem. B* **2001**, *105*, 4535.

(292) Boukherroub, R.; Wayner, D. D. M. *J. Am. Chem. Soc.* **1999**, *121*, 11513.

(293) Vermeir, I. E.; Kim, N. Y.; Laibinis, P. E. *Appl. Phys. Lett.* **1999**, *74*, 3860.

(294) Kim, A.; Filler, M. A.; Kim, S.; Bent, S. F. *J. Am. Chem. Soc.* **2005**, *127*, 6123.